9th International IFS and Contemporary Mathematics and Engineering Conference

July 08-11, 2023
Tarsus, Mersin, TURKEY

IFSCOM-E 2023

Proceeding Book

EDITOR-IN-CHIEF
Assoc. Prof. Dr. Gökhan Çuvalcıoğlu
Mersin University, TURKEY

EDITORS
Assis. Prof. Dr. Buğra Sarper
Tarsus University, TURKEY

Dr. Feride Tuğrul
Kahramanmaraş Sütçü İmam University, TURKEY

EDITING TEAM

Dr. Arif Bal
Mersin University, TURKEY

Ms.D. Şeyda Sezgek
Mersin University, TURKEY

Cansu Altıncı
Mersin University, TURKEY

ISBN: 978-605-68670-8-8

PREFACE

Dear Conference Participants,

Welcome to the Ninth International Conference on IFS and Contemporary Mathematics and Engineering (**IFSCOM-E 2023**). The aim of our conference is to bring together important engineers and mathematician researchers from all over the world with different engineering and mathematical interests. This conference is one of the leading international conferences to present new and fundamental advances in different fields of Engineering and Mathematics and to highlight interdisciplinary studies. We want to provide a suitable environment where researchers can exchange ideas, discuss the latest research findings and collaborate to generate new different ideas. We are happy to have outstanding researchers in different fields such as Mathematics and other fields related to Engineering sciences.

It is also the aim of the conference that young researchers and graduate students engage in such exceptional event. Their inputs and participation in such event should encourage them to do more research activities in the future.

We would like to thank all participating scientists who made the most important contribution to this conference. Their contributions are the key ingredient to the success of the conference.
We are sincerely grateful to all participants who really value our work and efforts that we develop every year to improve this conference. We are so proud to reach this respected level of success. Indeed, this was not possible without the outstanding work, efforts and supports from the members of the conference team: Scientific Committee Members, Referee Committee Members and Local Organizing Committee Members.

We are very pleased to present the abstracts of the Ninth International Conference on IFS and Contemporary Mathematics and Engineering (**IFSCOM-E 2023**). The conference was completed with **167** participants and **174** papers. The distribution of research papers delivered by the participants are classified by the following fields: Applied Mathematics, Algebra, Geometry, Topology, Analysis, Statistics and other fields such as Financial Mathematics, Fuzzy Sets, Game Theory, Geometric Computer Aided Design, Graph Theory, Intuitionistic Fuzzy, Machine Learning and Mathematical Modeling, Mechanical Engineering, Food Engineering, Information Visualization, Visualization Literacy, Environmental Engineering, Measurement of Fluid Properties, Civil Engineering, Natural Disaster, Industrial Engineering.

Two keynote speakers and four invited speakers attended the conference to share information about current studies in different fields with our participants. We have 167 participants participated from 21 countries: Canada, Mexico, India, Morocco, Poland, Russia, Turkey, etc..
This abstract booklet contains the titles and abstracts of all presented talks during the conference. Many submitted articles to this conference are considered in the following listed journals and books:

Journals:
- Journal of Universal Mathematics (JUM)
- Kahramanmaras Sutcu Imam University Journal of Engineering Sciences
- Karamanoğlu Mehmetbey University Journal of Engineering and Natural Sciences
- Notes on Intuitionistic Fuzzy Sets (Notes on IFS)

Books:
- IFSCOM-E 2023 Abstract Book with an ISBN number
- IFSCOM-E 2023 Proceeding Book with an ISBN number
- SPRINGER Book

We wish that all participants participate in all sessions, ask questions and be active in the conference. We also wish that this conference is a great place where you meet new friends, gain some knowledge, and get yourself involved in some research collaborations.

CHAIRMAN

Assoc. Prof. Gökhan ÇUVALCIOĞLU

July 2023

HONONARY CHAIRMAN

Orhan Aydın (Rector)(TR)

CHAIRMAN

Gökhan Çuvalcıoğlu (TR)

KEYNOTE SPEAKERS

İbrahim Dinçer (CA)
Oscar Castillo (MX)

INVITED SPEAKERS

Hanlar Reşidoğlu (TR)
Md. Hasanuzzaman (MY)
Poonam K. Sharma (IN)
Madhumangal Pal (IN)

SCIENTIFIC COMMITTEE MATH

Bijan Dawaz (IR)
Carlos M. da Fonseca (KW)
Ekrem Kadıoğlu (TR)
Evadokia Sotirova (BG)
Hamza Menken (TR)
Hüseyin Yıldırım (TR)
Janusz Kacprzyk (PL)
Krassimir Atanassov (BG)
Latif Hanna (KW)
Lois Aime Fono (CM)
Madhumangal Pal (IN)
Mehmet Çitil (TR)
M'hamed Elomari (MA)
Milica Andelic (KW)
Murat Güzeltepe (TR)
Kyriakos Papadopoulos (KW)
Oscar Castillo (MX)
Panagiotis Chountas (UK)
Piotr Nowak (PL)
Paramajit Kumar (IN)
Said Melliani (MA)
Sotir Sotirov (BG)
Şükran Konca (TR)
Taekyun Kim (KR)
Vassia Atanassova (BG)
Sinem Tarsuslu (Yılmaz) (TR)
Maya Altınok (TR)
Serap Şahinkaya (TR)
Halil Anaç (TR)

SCIENTIFIC COMMITTEE ENG

Aris Theofilatos (GR)
Ahmet Önen (OM)
Ahmet Kaya (TR)
Ahmet Alper Yontar (TR)
Alaattin Kaçal (TR)
Ali Kokangül (TR)

Ali Özen (TR)
Ali Şenol (TR)
Ata Hanlar (TR)
Aysel Özfidan (TR)
Berdan Özkurt (TR)
Buğra Sarper (TR)
Daver Ali (TR)
Deniz Üstün (TR)
Dilum Dissanayake (UK)
Dimitris Potoglou (UK)
Durmuş Yarımpabuç (TR)
Emel Yontar (TR)
Eren Özceylan (TR)
Erica Doutel (PT)
Ersan Harputlu (TR)
Fada Ragimov (AZ)
Faruk Geyik (TR)
Fecir Duran (TR)
Fehim Fındık (TR)
Ferruh Turan (TR)
Funda Kahraman (TR)
Gerhard Wilhelm Weber (PL)
Hüseyin Polat (TR)
Hüseyin Topaklı (TR)
Hüseyin Ünal (TR)
Indrasis Chakraborty (CA)
İrem Ersöz Kaya (TR)
İsmet Çelik (TR)
Kadri Süleyman Yiğit (TR)
Kamil Neyfel Çerçi (TR)
Kasım Ocakoğlu (TR)
Lin Li (CN)
Mahmoud Jourabian (IR)
Mine İnce Ocakoğlu (TR)
Mehmet Tahir Erdinç (TR)
Mehmet Eker (TR)
Mehmet Fatih Yılmaz (TR)
Metin Mutlu Aydın (TR)
Mustafa Berkan Biçer (TR)
Mustafa Egemen Taner (TR)
Mustara Kemal Külekci (TR)
Münir Süner (TR)
Olegas Prentkovskis (LT)

Onur Derse (TR)
Osman Murat Özkendir (TR)
Ömer Faruk Bay (TR)
Pawan Kumar (DE)
Raif Bayır (TR)
Ramazan Köse (TR)
Rovshan Aliyev (AZ)
Serhat OBUZ (TR)
Serdar Coşkun (TR)
Serdar Çiçek (TR)
Sezgin Aydın (TR)
Şule Yücelbaş (TR)
Tahir Hanalioğlu (TR)
Tahir Hikmet Karakoç (TR)
Taner Çokyaşar (TR)
Victor H. Duenas (US)
Veysel Alcan (TR)
Youming Fan (CN)
Zehra Yıldız (TR)

REFEREE COMMITTEE MATH

Abdullah Alazemi
Krassimir T. Atanassov
Oscar Castillo
Gökhan Çuvalcıoğlu
Ekrem Kadıoğlu
Mehmet Küçükaslan
Said Melliani
Madhumangal Pal
Hanlar Reşidoğlu
Sotir Sotirov
Hüseyin Yıldırım

REFEREE COMMITTEE ENG

Ercan Köse (TR)
Salih Hakan Yetgin (TR)
Serap Akcan (TR)
Uğur Eşme (TR)
Volkan Ateş (TR)

LOCAL ORGANIZING COMMITTEE

Feride Tuğrul
Arif Bal
Şeyda Sezgek
Cansu Altıncı
Fatma Yamaç Sağırlı
Enise Çiçek Yıldırım
Yasin Koç
Ali Müftüoğulları
Melisa Albayrak

CONTENTS

IFSCOM-E 2023
9th Ifs And Contemporary Mathematics and Engineering Conference
08-11 July 2023 Tarsus, Mersin, Türkiye
ISBN: 978-605-68670-8-8
pp: 1-8

APPROXIMATE SOLUTIONS OF THE MODIFIED KRATZER POTENTIAL PLUS SCREENED COULOMB POTENTIAL IN N-DIMENSIONS

A. ÖZFİDAN

Abstract. We investigate the bound state solutions of the N-dimensional Klein-Gordon equation with the modified Kratzer potential plus screened Coulomb potential via the asymptotic iteration approach. By the use of Greene-Aldrich approximation, we construct the N-dimensional energy spectrum and the N-dimensional radial wavefunction in relativistic theory. To test the accuracy of our analytical approach, we compare the present results with other reported works.

1. Introduction

Recently, many researchers have focused on solving the relativistic and non-relativistic wave equations with the linear combination of two or more potentials. In this regard, a vast number of works have been carried out to investigate the Klein-Gordon equation with these potentials in both three dimensions and N-spatial dimensions[1-3]. One such potential is the modified Kratzer potential plus screened Coulomb potential[4].

In hyperspherical coordinates, the modified Kratzer potential plus screened Coulomb potential is given by

$$V(r) = D_e \left(\frac{r - r_e}{r} \right)^2 - \frac{V_0}{r} e^{-\alpha r} \tag{1.1}$$

where r_e and D_e are the equilibrium intermolecular separation, the dissociation energy, V_0 is the potential strength parameter, α is the screening parameter, respectively. Kratzer potential[5] appears in various fields of physics and chemistry, especially atomic and nuclear physics. Besides, the modified Kratzer potential has also been worked out by many authors [6-7]. The screened Coulomb potential[8] has played a key role in some physical systems such as dense plasmas, solid-state matter. For this reason, we consider the extensive theoretical modeling which is a

Date: July, 8, 2023.
2000 *Mathematics Subject Classification.* 81Q05; 33C05.
Key words and phrases. Asymptotic iteration method, Hyperspherical coordinates.

superposition of the modified Kratzer and the screened Coulomb potentials in the present work.

Hyperspherical coordinates are of great importance in quantum mechanical problems and their applications. N-dimensional space plays a foundational role throughout our calculations in this work. It should be mentioned that mathematical tools have been investigated by Louck and Shaffer [9], Louck [10-11], and Chatterjee [12] to generalize orbital angular momentum.

We need to use an approximation scheme in quest for l-state solutions of the exponential-type potential models. In this context, to overcome the centrifugal term, we apply the Greene-Aldrich approximation[13]. According to the best of our knowledge, no the l_{N-1}-state solutions of the Klein-Gordon equation with the modified Kratzer potential plus the screened Coulomb potential have been established within the framework of asymptotic iteration method(AIM) which has been proposed by Ciftci *et al.* [14-16]. The present letter aims to apply the AIM to probe the relativistic treatment of a spinless particle interacting with the relevant potential in hyperspherical coordinates.

The rest of this work is arranged as follows: In Sec. 2, the asymptotic iteration approach is briefly discussed. In Sec. 3, the Klein-Gordon equation in hyperspherical coordinates is examined and the relativistic wave equation in the presence of central potential is separated into radial and angular parts. We present also the approximate solutions of the N-dimensional Klein-Gordon equation for the modified Kratzer potential plus the screened Coulomb potential. Finally, some conclusions are given in Sec. 4.

2. Basic Concepts Of Asymptotic Iteration Method

In this section, we present briefly the asymptotic iteration method which is the procedure for solving the Klein-Gordon equation in hyperspherical coordinates. The related theoretical details of this method can be found in Refs. [14-16]. AIM can be used to solve the second-order differential equation of the form

$$y''(r) = \lambda_0(r)y'(r) + s_0(r)y(r) \tag{2.1}$$

in which $\lambda_0(r)$ and $s_0(r)$ functions in C_∞(a,b) are sufficiently differentiable. The general solution of Eq.(2.1) can be obtained in the following form

$$y(r) = exp\left(-\int^r \alpha dr'\right)\left[C_2 + C_1\int^r exp\left(\int^{r'}\left[\lambda_0(\tau) + 2\alpha(\tau)\right]d\tau\right)dr'\right] \tag{2.2}$$

For adequately large k,

$$\frac{s_k(r)}{\lambda_k(r)} = \frac{s_{k-1}(r)}{\lambda_{k-1}(r)} \equiv \alpha(r) \tag{2.3}$$

in which

$$\lambda_k = \lambda_{k-1}^{'} + s_{k-1} + \lambda_0\lambda_{k-1} \qquad s_k = s_{k-1}^{'} + s_0\lambda_{k-1} \tag{2.4}$$

If the eigenvalue problem has exact analytic solutions, the termination condition Eq.(2.3), or equivalently,

$$\delta_k(r) = \lambda_k(r)s_{k-1}(r) - \lambda_{k-1}(r)s_k(r) = 0 \tag{2.5}$$

produces, at each iteration, an expression that is independent of r. It is noted that k displays the iteration number. Physically meaningful solution of Eq.(2.1) is provided by the first term of Eq.(2.2) not the second term, so we can use the first term as the wavefunction generator

$$y(r) = C_2 exp\left(-\int^r \frac{s_k(r')}{\lambda_k(r')}dr'\right) \tag{2.6}$$

where C_2 is an integration constant that can be determined by normalization.

3. N-dimensional solutions of the modified Kratzer potential plus the screened Coulomb Potential in approximate analytic form

We briefly carry out the separation of variables for the N-dimensional Klein-Gordon equation. In hyperspherical coordinates, the Klein-Gordon equation with a non-central potential can be written as

$$-\hbar^2c^2\nabla_N^2\Psi(r,\theta_{N-1}) + \left[\left(\mu c^2 + S(r,\theta_{N-1})\right)^2 - \left(E - V(r,\theta_{N-1})\right)^2\right]\Psi(r,\theta_{N-1}) = 0 \tag{3.1}$$

where E and μ are relativistic energy and reduced mass of a spin-zero particle, c is the velocity of light and $\hbar$ is Planck constant. Eq.(3.1) for $S(r,\theta_{N-1}) = V(r,\theta_{N-1})$ reduces to Klein-Gordon equation in hyperspherical coordinates for the potential $2V$ in the non-relativistic limit. Following the works of Alhaidari et al.[17] , we draw conclusion that only the choice $S = +V$ produces a nontrivial non-relativistic limit with a potential function $2V$ and not V. A choice of $S = -V$ also reveals free fields in the non-relativistic limit. For this reason, if the potential terms in Eq.(3.1) are scaled, in case of the non-relativistic limit the interaction potential becomes V, not $2V$. Therefore, for the case of the equal scalar and vector potentials, the N-dimensional Klein-Gordon equation is obtained in the following form

$$-\hbar^2c^2\nabla_N^2\Psi(r,\theta_{N-1}) + \left[\left(E + \mu c^2\right)V(r,\theta_{N-1}) - \left(E^2 - \mu^2c^4\right)\right]\Psi(r,\theta_{N-1}) = 0 \tag{3.2}$$

The N-dimensional Laplacian is defined with respect to Cartesian coordinates $x_1, x_2, x_3, ...x_N$ as

$$\nabla_N^2 = \sum_{j=1}^{N}\frac{\partial^2}{\partial x_j^2} \tag{3.3}$$

In accordance with the works of Louck [10,11] and Chatterjee [12], we introduce the hyperspherical coordinates in N-dimensional space as follows

$$\begin{aligned}
x_1 &= rcos\theta_1 sin\theta_2 sin\theta_3 .....sin\theta_{N-1} \\
x_2 &= rsin\theta_1 sin\theta_2 sin\theta_3 .....sin\theta_{N-1} \\
x_3 &= rcos\theta_2 sin\theta_3 sin\theta_4 .....sin\theta_{N-1} \\
x_4 &= rcos\theta_3 sin\theta_4 sin\theta_5 .....sin\theta_{N-1} \\
&\vdots \\
x_j &= rcos\theta_{j-1} sin\theta_j sin\theta_{j+1} .....sin\theta_{N-1} \qquad 3 \le j \le N-1 \\
x_N &= rcos\theta_{N-1}
\end{aligned} \tag{3.4}$$

for $N = 3, 4, 5...$, where the range of the variables is $0 \leq r \leq \infty$, $0 \leq \theta_1 \leq 2\pi$, $0 \leq \theta_j \leq \pi$, for $j = 2, 3, ..., N-1$ and r is the radius of an N-dimensional sphere. The Laplacian is given in terms of hyperspherical coordinates by

(3.5)
$$\nabla_N^2 = \frac{1}{r^{N-1}}\frac{\partial}{\partial r}r^{N-1}\frac{\partial}{\partial r} + \frac{1}{r^2}\sum_{k=1}^{N-2}\frac{1}{\sin^2\theta_{k+1}\sin^2\theta_{k+2}.....\sin^2\theta_{N-1}}\left(\frac{1}{\sin^{k-1}\theta_k}\frac{\partial}{\partial_k}\sin^{k-1}\theta_k\frac{\partial}{\partial\theta_k}\right)+ \frac{1}{r^2}\left(\frac{1}{\sin^{N-2}\theta_{N-1}}\frac{\partial}{\partial\theta_{N-1}}\sin^{N-2}\theta_{N-1}\frac{\partial}{\partial\theta_{N-1}}\right)$$

We take the total wave function in hyperspherical coordinates as

$$\Psi(r, \theta_1, \theta_2, ..., \theta_{N-1}) = r^{-\frac{N-1}{2}}R(r)Y_{l_{N-1},l_{N-2}....,l_2,l_1}(\theta_1, \theta_2, ..., \theta_{N-1}) \tag{3.6}$$

where $R(r)$ is radial wave function and $Y_{l_{N-1},l_{N-2}....,l_2,l_1}(\theta_1, \theta_2, ..., \theta_{N-1})$ is generalized spherical harmonics. In this context, the radial part of the N-dimensional relativistic wave equation is obtained as

(3.7)
$$\frac{d^2R(r)}{dr^2}+\left[\frac{E^2-\mu^2c^4}{\hbar^2c^2} - \left(\frac{E+\mu c^2}{\hbar^2c^2}\right)V(r) - \frac{(N-1)(N-3)}{4r^2} - \frac{l_{N-1}\left(l_{N-1}+N-2\right)}{r^2}\right]R(r) = 0$$

and the angular parts of the N-dimensional relativistic wave equation are given in the following forms

$$\begin{aligned}\frac{d^2H\left(\theta_{N-1}\right)}{d\theta_{N-1}^2} &+ (N-2)\frac{\cos\theta_{N-1}}{\sin\theta_{N-1}}\frac{dH\left(\theta_{N-1}\right)}{d\theta_{N-1}} - \left[\left(\frac{E+\mu c^2}{\hbar^2c^2}\right)r^2V(\theta_{N-1})\right.\\ &+ \left.\frac{l_{N-2}\left(l_{N-2}+N-3\right)}{\sin^2\theta_{N-1}} - l_{N-1}\left(l_{N-1}+N-2\right)\right]H\left(\theta_{N-1}\right) = 0\end{aligned} \tag{3.8}$$

$$\frac{d^2H(\theta_1)}{d\theta_1^2} + l_1^2H(\theta_1) = 0 \tag{3.9}$$

It should be noted that the Klein-Gordon equation for the potential involved is separable into (N - 1) angular equations for the angular parameters $(\theta_1, \theta_2, ..., \theta_{N-1})$ and to one radial equation for the radial parameter r. More details can be found in Refs.[10-12].

3.1. **Radial Energy Eigenvalues and Eigenfunctions in Hyperspherical Coordinates.** When we plug Eq.(1.1) into Eq.(3.7), we get the radial Klein-Gordon equation for the modified Kratzer potential plus the screened Coulomb potential in N-dimensions as

$$\begin{aligned}\frac{d^2R(r)}{dr^2} &+ \left[\frac{\left(E^2-\mu^2c^4\right)}{\hbar^2c^2} - \frac{\left(E+\mu c^2\right)}{\hbar^2c^2}\left(D_e\left(\frac{r-r_e}{r}\right)^2 - \frac{V_0}{r}e^{-\alpha r}\right) - \frac{(N-1)(N-3)}{4r^2}\right.\\ &- \left.\frac{l_{N-1}\left(l_{N-1}+N-2\right)}{r^2}\right]R(r) = 0\end{aligned} \tag{3.10}$$

Due to the centrifugal term, Eq.(3.10) cannot be solved analytically for any l_{N-1}-state. As a result, in order to solve this equation, we must utilize an approximation scheme proposed by Greene-Aldrich as

$$\frac{1}{r^2} \approx \frac{\alpha^2}{\left(1-e^{-\alpha r}\right)^2} \tag{3.11}$$

By applying this approximation to Eq.(3.10) and making a change of variable $y = e^{-\alpha r}$, we can reconstruct the hyper-radial relativistic wave equation

$$\frac{d^2R(y)}{dy^2} + \frac{1}{y}\frac{dR(y)}{dy} + \left[-\frac{\varepsilon^2}{y^2} + \frac{\Lambda_0}{y^2\left(1-y\right)} + \frac{\Lambda_1}{y\left(1-y\right)} - \frac{\Lambda_2}{y^2\left(1-y\right)^2}\right] R\left(y\right) = 0 \tag{3.12}$$

with

$$\begin{aligned} \& -\varepsilon^2 = \frac{\left(E^2-\mu^2c^4\right) - D_e\left(E+\mu c^2\right)}{\alpha^2\hbar^2c^2} \quad , \quad \kappa = l_{N-1} + \frac{N-3}{2} \quad , \quad \Lambda_0 = \frac{\left(E+\mu c^2\right)}{\alpha\hbar^2c^2} 2D_e r_e \\ \& \Lambda_1 = \frac{\left(E+\mu c^2\right)}{\alpha\hbar^2c^2} V_0 \quad , \quad \Lambda_2 = \frac{\left(E+\mu c^2\right)}{\hbar^2c^2} D_e r_e^2 + \kappa(\kappa+1) \end{aligned} \tag{3.13}$$

In order to solve Eq.(3.12) through asymptotic iteration method, the wave function that ensures the boundary conditions is proposed in the following form

$$R\left(y\right) = \left(1-y\right)^{\gamma+1} y^{\nu} f(y) \tag{3.14}$$

where $f(y)$ is a function to be determined and γ and ν are defined as

$$\gamma = -\frac{1}{2} + \frac{\sqrt{\left(1+4\Lambda_2\right)}}{2} \quad , \quad \nu = \sqrt{\varepsilon^2 - \Lambda_0 + \Lambda_2} \tag{3.15}$$

When we substitute Eq.(3.14) into Eq.(3.12), the second-order homogeneous linear differential equation is obtained as follows

$$\frac{d^2f(y)}{dy^2} = \left[\frac{\left(2\gamma+2\nu+3\right)y - \left(2\nu+1\right)}{y(1-y)}\right]\frac{df(y)}{dy} + \left[\frac{\left(1+\gamma\right)\left(2\nu+1\right) + 2\Lambda_2 - \Lambda_0 - \Lambda_1}{y\left(1-y\right)}\right] f(y) \tag{3.16}$$

which is convenient to apply the asymptotic iteration method. We can find the values of λ_0 and s_0 with the comparison of Eq.(3.16) to Eq.(2.1). By using Eq.(2.4), we can derive λ_n and s_n as follows

$$
\begin{aligned}
\lambda_0 &= \frac{(2\gamma+2\nu+3)\,y-(2\nu+1)}{y(1-y)} \\
s_0 &= \frac{(1+\gamma)\,(2\nu+1)+2\Lambda_2-\Lambda_0-\Lambda_1}{y\,(1-y)} \\
\lambda_1 &= \frac{2\gamma+2\nu+3}{y(1-y)}-\frac{(2\gamma+2\nu+3)\,y-(2\nu+1)}{y^2\,(1-y)}+\frac{(2\gamma+2\nu+3)\,y-(2\nu+1)}{y\,(1-y)^2} \\
&\quad +\frac{(1+\gamma)\,(2\nu+1)+2\Lambda_2-\Lambda_0-\Lambda_1}{y\,(1-y)}+\frac{\left((2\gamma+2\nu+3)\,y-(2\nu+1)\right)^2}{y^2\,(1-y)^2} \\
s_1 &= -\frac{(1+\gamma)\,(2\nu+1)+2\Lambda_2-\Lambda_0-\Lambda_1}{y^2\,(1-y)}+\frac{(1+\gamma)\,(2\nu+1)+2\Lambda_2-\Lambda_0-\Lambda_1}{y\,(1-y)^2} \\
&\quad +\frac{\left((1+\gamma)\,(2\nu+1)+2\Lambda_2-\Lambda_0-\Lambda_1\right)\left((2\gamma+2\nu+3)\,y-(2\nu+1)\right)}{y^2\,(1-y)^2}
\end{aligned}
\tag{3.17}
$$

After building the energy eigenvalues via Eq.(2.3) and taking into consideration the used abbreviations, we obtain the N-dimensional relativistic energy spectrum for the modified Kratzer potential plus the screened Coulomb potential

$$
\begin{aligned}
&\frac{\left(E^2-\mu^2c^4\right)}{\hbar^2c^2\alpha^2}=\frac{\left(E+\mu c^2\right)}{\alpha^2\hbar^2c^2}D_e-\frac{\left(E+\mu c^2\right)}{\alpha\hbar^2c^2}2D_er_e+\frac{\left(E+\mu c^2\right)}{\hbar^2c^2}D_er_e^2+\kappa(\kappa+1) \\
&-\left(\frac{\frac{\left(E+\mu c^2\right)}{\alpha\hbar^2c^2}V_0+\frac{\left(E+\mu c^2\right)}{\alpha\hbar^2c^2}2D_er_e-\frac{\left(E+\mu c^2\right)}{\hbar^2c^2}2D_er_e^2-\left(n^2+n+\frac{1}{2}+\left(n+\frac{1}{2}\right)\sqrt{1+4\kappa(\kappa+1)+\frac{4D_er_e^2\left(E+\mu c^2\right)}{\hbar^2c^2}}+2\kappa(\kappa+1)\right)}{\left(2n+1+\sqrt{1+4\kappa(\kappa+1)+\frac{4D_er_e^2\left(E+\mu c^2\right)}{\hbar^2c^2}}\right)}\right)^2
\end{aligned}
\tag{3.18}
$$

In the non-relativistic limit, for $N=3$, Eq.(3.18) is in agreement with the one obtained previously in Refs.[4].

We can also construct the corresponding wavefunctions of the radial part of the Klein-Gordon equation with Eq.(1.1) by using the wavefunction generator given by Eq.(2.6).

$$
\begin{aligned}
f_0(y) &= C_2 = C_2\,{}_2F_1\left(0,2\gamma+2\nu+2,2\nu+1;y\right) \\
f_1(y) &= -C_2[(2\nu+1)-(2\gamma+2\nu+3)\,y] \\
&= -C_2\,(2\nu+1)\,{}_2F_1\left(-1,2\gamma+2\nu+3,2\nu+1;y\right) \\
f_2(y) &= C_2\left[(2\gamma+2\nu+4)\,(2\gamma+2\nu+5)\,y^2-2\,(2\gamma+2\nu+4)\,(2\nu+2)\,y+(2\nu+1)\,(2\nu+2)\right] \\
&= C_2\,(2\nu+1)\,(2\nu+2)\,{}_2F_1\left(-2,2\gamma+2\nu+4,2\nu+1;y\right) \\
f_3(x) &= -C_2\left[-(2\gamma+2\nu+7)\,(2\gamma+2\nu+6)\,(2\gamma+2\nu+5)\,y^3+3\,(2\gamma+2\nu+6)\,(2\gamma+2\nu+5)\,(2\nu+3)\,y^2\right. \\
&\quad \left.-3\,(2\gamma+2\nu+5)\,(2\nu+3)\,(2\nu+2)\,y+(2\nu+3)\,(2\nu+2)\,(2\nu+1)\right] \\
&= C_2\,(2\nu+1)\,(2\nu+2)\,(2\nu+3)\,{}_2F_1\left(-3,2\gamma+2\nu+5,2\nu+1;y\right) \\
&\vdots
\end{aligned}
$$

We can see that $f(y)$in the general form can be written as follows

$$
f_n\left(y\right)=C_2\,(2\nu+1)_n\,(-1)^n\,{}_2F_1\left(-n,\,2\gamma+2\nu+2+n,\,2\nu+1,y\right) \tag{3.19}
$$

As a result, we express the hyper-radial wave function as follows

(3.20)

$$R(y) = C_2 (1-y)^{\gamma+1} y^{\nu} (2\nu+1)_n (-1)^n {}_2F_1(-n,\, 2\gamma+2\nu+2+n, 2\nu+1, y)$$

in which C_2 denotes the normalization factor.

4. Conclusion

On constructing the l_{N-1}-state solutions of the Klein-Gordon equation with the modified Kratzer potential plus the screened Coulomb potential under the condition of equal vector and scalar potentials, we employ the asymptotic iteration approach. It is important to note that quantum systems with such potentials can be investigated with proper approximations. In this context, Greene-Aldrich approximation is applied to the centrifugal term in this work. Hence, for bound states, we derive the N-dimensional energy eigenvalues and obtain the N-dimensional radial wavefunction in the presence of the relevant potential in approximate analytic form.

The asymptotic iteration formalism is a reliable computing approach for obtaining analytical solutions of the N-dimensional relativistic wave equation in central potential field. The energy spectrum obtained within the asymptotic iteration approach is consistent with the other method in the available literature.

References

[1] A.I., Ahmadov, S.M., Aslanova, M.S., Orujova, S.V., Badalov, S.H., Dong, Approximate bound state solutions of the Klein-Gordon equation with the linear combination of Hulthen and Yukawa potentials, Physics Letters A, vol. 383, pp. 3010, (2019).

[2] K.R., Purohit, R.H., Parmar, A.K., Rai, Eigensolution and various properties of the screened cosine Kratzer potential in D dimensions via relativistic and non-relativistic treatment, European Physical Journal Plus, vol. 135, (2020).

[3] C.P., Onyenegecha, A.I., Opara, I.J., Njoku, S.C., Udensi, U.M., Ukewuihe, C.J., Okereke, A., Omame, Analytical solutions of D-dimensional Klein-Gordon equation with modified Mobius squared potential, Results in Physics, vol. 25, pp. 104144 (2021).

[4] C.E., Edet, U.S., Okorie, A.T., Ngiangia, A.N., Ikot, Bound-state solutions of the Schrödinger for the modified Kratzer potential plus screened Coulomb potential, Indian Journal of Physics, vol. 94, pp. 425 (2020).

[5] A., Kratzer, Die ultraroten rotationsspektren der halogenwasserstoffe, Zeitschrift für Physik, vol. 3, pp. 289, (1920).

[6] K.J., Oyewumi, Realization of the spectrum generating algebra for the generalized Kratzer potentials, International Journal of Theoretical Physics, vol. 49, pp. 1302, (2010).

[7] A., Durmuş, Non-relativistic treatment of diatomic molecules interacting with a generalized Kratzer potential in hyperspherical coordinates, Journal of Physics A: Mathematical and Theoretical, vol. 44, pp. 155205, (2007).

[8] H., Yukawa, On the interaction of elementary particles I, Proceedings of the Physico-Mathematical Society of Japan 3rd Series, vol. 17, pp. 48, (1935).

[9] J.D., Louck, W.H., Shaffer, Generalized orbital angular momentum and the n-fold degenerate quantum mechanical oscillator: Part I the twofold degenerate oscillator, Journal of Molecular Spectroscopy, vol. 4, pp. 285, (1960).

[10] J.D., Louck, Generalized orbital angular momentum and the n-fold degenerate quantum mechanical oscillator: Part II the n-fold degenerate oscillator, Journal of Molecular Spectroscopy, vol. 4, pp. 298, (1960).

[11] J.D., Louck, Generalized orbital angular momentum and the n-fold degenerate quantum mechanical oscillator: Part III radial integrals, Journal of Molecular Spectroscopy, vol. 4, pp. 334, (1960).

[12] A., Chatterjee, Large-N expansions in quantum mechanics, atomic physics and some O(N) invariant systems, Physics Reports, vol. 186, pp. 249, (1990).

[13] R. L., Greene, C., Aldrich, Variational wave functions for a screened Coulomb potential, Physical Review A, vol. 14, pp. 2363, (1976)
[14] H., Ciftci, R.L., Hall, N., Saad, Asymptotic iteration method for eigenvalue problems, Journal of Physics A: Mathematical and General, vol. 36, pp. 11807, (2003).
[15] H., Ciftci, R.L., Hall, N., Saad, Construction of exact solutions to eigenvalue problems by the asymptotic iteration method, Journal of Physics A: Mathematical and General, vol. 38, pp. 1147,(2005).
[16] H., Ciftci, R.L., Hall, N., Saad, Iterative solutions to the Dirac equation, Physical Review A, vol. 72, pp. 022101, (2005).
[17] A.D., Alhaidari, H., Bahlouli, A., Al-Hasan, Dirac and Klein-Gordon equations with equal scalar and vector potentials, Physics Letters A, vol. 349, pp. 87, (2006).

Tarsus University, Department of Natural and Mathematical Sciences, Mersin, Türkiye.
Email address: ayselozfidan@tarsus.edu.tr

IFSCOM-E 2023
9th Ifs And Contemporary Mathematics and Engineering Conference
08-11 July 2023 Tarsus, Mersin, Türkiye
ISBN: 978-605-68670-8-8
pp: 9-14

ON A GENERAL INCLUSION THEOREM

HİKMET SEYHAN ÖZARSLAN AND BAĞDAGÜL KARTAL

0000-0002-0437-032X and 0000-0001-6223-0838

Abstract. In the present study, a theorem which gives necessary and sufficient conditions for the inclusion relation between $\mid A, p_n, \beta; \delta \mid_k$ and $\mid B, p_n, \beta; \delta \mid_k$ summability methods is introduced.

1. Introduction

Let $\sum a_n$ be an infinite series with its partial sums (s_n). Let $A = (a_{nv})$ be a normal matrix, i.e., a lower triangular matrix of nonzero diagonal entries. Then A defines the sequence-to-sequence transformation, mapping the sequence $s = (s_n)$ to $As = (A_n(s))$, where $A_n(s) = \sum_{v=0}^{n} a_{nv} s_v, \quad n = 0, 1, ...$ Let (φ_n) be any sequence of positive real numbers. The series $\sum a_n$ is said to be summable $\varphi - |A|_k$, $k \geq 1$, if (see [1])

$$\sum_{n=1}^{\infty} \varphi_n^{k-1} \mid A_n(s) - A_{n-1}(s) \mid^k < \infty.$$

The series $\sum a_n$ is said to be summable $\mid A, p_n, \beta; \delta \mid_k$, $k \geq 1$, $\delta \geq 0$ and β is a real number, if (see [2])

$$\sum_{n=1}^{\infty} \left(\frac{P_n}{p_n} \right)^{\beta(\delta k + k - 1)} \mid A_n(s) - A_{n-1}(s) \mid^k < \infty,$$

where (p_n) is a sequence of positive numbers such that

$$P_n = \sum_{v=0}^{n} p_v \to \infty \quad as \quad n \to \infty, \quad (P_{-k} = p_{-k} = 0, \quad k \geq 1).$$

Let l^k denotes the set of sequence such that $l^k := \left\{ x = (x_j) : \sum |x_j|^k < \infty \right\}$.

Date: July, 8, 2023.
2020 *Mathematics Subject Classification.* 40D25, 40F05; 40G99.
Key words and phrases. Relative strength, Absolute matrix summability, Infinite series.

2. Known Results

Let $A=(a_{nv})$ be a normal matrix, then two lower semimatrices $\bar{A}=(\bar{a}_{nv})$ and $\hat{A}=(\hat{a}_{nv})$ are defined as:

$$\bar{a}_{nv}=\sum_{i=v}^{n}a_{ni},\quad n,v=0,1,...$$

$$\hat{a}_{00}=\bar{a}_{00}=a_{00},\quad \hat{a}_{nv}=\bar{a}_{nv}-\bar{a}_{n-1,v},\quad n=1,2,...$$

and

$$\bar{\Delta}A_n(s)=A_n(s)-A_{n-1}(s)=\sum_{v=0}^{n}\hat{a}_{nv}a_v. \tag{1}$$

If A is a normal matrix, then $A'=(a'_{nv})$ denotes the inverse of A, and $\hat{A}=(\hat{a}_{nv})$ is a normal matrix and it has two-sided inverse $\hat{A}'=(\hat{a}'_{nv})$ which is also normal (see [3]). There are some studies about sufficient or necessary conditions for absolute summability and absolute matrix summability of infinite series, equivalence theorems for summability, the relative strength of absolute summability methods, see [4–24]. Also, the following theorem on the relative strength of $\varphi-|A|_k$ and $\varphi-|B|_k$ methods is known [1].

Theorem 1. *Let $k>1$. Let $A=(a_{nv})$ and $B=(b_{nv})$ be two positive normal matrices. In order that*

$$\varphi-|A|_k\Rightarrow\varphi-|B|_k$$

it is necessary that

$$b_{nn}=O\left(a_{nn}\right). \tag{2}$$

If we suppose that

$$b_{n-1,v}\geq b_{nv}\ for\ n\geq v+1, \tag{3}$$

$$\overline{a}_{n0}=1,\quad \overline{b}_{n0}=1,\quad n=0,1,..., \tag{4}$$

$$a_{vv}-a_{v+1,v}=O(a_{vv}a_{v+1,v+1}), \tag{5}$$

$$\sum_{v=1}^{n-1}\left(b_{vv}\hat{b}_{n,v+1}\right)=O\left(b_{nn}\right), \tag{6}$$

$$\sum_{n=v+1}^{m+1}\left(\varphi_n b_{nn}\right)^{k-1}\hat{b}_{n,v+1}=O\left(\varphi_v^{k-1}b_{vv}^{k-1}\right),$$

$$\sum_{n=v+1}^{m+1}\left(\varphi_n b_{nn}\right)^{k-1}\left|\Delta_v\left(\hat{b}_{nv}\right)\right|=O\left(\varphi_v^{k-1}b_{vv}^{k}\right),$$

$$\sum_{v=r+2}^{n}\hat{b}_{nv}|\hat{a}'_{vr}|=O\left(\hat{b}_{n,r+1}\right), \tag{7}$$

then (2) is also sufficient.

Lemma 1. *[4] Let $k \geq 1$ and $A = (a_{nv})$ be an infinite matrix. In order that $A \in \left(l^k; l^k\right)$ it is necessary that*

$$a_{nv} = O(1) \quad (all \quad n, v) \tag{8}$$

3. Main Result

The object of the present study is to generalize Theorem 1.

Theorem 2. *Let $k > 1$. Let $A = (a_{nv})$ and $B = (b_{nv})$ be two positive normal matrices. In order that*

$$| A, p_n, \beta; \delta |_k \Rightarrow | B, p_n, \beta; \delta |_k \tag{9}$$

the condition (2) is necessary. If we suppose that (3)-(7) and

$$\sum_{n=v+1}^{m+1} \left(\frac{P_n}{p_n}\right)^{\beta(\delta k+k-1)} b_{nn}^{k-1} \hat{b}_{n,v+1} = O\left(\left(\frac{P_v}{p_v}\right)^{\beta(\delta k+k-1)} b_{vv}^{k-1}\right), \tag{10}$$

$$\sum_{n=v+1}^{m+1} \left(\frac{P_n}{p_n}\right)^{\beta(\delta k+k-1)} b_{nn}^{k-1} \left|\Delta_v\left(\hat{b}_{nv}\right)\right| = O\left(\left(\frac{P_v}{p_v}\right)^{\beta(\delta k+k-1)} b_{vv}^{k}\right), \tag{11}$$

then (2) is also sufficient, where $\delta \geq 0$ and $-\beta(\delta k + k - 1) + k > 0$.

Proof of Theorem 2

Necessity. Let (I_n) and (U_n) denote A-transform and B-transform of the series $\sum a_n$, respectively. By (1), we have $\bar{\Delta} I_n = \sum_{v=0}^{n} \hat{a}_{nv} a_v$ and $\bar{\Delta} U_n = \sum_{v=0}^{n} \hat{b}_{nv} a_v$. Then, we write $a_v = \sum_{r=0}^{v} \hat{a}'_{vr} \bar{\Delta} I_r$ and $\bar{\Delta} U_n = \sum_{v=0}^{n} \hat{b}_{nv} \sum_{r=0}^{v} \hat{a}'_{vr} \bar{\Delta} I_r$. Also, using the fact that $\hat{b}_{n0} = \bar{b}_{n0} - \bar{b}_{n-1,0} = 0$, we have

$$\begin{aligned}
\bar{\Delta} U_n &= \sum_{v=1}^{n} \hat{b}_{nv} \sum_{r=0}^{v} \hat{a}'_{vr} \bar{\Delta} I_r \\
&= \sum_{v=1}^{n} \hat{b}_{nv} \hat{a}'_{vv} \bar{\Delta} I_v + \sum_{v=1}^{n} \hat{b}_{nv} \hat{a}'_{v,v-1} \bar{\Delta} I_{v-1} + \sum_{v=1}^{n} \hat{b}_{nv} \sum_{r=0}^{v-2} \hat{a}'_{vr} \bar{\Delta} I_r \\
&= \hat{b}_{nn} \hat{a}'_{nn} \bar{\Delta} I_n + \sum_{v=1}^{n-1} \left(\hat{b}_{nv} \hat{a}'_{vv} + \hat{b}_{n,v+1} \hat{a}'_{v+1,v}\right) \bar{\Delta} I_v + \sum_{r=0}^{n-2} \bar{\Delta} I_r \sum_{v=r+2}^{n} \hat{b}_{nv} \hat{a}'_{vr}
\end{aligned}$$

By using the equality $\sum_{k=v}^{n} \hat{a}'_{nk} \hat{a}_{kv} = \delta_{nv}$ (Kronecker delta), we obtain

$$\begin{aligned}
\hat{b}_{nv} \hat{a}'_{vv} + \hat{b}_{n,v+1} \hat{a}'_{v+1,v} &= \frac{\hat{b}_{nv}}{\hat{a}_{vv}} + \hat{b}_{n,v+1} \left(-\frac{\hat{a}_{v+1,v}}{\hat{a}_{vv} \hat{a}_{v+1,v+1}}\right) \\
&= \frac{\hat{b}_{nv}}{a_{vv}} - \hat{b}_{n,v+1} \frac{(\bar{a}_{v+1,v} - \bar{a}_{vv})}{a_{vv} a_{v+1,v+1}} \\
&= \frac{\hat{b}_{nv}}{a_{vv}} - \hat{b}_{n,v+1} \frac{(a_{v+1,v+1} + a_{v+1,v} - a_{vv})}{a_{vv} a_{v+1,v+1}} \\
&= \frac{\Delta_v(\hat{b}_{nv})}{a_{vv}} + \hat{b}_{n,v+1} \frac{(a_{vv} - a_{v+1,v})}{a_{vv} a_{v+1,v+1}}.
\end{aligned}$$

Thus

$$\begin{aligned}\bar{\Delta}U_n &= \frac{b_{nn}}{a_{nn}}\bar{\Delta}I_n+\sum_{v=1}^{n-1}\frac{\Delta_v(\hat{b}_{nv})}{a_{vv}}\bar{\Delta}I_v+\sum_{v=1}^{n-1}\hat{b}_{n,v+1}\frac{(a_{vv}-a_{v+1,v})}{a_{vv}a_{v+1,v+1}}\bar{\Delta}I_v\\ &+ \sum_{r=0}^{n-2}\bar{\Delta}I_r\sum_{v=r+2}^{n}\hat{b}_{nv}\hat{a}'_{vr}\\ &= U_{n,1}+U_{n,2}+U_{n,3}+U_{n,4}.\end{aligned}$$

Let's write the matrix transforming $\left(\left(\frac{P_n}{p_n}\right)^{\frac{\beta(\delta k+k-1)}{k}}\bar{\Delta}I_n\right)$ into $\left(\left(\frac{P_n}{p_n}\right)^{\frac{\beta(\delta k+k-1)}{k}}\bar{\Delta}U_n\right)$ by (8). The argument (9) is equivalent to the argument that this matrix $\in \left(l^k;l^k\right)$. So, by Lemma 1, in order that $\mid A,p_n,\beta;\delta\mid_k \Rightarrow \mid B,p_n,\beta;\delta\mid_k$, the condition (2) is necessary.

Sufficiency. Let the conditions be satisfied. We will prove that $\mid A,p_n,\beta;\delta\mid_k \Rightarrow \mid B,p_n,\beta;\delta\mid_k$. For the proof, let's show that

$$\sum_{n=1}^{\infty}\left(\frac{P_n}{p_n}\right)^{\beta(\delta k+k-1)}\mid U_{n,r}\mid^k<\infty \quad for \quad r=1,2,3,4.$$

First

$$\sum_{n=1}^{m}\left(\frac{P_n}{p_n}\right)^{\beta(\delta k+k-1)}\mid U_{n,1}\mid^k = \sum_{n=1}^{m}\left(\frac{P_n}{p_n}\right)^{\beta(\delta k+k-1)}\frac{b_{nn}^k}{a_{nn}^k}|\bar{\Delta}I_n|^k.$$

By (2) and using the fact that $\sum a_n$ is summable $\mid A,p_n,\beta;\delta\mid_k$, it follows that

$$\sum_{n=1}^{m}\left(\frac{P_n}{p_n}\right)^{\beta(\delta k+k-1)}\mid U_{n,1}\mid^k = O(1)\sum_{n=1}^{m}\left(\frac{P_n}{p_n}\right)^{\beta(\delta k+k-1)}|\bar{\Delta}I_n|^k=O(1) \quad as \quad m\to\infty.$$

Now, we get

$$\begin{aligned}\sum_{n=2}^{m+1}\left(\frac{P_n}{p_n}\right)^{\beta(\delta k+k-1)}\mid U_{n,2}\mid^k &\le \sum_{n=2}^{m+1}\left(\frac{P_n}{p_n}\right)^{\beta(\delta k+k-1)}\sum_{v=1}^{n-1}\frac{|\Delta_v(\hat{b}_{nv})|}{a_{vv}^k}\left|\bar{\Delta}I_v\right|^k\\ &\times \left(\sum_{v=1}^{n-1}|\Delta_v(\hat{b}_{nv})|\right)^{k-1}\end{aligned}$$

by Hölder's inequality. Then, we obtain

$$\begin{aligned}\sum_{n=2}^{m+1}\left(\frac{P_n}{p_n}\right)^{\beta(\delta k+k-1)}\mid U_{n,2}\mid^k &\le \sum_{n=2}^{m+1}\left(\frac{P_n}{p_n}\right)^{\beta(\delta k+k-1)}b_{nn}^{k-1}\sum_{v=1}^{n-1}\frac{|\Delta_v(\hat{b}_{nv})|}{a_{vv}^k}\left|\bar{\Delta}I_v\right|^k\\ &\le \sum_{v=1}^{m}\frac{\left|\bar{\Delta}I_v\right|^k}{a_{vv}^k}\sum_{n=v+1}^{m+1}\left(\frac{P_n}{p_n}\right)^{\beta(\delta k+k-1)}b_{nn}^{k-1}|\Delta_v(\hat{b}_{nv})|\\ &= O(1)\sum_{v=1}^{m}\left(\frac{P_v}{p_v}\right)^{\beta(\delta k+k-1)}|\bar{\Delta}I_v|^k=O(1) \quad as \quad m\to\infty\end{aligned}$$

by (11) and (2).

By using (5), the Hölder's inequality, and the conditions (6), (10), we obtain

$$\begin{aligned}
\sum_{n=2}^{m+1}\left(\frac{P_n}{p_n}\right)^{\beta(\delta k+k-1)} |\, U_{n,3}\,|^k &= \sum_{n=2}^{m+1}\left(\frac{P_n}{p_n}\right)^{\beta(\delta k+k-1)}\left|\sum_{v=1}^{n-1}\hat{b}_{n,v+1}\frac{(a_{vv}-a_{v+1,v})}{a_{vv}a_{v+1,v+1}}\bar{\Delta}I_v\right|^k \\
&= O(1)\sum_{n=2}^{m+1}\left(\frac{P_n}{p_n}\right)^{\beta(\delta k+k-1)}\left(\sum_{v=1}^{n-1}\hat{b}_{n,v+1}\left|\bar{\Delta}I_v\right|\right)^k \\
&= O(1)\sum_{n=2}^{m+1}\left(\frac{P_n}{p_n}\right)^{\beta(\delta k+k-1)}\sum_{v=1}^{n-1}\hat{b}_{n,v+1}\frac{b_{vv}}{b_{vv}^k}\left|\bar{\Delta}I_v\right|^k \\
&\times \left(\sum_{v=1}^{n-1}\hat{b}_{n,v+1}b_{vv}\right)^{k-1} \\
&= O(1)\sum_{n=2}^{m+1}\left(\frac{P_n}{p_n}\right)^{\beta(\delta k+k-1)} b_{nn}^{k-1}\sum_{v=1}^{n-1}\hat{b}_{n,v+1}\left|\bar{\Delta}I_v\right|^k\frac{1}{b_{vv}^{k-1}} \\
&= O(1)\sum_{v=1}^{m}\frac{1}{b_{vv}^{k-1}}\left|\bar{\Delta}I_v\right|^k\sum_{n=v+1}^{m+1}\left(\frac{P_n}{p_n}\right)^{\beta(\delta k+k-1)} b_{nn}^{k-1}\hat{b}_{n,v+1} \\
&= O(1)\sum_{v=1}^{m}\left(\frac{P_v}{p_v}\right)^{\beta(\delta k+k-1)}|\bar{\Delta}I_v|^k = O(1)\quad as\quad m\to\infty.
\end{aligned}$$

Lastly, the condition (7) follows that

$$\begin{aligned}
\sum_{n=2}^{m+1}\left(\frac{P_n}{p_n}\right)^{\beta(\delta k+k-1)} |\, U_{n,4}\,|^k &= O(1)\sum_{n=2}^{m+1}\left(\frac{P_n}{p_n}\right)^{\beta(\delta k+k-1)}\left(\sum_{r=0}^{n-2}\left|\bar{\Delta}I_r\right|\hat{b}_{n,r+1}\right)^k \\
&= O(1)\quad as\quad m\to\infty,
\end{aligned}$$

as in $U_{n,3}$. This completes the proof of Theorem 2.

References

[1] H.S. Özarslan, T. Kandefer, On the relative strength of two absolute summability methods, J. Comput. Anal. Appl., 11(3), 576-583, (2009).

[2] H.S. Özarslan, A. Karakaş, A new study on absolute summability factors of infinite series, Maejo Int. J. Sci. Technol., 13(3), 257-265, (2019).

[3] R.G. Cooke, Infinite Matrices and Sequence Spaces. Macmillan & Co. Limited, London, 1950.

[4] H. Bor, On the relative strength of two absolute summability methods, Proc. Amer. Math. Soc., 113(4), 1009-1012, (1991).

[5] H. Bor, H.M. Srivastava, W.T. Sulaiman, A new application of certain generalized power increasing sequences, Filomat, 26(4), 871-879, (2012).

[6] H. Bor, R.P. Agarwal, A new application of almost increasing sequences to factored infinite series, Anal. Math. Phys., 10(3), Paper No. 26, 7 pp. (2020).

[7] H. Bor, R.N. Mohapatra, An application of a wider class of increasing sequences, Trans. A. Razmadze Math. Inst., 175(3), 327-330, (2021).

[8] A. Karakaş, On absolute matrix summability factors of infinite series, J. Class. Anal., 13(2), 133-139, (2018).

[9] B. Kartal, New results for almost increasing sequences, Ann. Univ. Paedagog. Crac. Stud. Math., 18, 85-91, (2019).

[10] B. Kartal, An extension of a theorem on Cesàro summability, Numer. Funct. Anal. Optim., 42(4), 474–479, (2021).

[11] B. Kartal, Cesàro summability involving δ-quasi-monotone and almost increasing sequences, J. New Theory, 41, 94-99 (2022).
[12] B. Kartal, On necessary and sufficient conditions for absolute matrix summability, Earthline J. Math. Sci., 12(1), 1-12, (2023).
[13] H.S. Özarslan, H.N. Özgen, Necessary conditions for absolute matrix summability methods, Boll. Unione Mat. Ital., 8(3), 223-228, (2015).
[14] H.S. Özarslan, B. Kartal, A generalization of a theorem of Bor, J. Inequal. Appl., 179, 8pp., (2017).
[15] H.S. Özarslan, A new factor theorem for absolute matrix summability, Quaest. Math., 42(6), 803-809, (2019).
[16] H.S. Özarslan, B. Kartal, Absolute matrix summability via almost increasing sequence, Quaest. Math., 43(10), 1477-1485, (2020).
[17] H.S. Özarslan, Generalized almost increasing sequences, Lobachevskii J. Math., 42(1), 167-172, (2021).
[18] H.S. Özarslan, Absolute Cesàro summability via quasi-power increasing sequences, Asian-Eur. J. Math., 16(3), 1-6, (2023).
[19] H.S. Özarslan, A new theorem on generalized absolute matrix summability, Azerb. J. Math., 13(1), 3-13, (2023).
[20] H.S. Özarslan, M.Ö. Şakar, B. Kartal, Applications of quasi power increasing sequences to infinite series, J. Appl. Math. & Informatics, 41(1), 1-9, (2023).
[21] H.N. Özgen, On two absolute matrix summability methods, Boll. Unione Mat. Ital., 9(3), 391-397, (2016).
[22] S.A. Sezer, İ. Çanak, Conditions for the equivalence of power series and discrete power series methods of summability, Filomat, 29(10), 2275-2280, (2015).
[23] S. Sonker, A. Munjal, Absolute $\varphi - |C, \alpha, \beta; \delta|_k$ summability of infinite series, J. Inequal. Appl., Paper No. 168, 7 pp., (2017).
[24] S. Sonker, A. Munjal, Sufficient conditions for infinite series by absolute φ-product summable factor, Tbilisi Math. J., 12(4), 29-41, (2019).

(Hikmet Seyhan ÖZARSLAN) Department of Mathematics, Erciyes University, 38039 Kayseri, Turkey
Email address: seyhan@erciyes.edu.tr

(Bağdagül KARTAL) Department of Mathematics, Erciyes University, 38039 Kayseri, Turkey
Email address: bagdagulkartal@erciyes.edu.tr

IFSCOM-E 2023
9th Ifs And Contemporary Mathematics and Engineering Conference
08-11 July 2023 Tarsus, Mersin, Türkiye
ISBN: 978-605-68670-8-8
pp: 15-20

ON INFRA FUZZY-SOFT TOPOLOGICAL SPACES

A. ATAY

0000-0002-3373-8699

Abstract. It is always interesting to obtain structures that retain some topological properties but have a weaker condition. In this study, we will introduce a topological structure that is not closed under arbitrary combination and is a subfamily of the family of fuzzy soft sets. Firstly we will give definitions of this subfamily. The basic properties of this space, which we will call infra-fuzzy soft topological spaces, will be investigated. We will show that the union of infra fuzzy-soft topological spaces is not a infra fuzzy-soft topological space. In the upcoming work we will examine the equivalents of some topological concepts in infra-fuzzy-soft topological spaces.

1. Introduction

In 1999, Molodtsov [1] introduced a new mathematical tool for handling vagueness, known as soft sets. He explored its connection with fuzzy sets and demonstrated its applications in various domains. Since then, numerous scholars and researchers have investigated the utility of soft sets in different areas, including decision-making problems [2], computer science [3], and medical science [4]. In 2003, Maji et al. [5] initiated a study on the fundamental concepts and principles of soft set theory. They delved into various operations such as intersection and union operators, the difference between two soft sets, and the complement of a soft set.

The necessity to address problems that cannot be adequately expressed using classical logic, coupled with advancements in scientific knowledge, has prompted mathematicians to develop new mathematical models and tools. In response to this demand, various theories have been introduced in the field of mathematics. One such theory is fuzzy set theory, proposed by Zadeh in 1965 [6]. Both fuzzy set and soft set theories have found widespread applications in expert systems, decision-making, modeling, social sciences, medical diagnostics, and other domains. These theories have also been utilized in the identification and analysis of COVID-19 patients, which has been a topic of great global interest. The field of mathematics has seen numerous studies focusing on soft set and fuzzy set theories, attracting

Date: July, 8, 2023.
Key words and phrases. Fuzzy soft set, Infra topology, Fuzzy soft topology.

the attention of researchers. Building upon fuzzy set theory, Chang provided a definition of fuzzy topology in 1968 [7]. Subsequently, Lowen introduced a more natural definition of fuzzy topology in 1976, distinct from Chang's definition [8]. Since Chang's pioneering work, several topological concepts have been adapted to a fuzzy setting.
In 2001, Maji et al. [9] merged fuzzy set and soft set theories and proposed the concept of a fuzzy soft set. Recent research has shown that a significant portion of studies in this field focuses on fuzzy soft topological spaces. To further explore fuzzy soft sets, Ahmad and Kharal [10] presented additional properties of fuzzy soft sets and introduced the notion of mappings on fuzzy soft sets. In 2011, Tanay et al. [11] established the topological structure of fuzzy soft sets. Subsequently, in 2012, Varol and Aygün [12] introduced fuzzy soft topology, while Şimşekler and Yüksel [13] introduced fuzzy soft topological spaces in 2013.
Soft topology has been extended to various structures, and one notable extension is infra soft topology [14]. The continuous investigation of infra soft topological structures is motivated by the fact that many topological properties are preserved within the framework of infra soft topologies. Furthermore, infra soft topologies allow for easy construction of examples that demonstrate the relationships among different topological concepts. This investigation has been carried out for concepts such as infra soft compactness and infra soft connectedness [15, 16]. In [17], they introduce the concept of infra soft topological spaces. Also the concept of a infra fuzzy topological spaces has been studied by Zanyar A. Ameen et al [18].
In this paper, we introduce the concept of infra fuzzy-soft topological spaces and delve into the main properties of infra fuzzy-soft topology. We will also show with an example that the union of infra-fuzzy-soft topological spaces may not be an infra-fuzzy-soft topology.

2. Preliminaries

In this section, we will review the necessary technical concepts used in this paper. Firstly, During this work, $Y \neq \emptyset$ will be an initial universal set, $J = [0,1] \subset \mathbb{R}$ and $P \neq \emptyset$ is the set of all possible parameters of Y. we use the notation 2^Y to represent the power set of Y, which denotes the set of all subsets of Y.

Definition 2.1. For $\emptyset \neq K \subseteq P$ and the mapping $\beta : K \longrightarrow 2^Y$, a pair $(\beta, K) = \left\{\beta(p) : p \in K \subseteq P, \beta : K \longrightarrow 2^Y\right\}$ is named a soft set on Y. $SS(Y)_K$ is a family of all these soft sets [1].

Definition 2.2. Let $B \subseteq Y$ and $G_B(y) : Y \to J$ be a mapping. Then

$$\tilde{B} = \{(y, G_B(y)) : y \in Y\}$$

defined as a fuzzy set in Y and $G_B(y)$ defined as a degree of membership of $y \in B$. A fuzzy set defined as

$$\tilde{C} = \{(y, G_C(y)) : G_C(y) = \alpha, \alpha \in [0,1], y \in C \subseteq Y\}$$

is called a fixed fuzzy set. Also for $\forall y \in Y$ fuzzy empty set and fuzzy universal set are defined as respectively,

$$0_Y : Y \to J, y \to 0_y(y) = 0, 1_Y : Y \to J, y \to 1_y(y) = 1$$

. For $B \subseteq Y$ the fuzzy sets, with membership function G_B, will be briefly denoted by G_B.The family of all fuzzy sets in Y is indicated by J^Y [6].

Definition 2.3. Let $K \subset P$. f_K is defined to be a fuzzy soft set on (Y, P) if $f : K \to J^Y$ is a mapping defined by $f(p) = \mu_f^p$ such that

$$f(p) = \begin{cases} \mu_f^p = \overline{0}, & p \in P - K \\ \mu_f^p \neq \overline{0}, & p \in K \end{cases}$$

where $\overline{0}(y) = 0$ for each $y \in Y$ [9].

Definition 2.4. The complement of a fuzzy soft set f_K is a fuzzy soft set on (Y, P), which is denoted by f_K^c, and $f^c : K \to J^Y$ is defined as follows:

$$f^c = \begin{cases} \mu_{f^c}^k = 1 - \mu_f^k, & k \in K \\ \mu_{f^c}^k = \overline{1}, & k \in P - K \end{cases}$$

where $\overline{1}(y) = 1$ for each $y \in Y$ [9].

Definition 2.5. The fuzzy soft set f_K is called the null fuzzy soft set if $f_K(p) = 0$ for each $p \in P$ and denoted by $\tilde{0}_P$. The fuzzy soft set f_K is called the universal fuzzy soft set if $f_K(p) = 1$ for each $p \in P$ and denoted by $\tilde{1}_P$ [9].

Clearly, $(\tilde{1}_P)^c = \tilde{0}_P$, and $(\tilde{0}_P)^c = \tilde{1}_P$.

From now on, we will use $\mathcal{F}(Y, P)$ instead of the family of all fuzzy soft sets over Y.

Definition 2.6. Let f_{K_1}, g_{K_2} be two fuzzy soft sets on $\mathcal{F}(Y, P)$ and $K_1 \subseteq K_2 \subset Y$. Then, f_{K_1} is called a fuzzy soft subset of g_{K_2}, denoted by $f_{K_1} \sqsubseteq g_{K_2}$, if $f_{K_1}(p) \leq g_{K_2}(p)$ for every $p \in P$. If g_{K_2} is a fuzzy soft subset of f_{K_2}, then f_{K_1} is called a fuzzy soft superset of g_{K_2} and denoted by $f_{K_1} \sqsupseteq g_{K_2}$ [9].

Definition 2.7. Let $f_{K_1}, g_{K_2} \in \mathcal{F}(Y, P)$. If $f_{K_1} \sqsubseteq g_{K_2}$ and $g_{K_2} \sqsubseteq f_{K_1}$, then f_{K_1} and g_{K_2} are said to be equal and denoted by $f_{K_1} = g_{K_2}$ [9].

Definition 2.8. Let f_{K_1}, g_{K_2} and h_{K_3} be fuzzy soft sets. For $f_{K_1} \sqcup g_{K_2} = h_{K_3}$, we say that h_{K_3} is the union of f_{K_1} and g_{K_2}, whose membership function $\mu_{h_{K_3}}^p(y) = \max\left\{\mu_{f_{K_1}}^p(y), \mu_{g_{K_2}}^p(y)\right\}$ for every $y \in Y$ [9].

Definition 2.9. Let f_{K_1}, g_{K_2} and h_{K_3} be fuzzy soft sets. For $f_{K_1} \sqcap g_{K_2} = h_{K_3}$, we say that h_{K_3} is the intersection of f_{K_1} and g_{K_2}, whose membership function $\mu_{h_{K_3}}^p(y) = \min\left\{\mu_{f_{K_1}}^p(y), \mu_{g_{K_2}}^p(y)\right\}$ for every $y \in Y$ [9].

Theorem 2.10. *Let f_{K_1}, g_{K_2} be two fuzzy soft sets on (Y, P). Then, the following holds [10]:*

(1) $f_{K_1}^c \sqcap g_{K_2}^c = (f_{K_1} \sqcup g_{K_2})^c$;
(2) $f_{K_1}^c \sqcup g_{K_2}^c = (f_{K_1} \sqcap g_{K_2})^c$.

Theorem 2.11. *Let I be an index set, $j \in I$ and $(f_{K_1})_j$ be a family of fuzzy soft sets on (Y, P). Then, the following holds [10]:*

(1) $\sqcap_j((f_{K_1})_j^c) = (\sqcup_j((f_{K_1})_j))^c$;
(2) $\sqcup_j((f_{K_1})_j^c) = (\sqcap_j((f_{K_1})_j))^c$.

Theorem 2.12. *Let I be an index set, $j \in I$ and $f_{K_1}, g_{K_2}, h_{K_3}, (g_L)_j \in \mathcal{F}(Y,P), \forall j \in J$; then, the following holds [11]:*

(1) $f_{K_1} \sqcap f_{K_1} = f_{K_1}, f_{K_1} \sqcup f_{K_1} = f_{K_1}$.
(2) $f_{K_1} \sqcap g_{K_2} = g_{K_2} \sqcap f_{K_1}, f_{K_1} \sqcup g_{K_2} = g_{K_2} \sqcup f_{K_1}$.
(3) $f_{K_1} \sqcap (g_{K_2} \sqcap h_{K_3}) = (f_{K_1} \sqcap g_{K_2}) \sqcap h_{K_3}, f_{K_1} \sqcup (g_{K_2} \sqcup h_{K_3}) = (f_{K_1} \sqcup g_{K_2}) \sqcup h_{K_3}$.
(4) $f_{K_1} \sqcap (\bigsqcup_{j\in I}(g_L)_j) = \bigsqcup_{j\in I}(f_{K_1} \sqcap (g_L)_j), f_{K_1} \sqcup (\sqcap_{j\in I}(g_L)_j) = \sqcap_{j\in I}(f_{K_1} \sqcup (g_L)_j)$.
(5) *If* $f_{K_1} \sqsubseteq g_{K_2}$, *then* $(g_{K_2})^c \sqsubseteq (f_{K_1})^c$.
(6) $f_{K_1} \sqcap g_{K_2} \sqsubseteq f_{K_1}, g_{K_2}$ *and* $f_{K_1}, g_{K_2} \sqsubseteq f_{K_1} \sqcup g_{K_2}$.

Definition 2.13. A fuzzy soft topological space is a pair $(Y, \mathcal{T})$ where Y is a nonempty set and $\mathcal{T}$ a family of fuzzy soft sets over Y satisfying the following properties:

(1) $\tilde{0}_P, \tilde{1}_P \in \mathcal{T}$,
(2) If $f_{K_1}, g_{K_2} \in \mathcal{T}$, then $f_{K_1} \sqcap g_{K_2} \in \mathcal{T}$,
(3) If $(f_L)_j \in \mathcal{T}, \forall j \in I$, then $\bigsqcup_{j\in I}(f_L)_j \in \mathcal{T}$.

$\mathcal{T}$ is called a topology of fuzzy soft sets on Y. Every member of $\mathcal{T}$ is called fuzzy soft open. If $(g_K)^c \in \mathcal{T}$, then g_K is called fuzzy soft closed in $(Y, \mathcal{T})$ [11].

Example

Let $P = \{p_1, p_2, p_3\}$, $Y = \{a, b, c\}$. Then $\mathcal{T} = \{\tilde{0}_P, \tilde{1}_P\}$ is a s a fuzzy soft indiscrete topology and $(Y, \mathcal{F}(Y,P)$ is a fuzzy soft discrete topological space. Also for the fuzzy soft sets $f_{K_1} = \{(p_1, \{0.9/a, 0.5/b\}), (p_2, \{0.2/a, 0.7/c\}), (p_3, Y)\}$ and $g_{K_2} = \{(p_1, \{0.3/a, 0.1/b\}), (p_3, \{0.5/a, 0.9/b, 0.7/c\})\}$ the family $\{\tilde{0}_P, \tilde{1}_P, f_{K_1}, g_{K_2}\}$ is a fuzzy soft topology on Y.

3. Infra Fuzzy-Soft Topological Spaces

In this section, we introduce the concept of infra fuzzy-soft topology and discuss various methods for constructing this concept. We explore the basis of infra fuzzy-soft topology, infra fuzzy-soft neighborhood systems, and infra fuzzy-soft interior. We present these concepts and techniques to provide a comprehensive understanding of infra fuzzy-soft topology.

To illustrate the obtained results and the relationships between different concepts, we provide several examples. These examples serve to clarify the application and significance of infra fuzzy-soft topology in practical scenarios.

Definition 3.1. A subcollection $\mathcal{T}$ of $\mathcal{F}(Y,P)$ is said to be an infra fuzzy-soft topology on Y if

(1) $\tilde{0}_P, \tilde{1}_P \in \mathcal{T}$,
(2) $f_{K_1} \sqcap g_{K_2} \in \mathcal{T}$ whenever $f_{K_1}, g_{K_2} \in \mathcal{T}$.

The pair $(Y, \mathcal{T})$ is called an infra fuzzy-soft topological space, and the set of all infra fuzzy-soft topologies on Y is denoted by IFST(Y). The members of $\mathcal{T}$ are called infra fuzzy-soft open (or IFS-open) subsets of Y, and their complements are called infra fuzzy-soft closed (or IFS-closed) sets. The members of $\mathcal{T}^c$ are also called IFS-closed sets.

Remark 3.2. Evidently, each fuzzy-soft topology is an infra fuzzy-soft topology, but not conversely.

Lemma 3.3. *Let $\{\mathcal{T}_\lambda : \lambda \in \Lambda\}$ be a subclass of IFST(Y), where Λ is any index set. Then, $\{\mathcal{T} = \sqcap_{\lambda\in\Lambda}\mathcal{T}_\lambda \in$ IFST(Y).*

Proof. Straightforward. □

Lemma 3.4. *Let $\mathcal{U}$ be a subclass of $\mathcal{F}(Y, P)$. There exists a unique $\mathcal{T} \in$ IFST(Y) containing $\mathcal{U}$, and if $\mathcal{T}' \in$ IFST(Y) that includes $\mathcal{U}$, then $\mathcal{T} \sqsubseteq \mathcal{T}'$.*

Proof. Note that such an infra fuzzy-soft topology always exists because $\mathcal{F}(Y, P)$ is the infra fuzzy-soft topology on Y which includes $\mathcal{U}$. Consider $\mathcal{T}$, the intersection of all those infra fuzzy-soft topologies on Y which include $\mathcal{T}$. Then, it follows from Lemma 3.3 that $\mathcal{T}$ is the required infra fuzzy-soft topology. □

Definition 3.5. Let $\mathcal{U}$ be a subclass of $\mathcal{F}(Y, P)$. The unique $\mathcal{T} \in$ IFST(Y) obtained in the above lemma is called the infra fuzzy-soft topology on Y generated by the collection $\mathcal{U}$ and is denoted by $\mathcal{T}(\mathcal{U})$, which is the smallest infra fuzzy-soft topology on Y containing $\mathcal{U}$.

If $\mathcal{T}_1, \mathcal{T}_2 \in$ IFST(Y), then $\mathcal{T}_1 \sqcup \mathcal{T}_2 \in$ IFST(Y) is false in general.

Example

Let $P = \{p_1, p_2, p_3\}$, $Y = \{a, b, c\}$. F or the fuzzy soft sets
$f_{K_1} = \{(p_1, \{0.8/a, 0.5/b\}), (p_2, \{0.1/a, 0.5/c\}), (p_3, \{0.4/a, 0.2/c\})\}$,
$g_{K_2} = \{(p_1, \{0.2/a, 0.7/b\}), (p_3, \{0.9/b, 0.6/c\})\}$ and
$h_{K_3} = \{(p_1, \{0.2/a, 0.5/b\}), (p_3, \{0.2/c\})\}$
the families $\mathcal{T}_1 = \{\tilde{0}_P, \tilde{1}_P, f_{K_1}\}$ and $\mathcal{T}_2 = \{\tilde{0}_P, \tilde{1}_P, g_{K_2}\}$ are fuzzy soft topology on Y. But $\mathcal{T}_1 \sqcup \mathcal{T}_2$ is not. Becasuse $f_{K_1} \sqcap g_{K_2} = h_{K_3}$ and $h_{K_3} \notin \mathcal{T}_1 \sqcup \mathcal{T}_2 = \{\tilde{0}_P, \tilde{1}_P, f_{K_1}, g_{K_2}\}$.

4. CONCLUSION

In this study, we introduced and exemplified a new structure, infra-fuzzy-soft topological space, and talked about some results. In our future studies, as a continuation of this study, the results to be obtained by introducing the base, neighborhood, interior, exterior, boundary and similar topological concepts on infra-fuzzy-soft topological space will be included.

References

[1] D. Molodtsov, "Soft set theory–first results," Computers & Mathematics with Applications, vol. 37, no. 4-5, pp. 19–31, (1999).
DOI:10.1016/S0898-1221(99)00056-5

[2] J. Yang and Y. Yao, "Semantics of soft sets and three-way decision with soft sets," Knowledge-Based Systems, vol. 194, article 105538, (2020).
DOI: 10.1016/j.knosys.2020.105538

[3] N. Çağman and S. Enginoğlu, "Soft matrix theory and its decision making," Computers and Mathematics with Applications, vol. 59, no. 10, pp. 3308–3314, (2010).
DOI:10.1016/j.camwa.2010.03.015

[4] M. K. El-Bably and A. A. El Atik, "Softβ-rough sets and their application to determine COVID-19," Turkish Journal of Mathematics, vol. 45, no. 3, pp. 1133–1148, (2021).
DOI: 10.3906/mat-2008-93

[5] P. K. Maji, R. Biswas, and R. Roy, "Soft set theory," Computers & Mathematics with Applications, vol. 45, no. 4-5, pp. 555– 562, (2003).
DOI:10.1016/S0898-1221(03)00016-6

[6] L. A. Zadeh, Fuzzy sets, Inform. Control, vol. 8, pp. 338-353, (1965).
DOI:10.1016/S0019-9958(65)90241-X

[7] C. L. Chang, Fuzzy topological spaces, J. Math. Appl., vol. 24, pp. 182-193, (1968).
DOI:10.1016/0022-247X(68)90057-7

[8] R. Lowen, Fuzzy topological spaces and fuzzy compactness, J. Math. Anal. Appl., vol. 56, pp. 621-633, (1976).
DOI:10.1016/0022-247X(76)90029-9
[9] P. K. Maji, R. Biswas, A. R. Roy, Fuzzy soft sets, J. Fuzzy Math., vol. 9, pp. 589-602, (2001).
[10] B. Ahmat, A. Kharal, On fuzzy soft sets, Adv. Fuzzy Syst., vol. 2009, pp. 586507, (2009).
DOI:10.1155/2009/586507
[11] B. Tanay, M. B. Kandemir, Topological structures of fuzzy soft sets, Comput. Math. Appl., vol. 61, pp. 412-418, (2011).
DOI:10.1016/j.camwa.2011.03.056
[12] B. P. Varol, H. Aygün, Fuzzy soft topology, Hacettepe J. Math. Stat., vol. 41, pp. 407-419, (2012).
[13] T. Şimşekler, S. Yüksel, Fuzzy soft topological spaces, Ann. Fuzzy Math. Inform., vol. 5, pp. 87-96, (2013).
[14] T. M. Al-shami, "New soft structure: infra soft topological spaces," Mathematical Problems in Engineering, vol. 2021, Article ID 3361604, 12 pages, (2021).
[15] T. M. Al-shami, "Infra soft compact spaces and application to fixed point theorem," Journal of Function Spaces, vol. 2021, Article ID 3417096, 9 pages, (2021).
[16] T. M. Al-shami and E. A. Abo-Tabl, "Connectedness and local connectedness on infra soft topological spaces," Mathematics, vol. 9, no. 15, (2021).
[17] T. M. Al-shami, "New Soft Structure: Infra Soft Topological Spaces", Mathematical Problems in Engineering, vol. 2021, 12 pages, (2021).
DOI: 10.1155/2021/3361604
[18] Zanyar A. Ameen, T. M. Al-shami, A. A. Azzam and Abdelwaheb Mhemdi, "A Novel Fuzzy Structure: Infra-Fuzzy Topological Spaces", Journal of Function Spaces, vol. 2022, 11 pages, (2022).
DOI:10.1155/2022/9778069

(A. Atay) Dicle university, Mathematics department, 21280, Diyarbakir, Türkiye
Email address, A. Atay: arifea@dicle.edu.tr

IFSCOM-E 2023
9th Ifs And Contemporary Mathematics and Engineering Conference
08-11 July 2023 Tarsus, Mersin, Türkiye
ISBN: 978-605-68670-8-8
pp: 21-32

AN ALMOST UNBIASED RIDGE ESTIMATOR IN BETA REGRESSION

Y.ASAR

0000-0003-1109-8456

Abstract. In this paper we introduced an almost unbiased beta ridge estimator to overcome the problem of multicollinearity in the beta regression model. The proposed estimator is based on the well-known ridge estimator and its extension to the beta regression model. Although, the beta ridge estimator is useful in the presence of ill–conditioned data matrices, it has large bias. Thus, it is reasonable to propose an almost unbiased ridge type estimator in beta regression. An extensive Monte Carlo simulation study is performed to compare the performance of the proposed almost unbiased beta ridge estimator to beta ridge estimator and the maximum likelihood estimator. According to the results of the simulation study, almost unbiased beta ridge estimator has lower mean squared error and squared bias values for certain scenarios.

1. Introduction

The dependent variable may be restricted to the interval of $(0, 1)$ in many empirical contexts, such as rates and proportions. For these situations, a beta regression model was proposed based on the assumption that the dependent variable is distributed as beta distribution in [1].

The parameters of beta regression model are generally estimated by the maximum likelihood method. However, the maximum likelihood estimator (MLE) may perform poorly in the presence of ill-conditioned data matrices, as it is the situation in generalized linear models. This problem is called multicollinearity.

A number of methods are introduced to overcome this problem in the beta regression models. For example, the well-known ridge estimator [2] is extended to beta regression model in [3] and [4]. Ogundimu and Collins [3] used the penalized maximum likelihood approach while Qasim et al. [4] used a Lagrange multiplier method to define the beta ridge estimator (RE) in beta regression model.

It has been shown that ridge estimator has large bias when the biasing parameter is chosen as a large real value. Therefore, a bias adjusted version of beta ridge

Date: July, 8, 2023.
2000 *Mathematics Subject Classification.* 62J02; 62J07.
Key words and phrases. Beta regression, Ridge estimator, Almost unbiased, Maximum likelihood method, Multicollinearity.

estimator is proposed to reduce the bias and overcome the multicollinearity at the same time. Thus, the purpose of this study is to introduce a bias adjusted beta ridge estimator which can also be named as almost unbiased beta ridge estimator in the beta regression model.

The plan of the paper is as follows: In Section 2, a brief introduction of beta regression is given. In Section 3, an almost unbiased beta ridge estimator (AURE) is proposed, and its theoretical properties are studied. In Section 4, an extensive Monte Carlo simulation experiment is designed to compare the performances of MLE, RE and AURE for different scenarios. Finally, a conclusion is provided in Section 5.

2. Beta Regression Model

Assume that $\mathbf{y} = [y_1, y_2, \ldots, y_n]'$ be the vector of observations of the response variable following independent beta distribution with the following probability distribution function

$$f(y_i;\mu,\phi) = \frac{\Gamma(\phi)}{\Gamma(\mu\phi)\Gamma(\phi(1-\mu))} y^{\mu\phi-1}(1-y)^{(1-\mu)\phi-1},\ y \in (0,1), \tag{2.1}$$

where $0 < \mu < 1$ and $\phi > 0$ such that $y_i \sim Beta\,(\mu\phi, (1-\mu)\phi)$. Therefore, the mean and variance of each observation becomes, respectively, $E(y_i) = \mu$ and $Var(y_i) = V(\mu)/(1+\phi)$ where $V(\mu) = \mu(1-\mu)$.

The beta regression model is expressed by assuming that the mean of y_i can be written as

$$g(\mu_i) = \sum_{j=1}^{p} x_{ij}\beta_j = \mathbf{x}_i^\top \boldsymbol{\beta} = \eta_i \tag{2.2}$$

where $\mathbf{x}_i^\top$ is the ith observation vector such that $\mathbf{X} = \left[\mathbf{x}_1^\top, \mathbf{x}_2^\top, \ldots, \mathbf{x}_n^\top\right]$ which is the data matrix of explanatory variables of order $n \times p$, $\boldsymbol{\beta} = [\beta_1, \beta_2, \ldots, \beta_p]^\top$ is a $p \times 1$ vector of regression parameters. In Equation (2.2), the link function $g(.)$ is assumed to be strictly monotone and twice differentiable function from the interval $(0,1)$ to $\mathbb{R}^p$.

The logit link function is defined as $g(\mu) = \log(\mu/(1-\mu)$ such that

$$\mu_i = \frac{\exp(\mathbf{x}_i^\top \boldsymbol{\beta})}{1+\exp(\mathbf{x}_i'\boldsymbol{\beta})} \tag{2.3}$$

for $i = 1, 2, \ldots, n$. Therefore, the corresponding log-likelihood function of the beta regression model given in (2.2) can be written as

$$\begin{aligned} l(\boldsymbol{\beta}) = \sum_{i=1}^{n} &\log(\Gamma(\phi)) - \log(\Gamma(\mu_i\phi)) - \log(\Gamma((1-\mu_i)\phi)) + (\phi\mu_i - 1)\log(y_i) \\ &+ ((1-\mu_i)\phi - 1)\log(1-y_i). \end{aligned} \tag{2.4}$$

In order to estimate the regression parameters, an iterative algorithm must be utilized due to the nonlinearity of the log-likelihood function. Therefore, following [5], Fisher's scoring algorithm is considered for estimation of $\boldsymbol{\beta}$, assuming that ϕ is fixed. The score function can be found by taking the partial derivative of the log-likelihood function with respect to $\boldsymbol{\beta}$ as follows:

$$U_{\boldsymbol{\beta}}(\boldsymbol{\beta}) = \phi \mathbf{X}^\top \mathbf{T}(\mathbf{y}^* - \boldsymbol{\mu}^*) \tag{2.5}$$

where $\mathbf{T} = diag\{1/g'(\mu_1), \ldots, 1/g'(\mu_n)\}$, $\mathbf{y}^* = (y_1^*, \ldots, y_n^*)'$, $\boldsymbol{\mu}^* = (\mu_1^*, \ldots, \mu_n^*)'$ such that $y_i^* = \log(y_i/(1-y_i))$ and $\mu_i^* = \psi(\mu_i\phi) - \psi((1-\mu_i)\phi)$, here $\psi(.)$ denotes the digamma function.

The Fisher's information matrix for $\boldsymbol{\beta}$ is

$$\mathbf{K}_{\boldsymbol{\beta}\boldsymbol{\beta}} = \phi \mathbf{X}^\top \mathbf{W} \mathbf{X} \tag{2.6}$$

where $\mathbf{W}$ is a diagonal matrix whose diagonal elements are

$$w_i = \phi \left(\psi'(\mu_i\phi) + \psi'((1-\mu_i)\phi)\right) \frac{1}{[g'(\mu_i)]^2}$$

where $\psi'(.)$ denotes the trigamma function. A detailed discussion of the derivations of the score functions and Fisher's information matrix is given in the appendix of [1]. Under the assumption that ϕ is known, the Fisher's scoring procedure can be expressed as

$$\boldsymbol{\beta}^{(m+1)} = \boldsymbol{\beta}^{(m)} + \left(\mathbf{K}_{\boldsymbol{\beta}\boldsymbol{\beta}}^{(m)}\right)^{-1} U_{\boldsymbol{\beta}}(\boldsymbol{\beta})^{(m)} \tag{2.7}$$

where m shows the iterations which continues until some convergence criterion is reached. By inserting the score function and Fisher's information for $\boldsymbol{\beta}$ as specified in (2.5) and (2.6) into the iterative procedure in (2.7), we obtain mth step of the scoring algorithm as

$$\boldsymbol{\beta}^{(m+1)} = \left(\mathbf{X}^\top \mathbf{W}^{(m)} \mathbf{X}\right)^{-1} \mathbf{X}^\top \mathbf{W}^{(m)} \mathbf{z}^{(m)} \tag{2.8}$$

where $\mathbf{z}^{(m)} = \boldsymbol{\eta}^{(m)} + (\mathbf{W}^{(m)})^{-1}\mathbf{T}^{(m)}\left(\mathbf{y}^* - \boldsymbol{\mu}^{*(m)}\right)$. After some convergence is reached, the maximum likelihood estimator of $\boldsymbol{\beta}$ can be written as follows:

$$\widehat{\boldsymbol{\beta}}_{\text{MLE}} = \left(\mathbf{X}^\top \widehat{\mathbf{W}} \mathbf{X}\right)^{-1} \mathbf{X}^\top \widehat{\mathbf{W}} \widehat{\mathbf{z}} \tag{2.9}$$

where $\widehat{\mathbf{z}} = \widehat{\boldsymbol{\eta}} + (\widehat{\mathbf{W}})^{-1}\widehat{\mathbf{T}}\left(\mathbf{y}^* - \widehat{\boldsymbol{\mu}}\right)$ which is called the working response in the sence that the iterations given in (2.8) describes an iteratively re-weighted least squares estimations and here $\widehat{\mathbf{z}}$, $\widehat{\mathbf{W}}$ and $\widehat{\mathbf{T}}$ are computed at the final iteration of the algorithm.

The asymptotic covariance matrix of $\widehat{\boldsymbol{\beta}}_{\text{MLE}}$ is

$$\text{Cov}\left(\widehat{\boldsymbol{\beta}}_{\text{MLE}}\right) = \psi \left(\mathbf{X}^\top \widehat{\mathbf{W}} \mathbf{X}\right)^{-1} \tag{2.10}$$

and hence the scalar mean squared error (MSE) of $\widehat{\boldsymbol{\beta}}_{\text{MLE}}$ can be given as

$$\text{MSE}\left(\widehat{\boldsymbol{\beta}}_{\text{MLE}}\right) = \psi \sum_{j=1}^{p} \frac{1}{\lambda_j} \tag{2.11}$$

where $tr(.)$ is trace operator and λ_j is the jth eigenvalue of the matrix $\mathbf{X}^\top \widehat{\mathbf{W}} \mathbf{X}$ and $\psi = \frac{1}{\phi}$. It is obvious from Equation (2.11) that the variance of MLE may be affected negatively due to ill-conditioning of the data matrix $\mathbf{X}$ which is known as the multicollinearity problem.

Let $\mathbf{Q}^\top \mathbf{X}^\top \widehat{\mathbf{W}} \mathbf{X} \mathbf{Q} = \boldsymbol{\Lambda} = diag\left(\lambda_1, \lambda_2, \ldots, \lambda_p\right)$, where $\lambda_1 \geq \lambda_2 \geq \ldots \geq \lambda_p > 0$ are the ordered eigenvalues of $\mathbf{X}^\top \widehat{\mathbf{W}} \mathbf{X}$ and the $p \times p$ matrix $\mathbf{Q}$ whose columns are the normalized eigenvectors of $\mathbf{X}^\top \widehat{\mathbf{W}} \mathbf{X}$. Therefore, we have $\boldsymbol{\alpha} = \mathbf{Q}^\top \boldsymbol{\beta}$ and the canonical form of MLE can be written by $\widehat{\boldsymbol{\alpha}}_{\text{MLE}} = \mathbf{Q}^\top \widehat{\boldsymbol{\beta}}_{\text{MLE}}$.

3. Almost Unbiased Beta Ridge Estimator

3.1. **Definition of Almost Unbiased Beta Ridge Estimator.** The ridge estimator is extended to the beta regression model by Ogundimu and Collins [3] and Qasim et al. [4] and it is called the beta ridge estimator (RE) in this study. RE is defined as follows

$$\widehat{\boldsymbol{\beta}}_{\mathrm{RE}} = (\mathbf{X}^\top \widehat{\mathbf{W}}\mathbf{X} + k\mathbf{I})^{-1}\mathbf{X}^\top \widehat{\mathbf{W}}\widehat{\mathbf{z}},\ k > 0. \tag{3.1}$$

It is easy to obtain the bias vector $b(\widehat{\boldsymbol{\beta}}_{\mathrm{RE}})$ and covariance matrix $Cov(\widehat{\boldsymbol{\beta}}_{\mathrm{RE}})$ as follows:

$$b(\widehat{\boldsymbol{\beta}}_{\mathrm{RE}}) = -k(\mathbf{X}^\top \widehat{\mathbf{W}}\mathbf{X} + k\mathbf{I})^{-1}\boldsymbol{\beta} \tag{3.2}$$

$$Cov(\widehat{\boldsymbol{\beta}}_{\mathrm{RE}}) = (\mathbf{X}^\top \widehat{\mathbf{W}}\mathbf{X} + k\mathbf{I})^{-1}\mathbf{X}^\top \widehat{\mathbf{W}}\mathbf{X}(\mathbf{X}^\top \widehat{\mathbf{W}}\mathbf{X} + k\mathbf{I})^{-1}. \tag{3.3}$$

The MSE of RE is obtained as [4]

$$MSE(\widehat{\boldsymbol{\beta}}_{\mathrm{RE}}) = \psi \sum_{j=1}^{p} \frac{\lambda_j}{(\lambda_j + k)^2} + \sum_{j=1}^{p} \frac{k^2\alpha_j^2}{(\lambda_j + k)^2} \tag{3.4}$$

where the first term is the total variance and the second term is the square bias of the beta ridge estimator. Thus, the square bias of RE is given as

$$SB(\widehat{\boldsymbol{\beta}}_{\mathrm{RE}}) = \sum_{j=1}^{p} \frac{k^2\alpha_j^2}{(\lambda_j + k)^2}. \tag{3.5}$$

Definition 3.1. [6] Suppose $\hat{\beta}$ is a biased estimator of parameter vector β, and if the bias vector of $\hat{\boldsymbol{\beta}}$ is given by $b(\hat{\boldsymbol{\beta}}) = E(\hat{\boldsymbol{\beta}}) - \boldsymbol{\beta} = \mathbf{R}\boldsymbol{\beta}$, which shows that $E(\hat{\boldsymbol{\beta}} - \mathbf{R}\boldsymbol{\beta}) = \boldsymbol{\beta}$, then we call the estimator $\tilde{\boldsymbol{\beta}} = \hat{\boldsymbol{\beta}} - \mathbf{R}\hat{\boldsymbol{\beta}} = (\mathbf{I} - \mathbf{R})\hat{\boldsymbol{\beta}}$ is the almost unbiased estimator based on the biased estimator $\hat{\boldsymbol{\beta}}$.

Based on the Definition 3.1, the almost unbiased beta ridge estimator (AURE) can be defined by

$$\begin{aligned}
\widehat{\boldsymbol{\beta}}_{\mathrm{AURE}} &= [\mathbf{I} - ((\mathbf{X}^\top \widehat{\mathbf{W}}\mathbf{X} + k\mathbf{I})^{-1}\mathbf{X}^\top \widehat{\mathbf{W}}\mathbf{X} - \mathbf{I})]\widehat{\boldsymbol{\beta}}_{\mathrm{RE}} \\
&= [2\mathbf{I} - (\mathbf{X}^\top \widehat{\mathbf{W}}\mathbf{X} + k\mathbf{I})^{-1}\mathbf{X}^\top \widehat{\mathbf{W}}\mathbf{X}]\widehat{\boldsymbol{\beta}}_{\mathrm{RE}} \\
&= [2\mathbf{I} - (\mathbf{X}^\top \widehat{\mathbf{W}}\mathbf{X} + k\mathbf{I})^{-1}\mathbf{X}^\top \widehat{\mathbf{W}}\mathbf{X}](\mathbf{X}^\top \widehat{\mathbf{W}}\mathbf{X} + k\mathbf{I})^{-1}\mathbf{X}^\top \widehat{\mathbf{W}}\widehat{\mathbf{z}} \\
&= [\mathbf{I} + (\mathbf{X}^\top \widehat{\mathbf{W}}\mathbf{X} + k\mathbf{I})^{-1}\mathbf{X}^\top \widehat{\mathbf{W}}\mathbf{X}](\mathbf{X}^\top \widehat{\mathbf{W}}\mathbf{X} + k\mathbf{I})^{-1}\mathbf{X}^\top \widehat{\mathbf{W}}\mathbf{X}\widehat{\boldsymbol{\beta}}_{\mathrm{MLE}} \\
&= [\mathbf{I} + k(\mathbf{X}^\top \widehat{\mathbf{W}}\mathbf{X} + k\mathbf{I})^{-1}][\mathbf{I} - k(\mathbf{X}^\top \widehat{\mathbf{W}}\mathbf{X} + k\mathbf{I})^{-1}]\widehat{\boldsymbol{\beta}}_{\mathrm{MLE}} \\
&= [\mathbf{I} - k^2(\mathbf{X}^\top \widehat{\mathbf{W}}\mathbf{X} + k\mathbf{I})^{-2}]\widehat{\boldsymbol{\beta}}_{\mathrm{MLE}} \qquad (3.6)
\end{aligned}$$

where $k > 0$ is a biasing parameter [7]. To the best of our literature review, this estimator has not been proposed or studied in the beta regression model. The bias vector $b(\widehat{\boldsymbol{\beta}}_{\mathrm{AURE}})$ and covariance matrix $Cov(\widehat{\boldsymbol{\beta}}_{\mathrm{AURE}})$ are obtained respectively as follows:

$$b(\widehat{\boldsymbol{\beta}}_{\mathrm{AURE}}) = -k^2(\mathbf{X}^\top \widehat{\mathbf{W}}\mathbf{X} + k\mathbf{I})^{-2}\boldsymbol{\beta} \tag{3.7}$$

$$Cov(\widehat{\boldsymbol{\beta}}_{\mathrm{AURE}}) = \psi[\mathbf{I} - k^2(\mathbf{X}^\top \widehat{\mathbf{W}}\mathbf{X} + k\mathbf{I})^{-2}](\mathbf{X}^\top \widehat{\mathbf{W}}\mathbf{X})^{-1}[\mathbf{I} - k^2(\mathbf{X}^\top \widehat{\mathbf{W}}\mathbf{X} + k\mathbf{I})^{-2}]. \tag{3.8}$$

Therefore, the MSE function of AURE can be written as,

$$MSE(\widehat{\boldsymbol{\beta}}_{\text{AURE}}) = \psi \sum_{j=1}^{p} \left(1 - \frac{k^2}{(\lambda_j + k)^2}\right)^2 \frac{1}{\lambda_j} + \sum_{j=1}^{p} \frac{k^4 \alpha_j^2}{(\lambda_j + k)^4}$$

$$= \sum_{j=1}^{p} \frac{\psi \lambda_j (\lambda_j + 2k)^2 + k^4 \alpha_j^2}{(\lambda_j + k)^4} \tag{3.9}$$

where the first term is the total variance and the second term is the squared bias of AURE. Thus, the squared bias of AURE is given as

$$SB(\widehat{\boldsymbol{\beta}}_{\text{AURE}}) = \sum_{j=1}^{p} \frac{k^4 \alpha_j^2}{(\lambda_j + k)^4}. \tag{3.10}$$

In the next subsection, some theoretical comparisons between MLE, RE and AURE are derived.

3.2. **Theoretical Comparisons.** Firstly, we provide a comparison of the squared biases of RE and AURE in Theorem 3.2.

Theorem 3.2. *The squared bias of RE is greater than the squared bias of AURE* $\forall k > 0$, *i.e.* $SB(\widehat{\boldsymbol{\beta}}_{\text{RE}}) - SB(\widehat{\boldsymbol{\beta}}_{\text{AURE}}) > 0$.

Proof. The difference of the squared biases of RE and AURE is given as

$$SB(\widehat{\boldsymbol{\beta}}_{\text{RE}}) - SB(\widehat{\boldsymbol{\beta}}_{\text{AURE}}) = \sum_{j=1}^{p} \left(\frac{k^2 \alpha_j^2}{(\lambda_j + k)^2} - \frac{k^4 \alpha_j^2}{(\lambda_j + k)^4} \right)$$

$$= \sum_{j=1}^{p} \left(\frac{k^2 \alpha_j^2}{(\lambda_j + k)^4} \lambda_j \left(\lambda_j + 2k\right) \right) \tag{3.11}$$

which is always greater zero since $\lambda_j > 0, j = 1, \ldots, p$. □

Theorem 3.3. *The MSE of AURE is less than the MSE of MLE i.e.* $\Delta_1 = MSE(\widehat{\boldsymbol{\beta}}_{\text{MLE}}) - MSE(\widehat{\boldsymbol{\beta}}_{\text{AURE}}) > 0$ *if one of the following conditions holds:*

- *if* $\psi - \lambda_j \alpha_j^2 > 0$ *then* $\Delta_1 > 0$ *if and only if* $k > k_{2j} > 0$
- *if* $\psi - \lambda_j \alpha_j^2 < 0$ *then* $\Delta_1 > 0$ *if and only if* $0 < k < k_{2j}$

where

$$k_{2j} = \frac{-2\psi\lambda_j + \lambda_j \sqrt{2\psi^2 + 2\psi\lambda_j \alpha_j^2}}{\psi - \lambda_j \alpha_j^2}$$

for $j = 1, \ldots, p$.

Proof. Using Equations (2.11) and (3.9), the difference between the MSE functions of MLE and AURE is obtained as

$$\Delta_1 = MSE(\widehat{\boldsymbol{\beta}}_{\text{MLE}}) - MSE(\widehat{\boldsymbol{\beta}}_{\text{AURE}})$$

$$= \psi \sum_{j=1}^{p} \frac{1}{\lambda_j} - \sum_{j=1}^{p} \frac{\psi \lambda_j (\lambda_j + 2k)^2 + k^4 \alpha_j^2}{(\lambda_j + k)^4}$$

$$= \sum_{j=1}^{p} \frac{k^2}{\lambda_j (\lambda_j + 2k)^2} \left((\psi - \lambda_j \alpha_j^2) k^2 + 4\psi\lambda_j k + 2\psi\lambda_j^2 \right). \tag{3.12}$$

Investigating Equation (3.12), it is enough to obtain under which condition the quadratic functions $\psi-(\lambda_j\alpha_j^2)k^2+4\psi\lambda_j k+2\psi\lambda_j^2$ are positive. Using the discriminant method, the following roots are obtained

$$k_{1j}=\frac{-2\psi\lambda_j-\lambda_j\sqrt{2\psi^2+2\psi\lambda_j\alpha_j^2}}{\psi-\lambda_j\alpha_j^2}$$

and

$$k_{2j}=\frac{-2\psi\lambda_j+\lambda_j\sqrt{2\psi^2+2\psi\lambda_j\alpha_j^2}}{\psi-\lambda_j\alpha_j^2}$$

for $j=1,\ldots,p$. It is clear that the numerators of k_{1j}'s are negative and the numerators of k_{2j}'s are positive. Thus, one can conclude the followings:

- if $\psi-\lambda_j\alpha_j^2>0$ then $\Delta_1>0$ if and only if $k>k_{2j}>0$
- if $\psi-\lambda_j\alpha_j^2<0$ then $\Delta_1>0$ if and only if $0<k<k_{2j}$.

This finishes the proof. □

Finally, a comparison of MSE functions of RE and AURE is given in Theorem 3.4.

Theorem 3.4. *The MSE of AURE is less than the MSE of RE i.e.,* $\Delta_2=MSE(\widehat{\boldsymbol{\beta}}_{\mathrm{RE}})-MSE(\widehat{\boldsymbol{\beta}}_{\mathrm{AURE}})>0$ *if* $k>k_{4j}>0$ *where*

$$k_{4j}=\frac{3\psi-\lambda_j\alpha_j^2+\sqrt{\lambda_j^2\alpha_j^4+2\psi\lambda_j\alpha_j^2+9\psi^3}}{4\alpha_j^2}$$

for $j=1,\ldots,p$.

Proof. Using Equations (3.4) and (3.9), the difference between the MSE functions of RE and AURE is obtained as

$$\begin{aligned}\Delta_2&=MSE(\widehat{\boldsymbol{\beta}}_{\mathrm{RE}})-MSE(\widehat{\boldsymbol{\beta}}_{\mathrm{AURE}})\\&=\sum_{j=1}^{p}\frac{\psi\lambda_j+k^2\alpha_j^2}{(\lambda_j+k)^2}-\sum_{j=1}^{p}\frac{\psi\lambda_j(\lambda_j+2k)^2+k^4\alpha_j^2}{(\lambda_j+k)^4}\\&=\sum_{j=1}^{p}\frac{k\lambda_j}{(\lambda_j+k)^4}\left(2k^2\alpha_j^2+(\lambda_j\alpha_j^2-3\psi)k+2\psi\lambda_j\right).\end{aligned}\tag{3.13}$$

Investigating Equation (3.13) and using the same procedure as in the proof of Theorem 3.3, it is enough to obtain under which condition the quadratic functions $2k^2\alpha_j^2+(\lambda_j\alpha_j^2-3\psi)k+2\psi\lambda_j$ are positive. Using the discriminant method, the following roots are obtained

$$k_{3j}=\frac{3\psi-\lambda_j\alpha_j^2-\sqrt{\lambda_j^2\alpha_j^4+2\psi\lambda_j\alpha_j^2+9\psi^3}}{4\alpha_j^2}$$

and

$$k_{4j}=\frac{3\psi-\lambda_j\alpha_j^2+\sqrt{\lambda_j^2\alpha_j^4+2\psi\lambda_j\alpha_j^2+9\psi^3}}{4\alpha_j^2}$$

for $j=1,\ldots,p$. It is clear that k_{3j}'s are negative, whereas k_{4j}'s are positive. Thus, $\Delta_2>0$ if $k>k_{4j}>0$. This finishes the proof. □

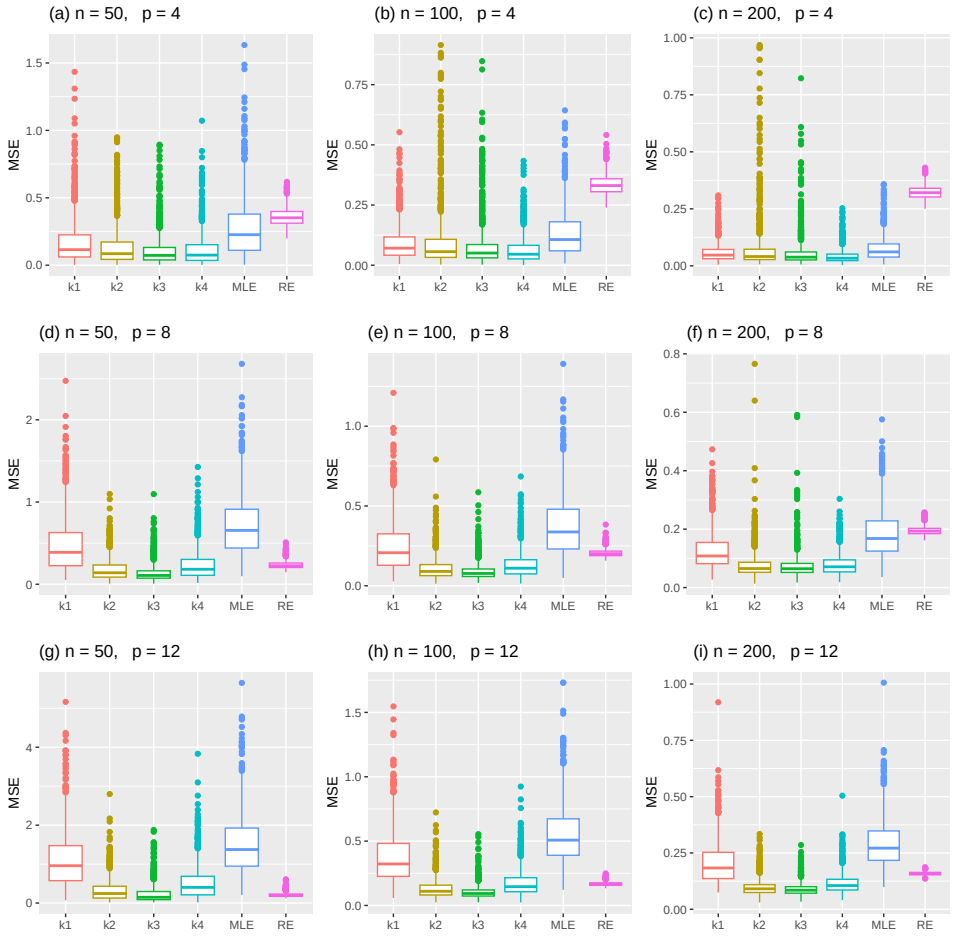

FIGURE 1. $MSE(\beta)$ values of the estimators when $\rho = 0.90$

3.3. **Selection of the parameter k.** The MSE function of AURE is given in Equation 3.9. It is a function of the parameter k. In order to obtain smaller MSE values than that of MLE and RE, one needs to choose the biasing parameter k carefully. Thus, to attain the minimum MSE value of $MSE(\widehat{\boldsymbol{\beta}}_{\text{AURE}})$, we try to minimize this function by taking the derivate of this function with respect to k and equating the derivative to zero. The following is obtained

$$\frac{\partial(MSE(\widehat{\boldsymbol{\beta}}_{\text{AURE}}))}{\partial k} = \sum_{j=1}^{p} \frac{-4\psi k\lambda_j^2 - 8\psi k^2\lambda_j + 4k^3\lambda_j\alpha_j^2}{(\lambda_j + k)^5} = 0. \tag{3.14}$$

Now, using the same strategy as in the proof of theorems, we find the roots of the function $-4\psi k\lambda_j^2 - 8\psi k^2\lambda_j + 4k^3\lambda_j\alpha_j^2$ which is equivalent to solving

$$k^2\alpha_j^2 - 2\psi k - \psi\lambda_j = 0.$$

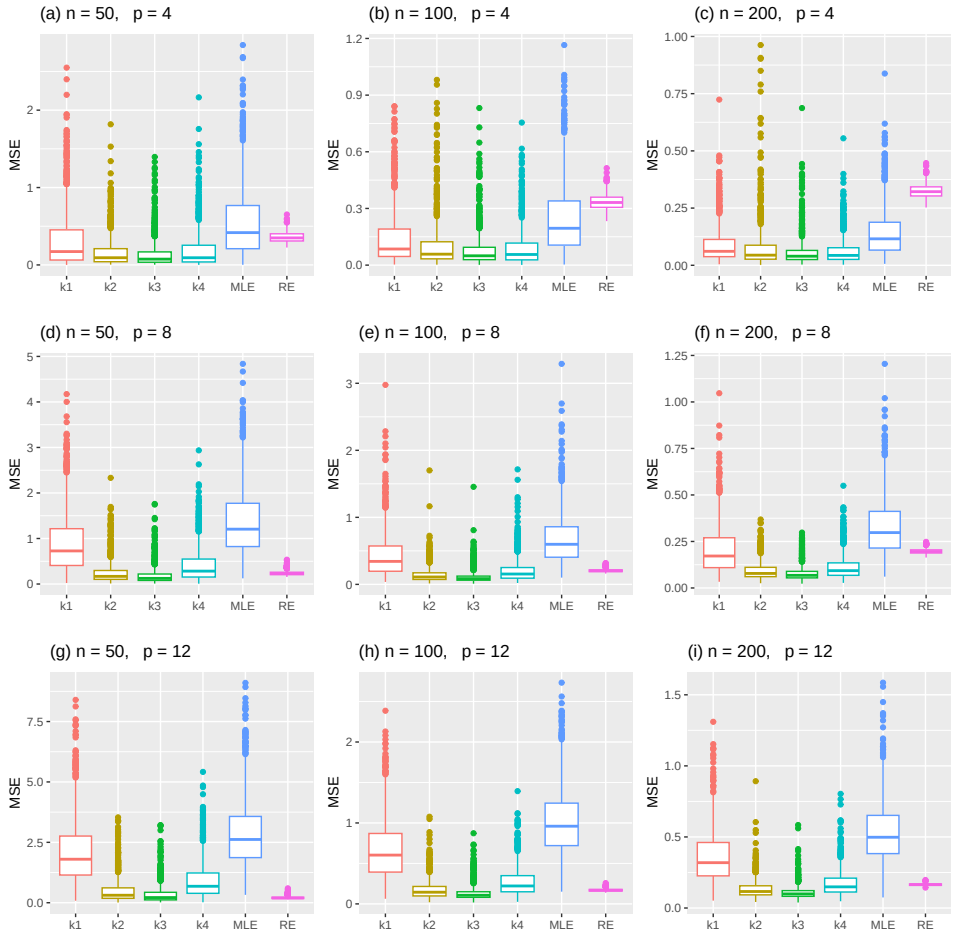

FIGURE 2. $MSE(\beta)$ values of the estimators when $\rho = 0.95$

Upon using the discriminant method, we find the following roots:

$$k_{5j} = \frac{\psi - \sqrt{\psi(\psi + \lambda_j \alpha_j^2)}}{\alpha_j^2} < 0$$

and

$$k_{6j} = \frac{\psi + \sqrt{\psi(\psi + \lambda_j \alpha_j^2)}}{\alpha_j^2} > 0.$$

Since k_{5j}'s are negative and k_{6j}'s are positive, and we only need to estimate the parameter k, we propose to use the following estimators of k:

- $k_1 = min(k_{6j})$
- $k_2 = median(k_{6j})$
- $k_3 = \prod_{j=1}^{p} (k_{6j})^{1/p}$ which is the geometric mean of k_{6j}'s.
- $k_4 = \frac{p}{\sum_{j=1}^{p} \frac{1}{k_{6j}}}$ which is the harmonic mean of k_{6j}'s.

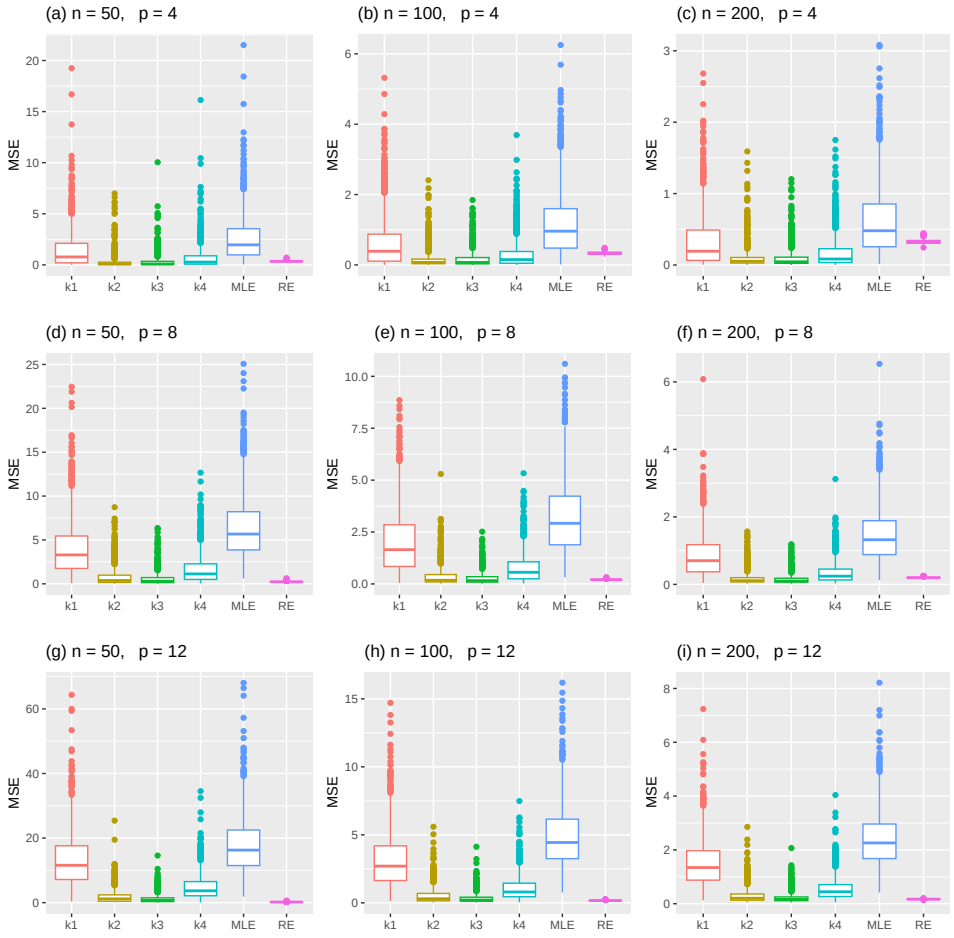

FIGURE 3. $MSE(\beta)$ values of the estimators when $\rho = 0.99$

Since the true values of ψ and $\boldsymbol{\alpha}$ are unknown, we replace them by the respective estimators as $\widehat{\psi}$ and $\widehat{\boldsymbol{\alpha}}_{\text{MLE}}$ in $k_1, \ldots, k_4$. In the next section, we show that the performance of AURE becomes better than RE and MLE using the estimators $k_1, \ldots, k_4$ in most of the situations considered.

4. A Monte Carlo Simulation

In this section, a Monte Carlo simulation experiment is designed to compare the performances of the estimators. The explanatory variables are generated by

$$x_{ij} = (1-\rho^2)^{1l2} w_{ij} + \rho w_{ip+1}, \quad i = 1, 2, ..., n, \quad j = 1, 2, ..., p,$$

where w_{ij} are independent standard normal pseudo-random numbers, and ρ determines the degree of correlation between any two explanatory variables which is given by ρ^2 [8, 9]. Thus, we can examine the performance of the methods under different degrees of the strength of the correlation in the data. Therefore, the following different values are considered: $\rho = 0.9, 0.95$ and 0.99.

The slope parameters are decided such that $\sum_{j=1}^{p} \beta_j^2 = 1$, which is a commonly used restriction in the field [9, 10]. The response variable is generated using the beta distribution such that $y_i \sim Beta\left(\mu_i\phi, (1-\mu_i)\phi\right)$ where

$$\mu_i = \frac{\exp(\mathbf{x}_i'\boldsymbol{\beta})}{1+\exp(\mathbf{x}_i'\boldsymbol{\beta})}.$$

which is known as the logit link function and the dispersion parameter is fixed to be 5 for this study.

Moreover, the sample size is taken to be as 50, 100, and 200 in the simulation. The number of explanatory variables is taken to be $4, 8$ and 12 to be able to understand the effect of the number of covariates on the performances of estimators.

The simulation is repeated 1000 times for each value of the parameters mentioned above. The simulated MSE and the squared bias (SB) of an estimator $\widehat{\boldsymbol{\beta}}^*$ are computed to evaluate the performances of the estimators. They are respectively given by

$$\begin{aligned} \text{MSE}\left(\widehat{\boldsymbol{\beta}}^*\right) &= \frac{1}{1000}\sum_{r=1}^{1000}\left(\widehat{\boldsymbol{\beta}}^* - \mathbf{b}\right)_r^\top \left(\widehat{\boldsymbol{\beta}}^* - \mathbf{b}\right) \\ \text{SB}\left(\widehat{\boldsymbol{\beta}}^*\right) &= \left(\overline{\widehat{\boldsymbol{\beta}}^*} - \mathbf{b}\right)^\top \left(\overline{\widehat{\boldsymbol{\beta}}^*} - \mathbf{b}\right), \ \overline{\widehat{\boldsymbol{\beta}}^*} = \frac{1}{1000}\sum_{r=1}^{1000} {}_r\widehat{\boldsymbol{\beta}}^* \end{aligned}$$

where $\left(\widehat{\boldsymbol{\beta}}^* - \mathbf{b}\right)_r$ shows the difference between the estimated and true parameter vectors and ${}_r\widehat{\boldsymbol{\beta}}^*$ shows the estimate of $\widehat{\boldsymbol{\beta}}^*$ at the rth iteration of the simulation. All the computations are performed using the R Programming Language [11].

The results of the simulation study are summarized in Figures 1-3 and Table 1. The boxplots of the simulated MSE values are provided in Figures 1-3 and the simulated squared bias values are given in Table 1.

TABLE 1. Simulated squared bias values

	$\rho = 0.90$			$\rho = 0.95$			$\rho = 0.99$		
n	50	100	200	50	100	200	50	100	200
					$p = 4$				
RE	0.3556	0.3340	0.3220	0.3564	0.3333	0.3241	0.3546	0.3325	0.3240
k1	0.0031	0.0063	0.0133	0.0032	0.0088	0.0177	0.0082	0.0227	0.0324
k2	0.0216	0.0292	0.0348	0.0112	0.0229	0.0256	0.0063	0.0154	0.0198
k3	0.0217	0.0275	0.0304	0.0117	0.0218	0.0231	0.0063	0.0153	0.0194
k4	0.0048	0.0078	0.0135	0.0040	0.0096	0.0162	0.0060	0.0164	0.0227
					$p = 8$				
RE	0.2317	0.2032	0.1941	0.2351	0.2048	0.1971	0.2357	0.2088	0.1990
k1	0.0377	0.0530	0.0433	0.0624	0.0767	0.0568	0.2235	0.3015	0.1263
k2	0.0397	0.0473	0.0492	0.0426	0.0499	0.0504	0.0672	0.0761	0.0603
k3	0.0450	0.0504	0.0546	0.0437	0.0501	0.0511	0.0607	0.0684	0.0573
k4	0.0342	0.0422	0.0413	0.0452	0.0537	0.0494	0.1078	0.1313	0.0763
					$p = 12$				
RE	0.2047	0.1644	0.1575	0.2067	0.1686	0.1638	0.2084	0.1702	0.1690
k1	0.1329	0.0651	0.0706	0.2748	0.0963	0.1047	1.3957	0.2910	0.2925
k2	0.0534	0.0563	0.0651	0.0819	0.0613	0.0776	0.2766	0.0816	0.1068
k3	0.0455	0.0608	0.0697	0.0668	0.0607	0.0767	0.1823	0.0717	0.0963
k4	0.0715	0.0540	0.0631	0.1335	0.0668	0.0814	0.5681	0.1235	0.1449

According to the figures and table, the following results are obtained:

- Based on the simulated MSE values, AURE outperforms the other estimators in most of the cases considered in the simulation.
- It is observed from Figure 1 that AURE with k_3 has the best performance than the others, when $\rho = 0.90$. In this case, as the number of explanatory variables is increased, RE has better performance however AURE with k_3 is superior to RE.
- The MLE becomes the worst estimator, in other words, it produces the highest MSE values in almost all of the cases, except for some situations when $p = 4$. Moreover, the MSE of MLE increases drastically when the degree of correlation ρ is increased.
- Generally, increasing the sample size has a positive effect on the estimators meaning that the MSEs decrease.
- Although, there is degeneracy of the monotonicity of the MSE values, the MSE values increase if the number of explanatory variables increase. This result can be seen especially when the degree of correlation is high, namely, $\rho = 0.99$.
- In general, increasing the degree of correlation has a negative effect on the estimators.
- On the other hand, considering the SB performances of the estimators, it is observed from Table 1 that AURE has the lowest SB values in all the cases.
- If the sample size increases, the SB values increase in general. But, there is no clear pattern for the SB values if there is a change in the number of variables or the degree of correlation.

5. Conclusion

In this study, an almost unbiased beta ridge estimator is introduced in order to overcome the effects of the problem of ill–conditioning in the beta regression models. The theoretical comparisons are provided in detail using the squared biases and mean squared errors of the considered estimators in this paper. Based on the results of the Monte Carlo simulation, it is concluded that AURE has better performance than the estimators MLE and RE in terms of both the simulated MSE and SB values. Thus, AURE can be useful for the researchers in the field.

References

[1] S. Ferrari, F. Cribari–Neto, Beta regression for modelling rates and proportions, Journal of applied statistics, 31(7), 799–815 (2004).
[2] A. E. Hoerl, R. W. Kennard, Ridge regression: Biased estimation for non-orthogonal problems. Technometrics 12(1), 55–67 (1970a).
[3] E. O. Ogundimu, G. S. Collins, Predictive performance of penalized beta regression model for continuous bounded outcomes, Journal of Applied Statistics, 45(6), 1030–1040 (2018).
[4] M. Qasim, K. Månsson, B. M. G. Kibria, On some beta ridge regression estimators: method, simulation and application, Journal of Statistical Computation and Simulation, 91 (9), 1699–1712 (2021).
[5] P. L. Espinheira, S. L. Ferrari, F. Cribari-Neto, On beta regression residuals, Journal of Applied Statistics, 35(4), 407–419 (2008).
[6] J. W. Xu, H. Yang, More on the bias and variance comparisons of the restricted almost unbiased estimators, Communication in Statistics–Theory and Methods, 40, 4053–4064 (2011).
[7] B. Singh, Y. P. Chaubey, T. D. Dwivedi, An almost unbiased ridge estimator, Sankhya: The Indian Journal of Statistics, Series B, 342–346 (1986).

[8] G. C. McDonald, D. I. Galarneau, A Monte Carlo evaluation of some ridge–type estimators, Journal of the American Statistical Association, 70(350), 407–416 (1975).
[9] M. Erişoğlu, N. Yaman, Ridge Tahminine Dayalı Kantil Regresyon Analizinde Yanlılık Parametresi Tahminlerinin Performanslarının Karşılaştırılması, NEU Journal of Science and Engineering, 1(2), 103–111 (2019).
[10] B. M. G. Kibria, Performance of some new ridge regression estimators, Communications in Statistics–Simulation and Computation, 32(2), 419–435 (2003).
[11] R Core Team (2021). R: A language and environment for statistical computing. R Foundation for Statistical Computing, Vienna, Austria. URL https://www.R-project.org/.

(Yasin Asar) Necmettin Erbakan University, Department of Mathematics and Computer Sciences, 42090, Konya, Turkey

Email address, Yasin Asar: yasar@erbakan.edu.tr

IFSCOM-E 2023
9th Ifs And Contemporary Mathematics and Engineering Conference
08-11 July 2023 Tarsus, Mersin, Türkiye
ISBN: 978-605-68670-8-8
pp: 33-38

REVOLUTIONIZING MATRIX COMPUTATIONS: A PRACTICAL APPROACH FOR EFFICIENT CALCULATION OF MATRIX SIGN FUNCTION

GUL KARADUMAN

0000-0002-2776-759X

Abstract. Matrix computations are fundamental operations in numerous scientific and engineering fields, such as machine learning, quantum mechanics, and numerical analysis. Calculating the matrix sign function, which determines the sign of each entry in a matrix, is of great significance in these applications. However, efficiently computing the matrix sign function remains challenging, especially for large matrices. This study introduces a way to approximate the matrix sign function using the Taylor expansion and Generalized Minimal Residual (GMRES) algorithm. The proposed approach reduces the computational complexity and enhances the numerical stability, making it highly practical for a wide range of applications.

1. Introduction

Matrix computations are at the core of many scientific and engineering problems. The matrix sign function, represented as $sign\,(A)$, assigns the sign of each element in matrix A. Despite its seemingly simple definition, accurately and efficiently computing the matrix sign function for large matrices remains complex. The matrix sign function is defined as,

$$sign\,(A) = U \times diag(sign(\lambda_1), sign(\lambda_2), \ldots, sign(\lambda_n) \times V^H, \tag{1.1}$$

where $A = U \times \Sigma \times V^H$ is the singular value decomposition (SVD) of A. λ_i represents the $i-th$ singular value of A, $sig(\lambda_i)$ is the $sign$ of λ_i, and

$$diag(sign(\lambda_1), sign(\lambda_2), \ldots, sign(\lambda_n), \tag{1.2}$$

is a diagonal matrix with the signs of the singular values [4].

Existing methods for calculating the matrix sign function have been developed over the years, each with advantages and limitations. These methods often suffer from high computational costs and numerical instability. The most straightforward approach is to directly compute the sign of each element in the matrix [3]. This

Date: July, 8, 2023.
Key words and phrases. Matrix functions, Matrix sign function, Iterative methods, Taylor expansion, GMRES.

method involves iterating over each entry and determining its sign using standard arithmetic operations. While straightforward, this approach can be computationally expensive, especially for large matrices, due to its $O\left(n^2\right)$ time complexity.

Another approach is Singular Value Decomposition (SVD). The matrix sign function can be calculated using the SVD of the matrix. The SVD decomposes the matrix into three components,

$$A = U \times \Sigma \times V^H, \tag{1.3}$$

where U and V are unitary matrices, and Σ is a diagonal matrix containing the singular values of A [2]. The matrix sign function can be obtained by computing the sign of each singular value and reconstructing the sign matrix. However, the SVD approach can be computationally expensive, particularly for large matrices, as it involves decomposing the matrix and manipulating the singular values.

Similar to the SVD approach, the matrix sign function can be calculated using the eigenvalue decomposition of the matrix. The SVD decomposes the matrix into eigenvectors and eigenvalues. By computing the sign of each eigenvalue and reconstructing the sign matrix, the matrix sign function can be obtained [6]. However, the SVD approach must also improve its computational complexity, especially for non-symmetric matrices.

Iterative approximation methods, such as Newton-Raphson or fixed-point iterations, can also compute the matrix sign function [1], [5]. These methods iteratively update an initial estimate of the sign function until convergence is achieved. While iterative methods can be computationally efficient, they may suffer from numerical instability or convergence issues, especially for ill-conditioned matrices.

This study presents a way to approximate the matrix sign function using Taylor expansion and Generalized Minimal Residual (GMRES) [7] as a component in a larger iterative scheme. The approach uses the Taylor expansion method, where GMRES is employed to solve linear systems of equations that arise during the computation of the rational approximation.

2. Approximation method

This study approximates the matrix sign function using GMRES as a component in a larger iterative scheme. To achieve this, the Taylor approximation method is utilized, employing GMRES to solve the linear systems of equations that arise during the computation of the rational approximation. A localized approximation is obtained around a selected expansion point by utilizing a Taylor expansion, enabling an accurate representation of the sign function's behavior in the immediate vicinity of that point. Throughout each iteration of the Taylor expansion, the GMRES algorithm is a reliable solver for emerging linear systems.

The Taylor series expansion is a powerful mathematical tool enabling a function to be expressed as an infinite sum of terms. These terms are determined by evaluating the function's derivatives at a specific point. The Taylor series expansion of a function $f(x)$ around a point a can be expressed as follows.

$$f(x) = f(a) + f'(a)(x-a) + f''(a)(x-a)^2/2! + f'''(a)(x-a)^3/3! + \ldots. \tag{2.1}$$

We can approximate the matrix sign function by substituting the matrix A into the Taylor series expansion and truncating the series after a certain number of terms.

Restarted GMRES (Generalized Minimal Residual) is an iterative method to solve large sparse linear systems of equations [7]. It is particularly effective for solving non-symmetric systems. The technique combines the advantages of the GMRES algorithm with a restart strategy to improve efficiency and reduce memory requirements. The GMRES algorithm aims to find an approximate solution to the linear system $Ax = b$ by constructing an orthogonal basis for the Krylov subspace generated by the matrix A and the residual vector $r = b - Ax$. This basis is then used to minimize the residual over the subspace, resulting in an approximate solution.

The following steps outline how the Taylor series coefficients are computed and how the GMRES algorithm is employed to solve the linear systems involved in each iteration. Denoting the matrix sign function as $sign(A)$, we can explain the combined GMRES and Taylor series expansion method as follows.

Suppose the sign function of the matrix $A \in R^{n\times n}$ is to be computed. We choose a suitable expansion point, denoted as a, around which the Taylor series expansion will be performed. We compute the Taylor series expansion of the matrix sign function centered at the chosen point as,

$$sign(A) = c_0 I + c_1(A - aI) + c_2(A - aI)^2 + c_3(A - aI)^3 + \dots. \tag{2.2}$$

Now, we truncate the series after a certain number of terms, denoted as k, to obtain the approximation of the matrix sign function as

$$sign(A) \approx c_0 I + c_1(A - aI) + c_2(A - aI)^2 + ... + c_k(A - aI)^k. \tag{2.3}$$

Next, we initialize an initial approximation matrix $X(0) \in R^{n\times n}$. Here, we set $X(0)$ equal to the matrix A. Residual matrix $R(i)$ is set to be,

$$R(i) = appfunc(X(i-1)) - A \tag{2.4}$$

where i is a number from 1 to n, and appfunc represents the Taylor series expansion of the matrix sign function evaluated at $X(i-1)$. Next, we use the GMRES method to solve the linear system of equations,

$$GMRES(A,\ R(i),\ x) \tag{2.5}$$

where A is the matrix, $R(i)$ is the right-hand side vector representing the residual, and x is the solution vector. Updating the approximation matrix by adding the solution vector x obtained from the GMRES solver to the previous approximation matrix $X(i-1)$, we get,

$$X(i) = X(i-1) + x \tag{2.6}$$

Finally, after n iterations, the matrix $X(n)$ will approximate the matrix sign function of A.

By combining the Taylor series expansion and GMRES method, this approach allows for iterative refinement of the approximation. The approximation function is evaluated using the current approximation matrix $X(i-1)$, and the resulting residual is used as the right-hand side for the linear system. The combined method leverages the benefits of both the Taylor series expansion and the efficient convergence of GMRES to improve the accuracy of the approximation. The level of accuracy depends on factors such as the choice of the expansion point, the number of terms in the Taylor series expansion, the number of iterations, and the properties of the matrix A.

Algorithm 1 Approximating the Matrix Sign Function $sign\,(A)$

Require: Matrix $A \in R^{(n\times n)}$, expansion point a, number of terms in Taylor series k, initial approximation matrix $X0 \in R^{(n\times n)}$, number of iterations n.
Ensure: Approximation matrix X after n iterations.

```
Initialize X = X0
Compute the Taylor series coefficients I = eye(size(A))
for j = 0 : k do
    if j = 0 then
        coefficient(j) = 1
    else[coefficient(j) = 1/factorial(j)]
    end if
end for
for i = 0 : n do
    R = ApproximationFunction(X) − A
    x = GMRES(A, R)
    X = X + x
end for
```

Note: We employed an approximation function and the GMRES method as separate built-in functions.

3. Results

We conducted a thorough performance evaluation to assess the proposed approach's efficacy. Specifically, we computed the matrix sign function for two randomly generated real matrices. In this calculation, we utilized MATLAB's random matrix generator. The algorithm continued until the residual reached a 10^{-8}, at which point it terminated.

Experiment 1: Let $A = rand(20, 20)$ be 20×20 real matrix. We computed the matrix sign function.

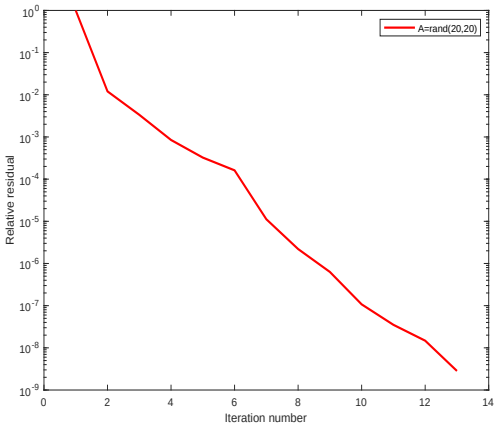

Figure 1. Relative residual *vs*. iteration number

During the computational analysis of the problem, we utilized a highly regarded numerical technique known for its efficiency and reliability. This method demonstrated significant convergence, successfully reaching the desired solution after 13 iterations of an iterative process. The method's exceptional computational prowess enabled it to complete its calculations within a mere 0.102 seconds swiftly. This impressive performance emphasizes both the computational efficiency and effectiveness of the method.

Experiment 2: Let $A = rand(50, 50)$ be 50×50 real matrix. We computed the matrix sign function.

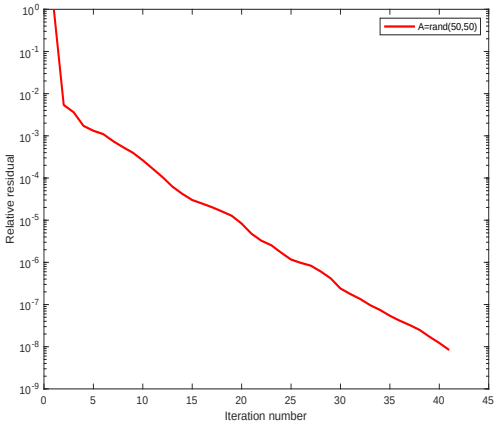

FIGURE 2. Relative residual *vs*. iteration number

This method shows a remarkable convergence, achieving the desired solution through 41 iterations of an iterative process. With its exceptional computational prowess, the methodology executed its calculations swiftly, wrapping up within an impressive time of just 0.216 seconds.

The evaluation shows the revolutionary approach's computational efficiency and numerical accuracy for calculating the matrix sign function. Experimental results demonstrate the superiority of the proposed method, showing significant results in terms of computational time, memory utilization, and numerical stability.

4. Conclusion

This article presents a novel approach that revolutionizes the computation of the matrix sign function, offering a practical and efficient solution. Combining the Taylor series expansion and the GMRES method provides a powerful tool for matrix computations, enhancing efficiency and accuracy. The approach presented in this article opens up new possibilities for solving complex problems that involve the matrix sign function and paves the way for future advancements in matrix computations.

References

[1] R. L. Burden and J. D. Faires. *Numerical Analysis*. PWS-Kent Publishing Company, Boston, fourth edition, 1989.

[2] J. W. Demmel. *Applied Numerical Linear Algebra*. Society for Industrial and Applied Mathematics, 1997.
[3] E. D. Denman and A. N. Beavers. The matrix sign function and computations in systems. *Applied Mathematics and Computation*, 2(1):63–94, 1976.
[4] N. J. Higham. *Functions of Matrices*. Society for Industrial and Applied Mathematics, 2008.
[5] C. Kenney and A. J. Laub. Rational iterative methods for the matrix sign function. *SIAM Journal on Matrix Analysis and Applications*, 12(2):273–291, 1991.
[6] C.S. Kenney and A.J. Laub. The matrix sign function. *IEEE Transactions on Automatic Control*, 40(8):1330–1348, 1995.
[7] Y. Saad and M. H. Schultz. Gmres: A generalized minimal residual algorithm for solving nonsymmetric linear systems. *SIAM Journal on Scientific and Statistical Computing*, 7(3):856–869, 1986.

Vocational School of Health Services, Karamanoglu Mehmetbey University, Karaman, 70200, Turkey
Email address: gulk@bu.edu

IFSCOM-E 2023
9th Ifs And Contemporary Mathematics and Engineering Conference
08-11 July 2023 Tarsus, Mersin, Türkiye
ISBN: 978-605-68670-8-8
pp: 39-49

RELATIVE CONTROLLABILITY OF THE μ-CAPUTO FRACTIONAL DELAYED SYSTEM WITH IMPULSES

MUSTAFA AYDIN

0000-0003-0132-9636

Abstract. In this paper we consider the impulsive fractional delayed differential system with the Caputo derivative with respect to another function. We determine an explicit solution in the light of the available studies in this subject and discuss its existence and uniqueness. we investigate stability and controllability of the given system.

1. Introduction

Fractional calculus is regarded as a generalization of integer calculus. Of course, this generalization contributes different positive capabilities which integer calculus does not have to fractional calculus. For example, according to researchers in this field, this enables fractional calculus to model almost all of scientific problem more suitable than integer order, numerical approaches to fractional calculus give better results compared to integer calculus, etc. Fractional calculus begin to be used in many areas such as mathematical physics, biophysics, engineering, signal processing, etc. For more details, all of reference section can be scanned. An differential equation which consists of the present state and its rate of changes is said to be a delayed differential equation[4]-[6] if it also includes the past state. It is difficult to work on such a equation according to equivalent studies. When we have look at the literature, these kinds of systems have been investigated in terms of existence and uniqueness of solutions, stability and controllability[12]-[15] of the systems. Generally, a differential equation has been used to formulate the dynamics of changing processes. The dynamics of several changing processes count on sudden changes such as natural disasters, shocks. These sorts of phenomena have short-term perturbations(deviations) from continuous dynamics. When the duration of the whole development is considered, its duration is negligible. While such deviations are modelled, these deviations treat in the form of ''impulses"or instantaneously. As

Date: July, 8, 2023.
Key words and phrases. Impulsive fractional delayed system, Existence uniqueness, Ulam-Hyers stability, Relative controllability.

a consequence, modelling impulsive problems produce impulsive differential equations in industrial robotics, population dynamics, physics, ecology, optimal control and so on [16, 17, 18, 19].

Inspired by the above-cited studies, we consider the following nonhomogeneous linear Ψ-Caputo fractional delayed differential system with impulses

$$(1.1)\quad \begin{cases} {}^{C}_{-r^+}D^{\beta}_{\mu}w(t) = Mw(t) + Aw(t-r) + g(t,w(t)), \quad 0 < t \leq T, \quad r > 0, \\ w(t) = \psi(t), \quad -r \leq t \leq 0, \\ w\left(t_i^+\right) = w\left(t_i^-\right) + f\left(w\left(t_i\right)\right), \quad t_i \in J, \end{cases}$$

where ${}^{C}_{-r^+}D^{\beta}_{\mu}$ is μ-Caputo derivative of order β, $\mu(t) : \mathbb{R} \to \mathbb{R}$ is increasing and $\mu'(t) \neq 0$ for every $t \in [-r, T]$, $M, A \in \mathbb{R}^n$ which do not have to be commutative, $g \in C\left([0,T] \times \mathbb{R}^n, \mathbb{R}^n\right)$, $f \in C\left(\mathbb{R}^n, \mathbb{R}^n\right)$, and $\psi(x) \in C^1\left([-h, 0], \mathbb{R}^n\right)$, $J = \{t_1, t_2, ..., t_m\}$ is the impulsive times with $0 < t_1 < ... < t_m < T$, $T = lr$ for a fixed $l \in \mathbb{N}$. The jumps

$$w\left(t_i^+\right) = \lim_{\varepsilon \to 0^+} w\left(t_i + \varepsilon\right), \qquad w\left(t_i^-\right) = \lim_{\varepsilon \to 0^-} w\left(t_i + \varepsilon\right)$$

stand for the right and left limits of $w\left(t\right)$ at $t = t_i$, respectively

.

2. Preliminaries

In this section we will present most essential tools to be used in the following sections.

$\mathbb{R}^n$ is the famous Euclidean space with dimension $n \in \{1, 2, 3, ...\}$. For $a, b \in \mathbb{R}$ with $a < b$, let

$$C\left([a,b], \mathbb{R}^n\right) = \{f : [a,b] \to \mathbb{R}^n : f \text{ is continuous}\}$$

with the maximum norm $\|.\|_C$, which is

$$\|f\|_C = \max\{\|f\left(t\right)\|, t \in [a,b]\}$$

where $\|.\|$ is an arbitrary norm on $\mathbb{R}^n$. Let $AC[a,b]$ be the absolutely continuous functions' space. For $n \in \{1, 2, 3, ...\}$, $AC^n[a,b]$ the space of all complex-valued functions $f(t)$ such that $f^{(n-1)}(t) \in AC[a,b]$.

Lemma 2.1. [2] *$\mathcal{X}^{M,A,\mu}_{\beta,1,r}(t,s)$ is a solution of*

$${}^{C}_{-r^+}D^{\beta}_{\mu}\mathcal{X}^{M,A,\mu}_{\beta,1,r}(t,s) = M\mathcal{X}^{M,A,\mu}_{\beta,1,r}(t,s) + A\mathcal{X}^{M,A,\mu}_{\beta,1,r}(t,s+h).$$

Lemma 2.2. [2] *A continuous solution w of the equation (1.1) without the impulsive initial condition is*

$$\begin{aligned} w(t) =& \mathcal{X}^{M,A,\mu}_{\beta,1,r}(t,-r)\psi(-r) + \int_{-r}^{0} \mathcal{X}^{M,A,\mu}_{\beta,\beta,r}(t,s)\left[\left({}^{C}_{-r^+}D^{\beta}_{\mu}\psi\right)(s) - A\psi(s)\right]d\mu(s) \\ &+ \int_{0}^{t} \mathcal{X}^{M,A,\mu}_{\beta,\beta,r}(t,s)f(s,w(s))d\mu(s) \end{aligned}$$

here, μ-delay perturbation of two-parameter Mittag-Leffler function $\mathcal{X}^{M,A,\mu}_{\beta,\alpha,r}$ is defined by

(2.1)
$$\mathcal{X}^{M,A,\mu}_{\beta,\alpha,r}(t,s)=\begin{cases}\Theta, & t-s\in[-r,0)\\ I, & t=s\\ \sum\limits_{i=0}^{\infty}\sum\limits_{j=0}^{l-1}\mathcal{Q}_{i+1}(jr)\frac{[\mu(t)-\mu(s+jr)]^{i\beta+\alpha-1}}{\Gamma(i\beta+\alpha)}, & t-s\in((l-1)r,lr]\end{cases}$$

where $\mu(t):\mathbb{R}\to\mathbb{R}$ is an increasing function such that $\mu(0)=0$ and $\mu'(t)\neq 0$ for every $t\in[-r,T]$, I and Θ stand for the identity matrix and zero matrix, respectively. From [1]*, the recurresive matrices $\mathcal{Q}_i(s)$ are defined for $s=ir$ with $i=0,1,2,...$ as*

$$\mathcal{Q}_0(s)=\Theta,\quad \mathcal{Q}_1(0)=I,\quad \mathcal{Q}_i(-r)=\Theta,\quad \mathcal{Q}_{i+1}(s)=M\mathcal{Q}_i(s)+A\mathcal{Q}_i(s-r).$$

Lemma 2.3. [2] *If $t\in[0,T]$, $T=lr$ where $l\in\mathbb{N}$ and $r\in\mathbb{R}^+$, then the following inequality holds true*

$$\int_0^t\left\|\mathcal{X}^{M,A,\mu}_{\beta,\alpha,r}(t,s)\right\|d\mu(s)\leq[\mu(T)-\mu(0)]\mathcal{X}^{||M||,||A||,\mu}_{\beta,\alpha,r}(T,0). \tag{2.2}$$

Lemma 2.4. [2] *$\mathcal{X}^{M,A,\mu}_{\beta,\alpha,r}(t,s)$ is jointly continuous in $0<s<t<\infty$.*

From here on, we will offer our fundamental contributions.

3. The representation of a solution

Theorem 3.1. *A continuous solution w of the equation (1.1) is*

$$\begin{aligned}w(t)=&\mathcal{X}^{M,A,\mu}_{\beta,1,r}(t,-r)\psi(-r)+\int_{-r}^{0}\mathcal{X}^{M,A,\mu}_{\beta,\beta,r}(t,s)\left[\left({}^{C}_{-r^+}D^{\beta}_{\mu}\psi\right)(s)-A\psi(s)\right]d\mu(s)\\&+\int_0^t\mathcal{X}^{M,A,\mu}_{\beta,\beta,r}(t,s)g(s,w(s))d\mu(s)+\sum_{0<t_i<t}\mathcal{X}^{M,A,\mu}_{\beta,1,r}(t,t_i)\,f\left(w\left(t_i\right)\right)\end{aligned}$$

where $\mathcal{X}^{M,A,\mu}_{\beta,\alpha,r}$ is μ-delay perturbation of two-parameter Mittag-Leffler function given above.

Proof. If one combines Lemma 2.1 with Lemma 2.2, the proof is completed out of the satisfaction of the impulsive initial condition. Now, we will show that the solution satisfies the impulsive initial condition. For each $t\in(t_{k-1},t_k]$, the solution $w(t)$ is given by

$$\begin{aligned}w(t)=&\mathcal{X}^{M,A,\mu}_{\beta,1,r}(t,-r)\psi(-r)+\int_{-r}^{0}\mathcal{X}^{M,A,\mu}_{\beta,\beta,r}(t,s)\left[\left({}^{C}_{-r^+}D^{\beta}_{\mu}\psi\right)(s)-A\psi(s)\right]d\mu(s)\\&+\int_0^t\mathcal{X}^{M,A,\mu}_{\beta,\beta,r}(t,s)g(s,w(s))d\mu(s)+\sum_{i=1}^{k-1}\mathcal{X}^{M,A,\mu}_{\beta,1,r}(t,t_i)\,f\left(w\left(t_i\right)\right),\end{aligned}$$

and for each $t\in(t_k,t_{k+1}]$, we have

$$\begin{aligned}w(t)=&\mathcal{X}^{M,A,\mu}_{\beta,1,r}(t,-r)\psi(-r)+\int_{-r}^{0}\mathcal{X}^{M,A,\mu}_{\beta,\beta,r}(t,s)\left[\left({}^{C}_{-r^+}D^{\beta}_{\mu}\psi\right)(s)-A\psi(s)\right]d\mu(s)\\&+\int_0^t\mathcal{X}^{M,A,\mu}_{\beta,\beta,r}(t,s)g(s,w(s))d\mu(s)+\sum_{i=1}^{k}\mathcal{X}^{M,A,\mu}_{\beta,1,r}(t,t_i)\,f\left(w\left(t_i\right)\right),\end{aligned}$$

Since it is known that $\mathcal{X}_{\beta,1,r}^{M,A,\mu}(t_k,t_k)=I$, we acquire

$$\begin{aligned} w(t_k^+) =&\mathcal{X}_{\beta,1,r}^{M,A,\mu}(t,-r)\psi(-r)+\int_{-r}^{0}\mathcal{X}_{\beta,\beta,r}^{M,A,\mu}(t,s)\left[\left({}_{-r^+}^{C}D_{\mu}^{\beta}\psi\right)(s)-A\psi(s)\right]d\mu(s)\\ &+\int_0^t\mathcal{X}_{\beta,\beta,r}^{M,A,\mu}(t,s)g(s,w(s))d\mu(s)+\sum_{i=1}^{k}\mathcal{X}_{\beta,1,r}^{M,A,\mu}(t,t_i)\,f\left(w\left(t_i\right)\right)\\ &=w(t_k^-)+\mathcal{X}_{\beta,1,r}^{M,A,\mu}(t_k,t_k)\,f\left(w\left(t_k\right)\right)=w(t_k^-)+f\left(w\left(t_k\right)\right) \end{aligned}$$

which completes the proof. □

4. Existence uniqueness results

Unfortunately, the conditions given in the statements of the problem root is not enough to assure that the solution given in Theorem 3.1 is unique. So we need to make a couple of extra assumptions as follows:

A_1 :: The function g satisfies the Lipschitz condition with $L_g>0$

$$||g(t,w)-g(t,v)||\leq L_g||w-v||,\quad t\in[0,T],\quad w,v\in\mathbb{R}^n,$$

A_2 :: The function f satisfies the Lipschitz condition with $L_f>0$

A_3 :: $\left([\mu(T)-\mu(0)]\,L_g+mL_f\right)\max\left\{\mathcal{X}_{\beta,1,r}^{M,A,\mu}(T,0),\mathcal{X}_{\beta,\beta,r}^{M,A,\mu}(T,0)\right\}<1.$

Theorem 4.1. *Under all assumptions A_1,A_2, A_3, the integral equation given in Theorem 3.1 has a unique solution on $[-r,T]$.*

Proof. Define $G:C\left([-r,T],\mathbb{R}^n\right)\to C\left([-r,T],\mathbb{R}^n\right)$ by

$$\begin{aligned} Gw(t) =&\mathcal{X}_{\beta,1,r}^{M,A,\mu}(t,-r)\psi(-r)+\int_{-r}^{0}\mathcal{X}_{\beta,\beta,r}^{M,A,\mu}(t,s)\left[\left({}_{-r^+}^{C}D_{\mu}^{\beta}\psi\right)(s)-A\psi(s)\right]d\mu(s)\\ &+\int_0^t\mathcal{X}_{\beta,\beta,r}^{M,A,\mu}(t,s)g(s,w(s))d\mu(s)+\sum_{0<t_i<t}\mathcal{X}_{\beta,1,r}^{M,A,\mu}(t,t_i)\,f\left(w\left(t_i\right)\right). \end{aligned}$$

By taking arbitrary $w,v\in C\left([-r,T],\mathbb{R}^n\right)$, one can obtain for $\|Gw(t)-Gv(t)\|$:

$$\begin{aligned} &\leq L_g\int_0^t\left\|\mathcal{X}_{\beta,\alpha,r}^{M,A,\mu}(t,s)\right\|d\mu(s)\left\|w-v\right\|_C+L_f\sum_{0<t_i<t}\left\|\mathcal{X}_{\beta,1,r}^{M,A,\mu}(t,t_i)\right\|\left\|w-v\right\|_C\\ &\leq\left([\mu(T)-\mu(0)]\,L_g+mL_f\right)\max\left\{\mathcal{X}_{\beta,1,r}^{M,A,\mu}(T,0),\mathcal{X}_{\beta,\beta,r}^{M,A,\mu}(T,0)\right\}\left\|w-v\right\|_C. \end{aligned}$$

In the light of A_3, G is a contraction. By Banach fixed point theorem, G has a unique fixed point. □

5. Stability results

In this section, we firstly share fundamental definition and remark to prove that the system (1.1) is Ulam-Hyers stable.

Definition 5.1. If $\forall\epsilon>0$ and for any solution $w\in C\left([0,T],\mathbb{R}^n\right)$ of inequality

$$\left\|{}_{-r^+}^{C}D_{\mu}^{\beta}w(t)-Mw(t)-Aw(t-r)-g(t,w(t))\right\|\leq\epsilon \tag{5.1}$$

then there is a solution $w\in C\left([0,T],\mathbb{R}^n\right)$ of (1.1), and a $\eta>0$ such that

$$\|w(t)-v(t)\|\leq\eta.\varepsilon\quad t\in[0,T] \tag{5.2}$$

then (1.1) is stable in the sense of Ulam-Hyers.

Remark 5.2. A function $w \in C^1([0,T],\mathbb{R}^n)$ is a solution of the inequality (5.1) iff there is at least $h \in C([0,T],\mathbb{R}^n)$ filfulling

- $\|h(t)\| \leq \epsilon \ \ (\epsilon > 0)$,
- ${}_{-r^+}^{C}D_{\mu}^{\beta} w(t) = Mw(t) + Aw(t-r) + g(t,w(t)) + h(t)$.

Theorem 5.3. *Under all of circumstances in Theorem 4.1, the system (1.1) is stable in the sense of Ulam-Hyers.*

Proof. Suppose $w \in C([0,T],\mathbb{R}^n)$ which satisfies the inequality (5.1), and let $v \in C([0,T],\mathbb{R}^n)$ which is the unique solution of system (1.1) with the initial condition $v(t) = w(t)$ for all $t \in [-r,0]$, $w\left(t_i^+\right) - w\left(t_i^-\right) = v\left(t_i^+\right) - v\left(t_i^-\right) = f(w(t_i))$. By keepimg the definition of G and Remark 5.2 in mind, one acquires

$$\|h(t)\| < \epsilon, \quad w(t) = Gw(t) + \int_0^t \mathcal{X}_{\beta,\beta,r}^{M,A,\mu}(t,s) h(s)\, ds,$$

and also $v(t) = (Gv)(t)$ for each $t \in [0,T]$. One gets

$$\|Gw(t) - w(t)\| \leq \int_0^t \left\| \mathcal{X}_{\beta,\beta,r}^{M,A,\mu}(t,s) \right\| \|h(s)\|\, ds \leq [\mu(T) - \mu(0)] \mathcal{X}_{\beta,\beta,r}^{||M||,||A||,\mu}(T,0)\epsilon.$$

We are set to make an estimation $\|v(t) - w(t)\|$:

$$\begin{aligned}
&\|v(t) - w(t)\| \leq \|v(t) - Gw(t)\| + \|Gw(t) - w(t)\| \\
&\leq ([\mu(T) - \mu(0)] L_g + mL_f) \max\left\{ \mathcal{X}_{\beta,1,r}^{M,A,\mu}(T,0), \mathcal{X}_{\beta,\beta,r}^{M,A,\mu}(T,0) \right\} \|v - w\|_C \\
&+ [\mu(T) - \mu(0)] \mathcal{X}_{\beta,\beta,r}^{||M||,||A||,\mu}(T,0)\epsilon,
\end{aligned}$$

which provides

$$\|v - w\|_C \leq \eta\epsilon,$$

where

$$\eta = \frac{[\mu(T) - \mu(0)] \mathcal{X}_{\beta,\beta,r}^{||M||,||A||,\mu}(T,0)}{1 - ([\mu(T) - \mu(0)] L_g + mL_f) \max\left\{ \mathcal{X}_{\beta,1,r}^{M,A,\mu}(T,0), \mathcal{X}_{\beta,\beta,r}^{M,A,\mu}(T,0) \right\}} > 0.$$

The proof is completed. □

6. Relative Controllability Results

In this section we investigate the relative controllability of the impulsive fractional delayed differential systems having Caputo fractional derivatives with respect to another function while it is not only linear but also semilinear.

Definition 6.1. System (1.1) is called relatively controllable, if for the final state $w_\tau \in \mathbb{R}^n$ with time τ, any initial function $\phi \in C^1([-r,0],\mathbb{R}^n)$, and initial function $f \in C(\mathbb{R}^n,\mathbb{R}^n)$, there is a control $u \in L^2(J = [0,T],\mathbb{R}^n)$(the Hilbert space of all square integrable functions) such that system (1.1) has a solution $w \in C^1([-r,\tau],\mathbb{R}^n)$ that holds the initial delayed condition, the initial impulsive condition, and $w(\tau) = w_\tau$.

6.1. **The relative controllability of linear case.** We will consider the following control system

$$\left\{\begin{array}{r} {}_{-r^+}^{C}D_{\mu}^{\beta}w(t) = Mw(t) + Aw(t-r) + Su(t), \quad 0 < t \leq T, \quad r > 0, \\ w(t) = \psi(t), \quad -r \leq t \leq 0, \\ w\left(t_i^+\right) = w\left(t_i^-\right) + f\left(w\left(t_i\right)\right), \quad t_i \in J, \end{array}\right. \tag{6.1}$$

whose solution is given by

$$\begin{aligned} w(t) =& \mathcal{X}_{\beta,1,r}^{M,A,\mu}(t,-r)\psi(-r) + \int_{-r}^{0} \mathcal{X}_{\beta,\beta,r}^{M,A,\mu}(t,s)\left[\left({}_{-r^+}^{C}D_{\mu}^{\beta}\psi\right)(s) - A\psi(s)\right]d\mu(s) \\ &+ \int_{0}^{t} \mathcal{X}_{\beta,\beta,r}^{M,A,\mu}(t,s)Su(s)d\mu(s) + \sum_{0<t_i<t} \mathcal{X}_{\beta,1,r}^{M,A,\mu}\left(t,t_i\right) f\left(w\left(t_i\right)\right). \end{aligned}$$

Theorem 6.2. *The system (6.1) is relatively controllable if and only if the following Gramian matrix*

$$W[0,\tau] = \int_{0}^{\tau} \mathcal{X}_{\beta,\beta,r}^{M,A,\mu}(\tau,s)SS^{*}\mathcal{X}_{\beta,\beta,r}^{M^{*},A^{*},\mu}(\tau,s)d\mu(s)$$

is nonsingular, where . stands for the transpose of a matrix.*

Proof. $\Rightarrow$: Let $W[0,\tau]$ be singular while the system (6.1) is relatively controllable. There is nonzero $\pi \in \mathbb{R}^n$

$$W[0,\tau]\pi = 0.$$

One gets

$$\int_{0}^{\tau} \pi^{*}\mathcal{X}_{\beta,\beta,r}^{M,A,\mu}(\tau,s)SS^{*}\mathcal{X}_{\beta,\beta,r}^{M^{*},A^{*},\mu}(\tau,s)\pi d\mu(s) = 0$$

which provides

$$\pi^{*}\mathcal{X}_{\beta,\beta,r}^{M,A,\mu}(\tau,s)S, \quad 0 \leq s \leq \tau.$$

Based on the relative controllability of the system, we can find u_1 and u_2 for the different final $0, \pi \in \mathbb{R}^n$,respectively so that

$$\pi^{*}\pi = \int_{0}^{\tau} \pi^{*}\mathcal{X}_{\beta,\beta,r}^{M,A,\mu}(\tau,s)S(u_2(s) - u_1(s))d\mu(s) = 0$$

from which $\pi = 0$ is obtained. This is a contradiction.
$\Leftarrow$: By means of the invertibility of the Gramian matrix, it is known that its inverse is well-defined. If one regards the following continuous function

$$u(t) = S^{*}\mathcal{X}_{\beta,\beta,r}^{M^{*},A^{*},\mu}(\tau,t)W^{-1}[0,\tau]\vartheta$$

where

$$\begin{aligned} \vartheta =& w_{\tau} - \mathcal{X}_{\beta,1,r}^{M,A,\mu}(\tau,-r)\psi(-r) - \int_{-r}^{0} \mathcal{X}_{\beta,\beta,r}^{M,A,\mu}(\tau,s)\left[\left({}_{-r^+}^{C}D_{\mu}^{\beta}\psi\right)(s) - A\psi(s)\right]d\mu(s) \\ &- \sum_{0<t_i<t} \mathcal{X}_{\beta,1,r}^{M,A,\mu}\left(\tau,t_i\right) f\left(w\left(t_i\right)\right), \end{aligned}$$

as a control, one can easily observe $w(\tau) = w_{\tau}$, and w fulfills all of the initial conditions. □

6.2. **The relative controllability of semilinear case.** We will consider the following control system

$$(6.2)\quad \begin{cases} {}^{C}_{-r^+}D^{\beta}_{\mu}w(t) = Mw(t) + Aw(t-r) + g(t,w(t)) + Su(t), \quad 0 < t \leq T, \\ w(t) = \psi(t), \quad -r \leq t \leq 0, \quad r > 0, \\ w\left(t_i^+\right) = w\left(t_i^-\right) + f\left(w\left(t_i\right)\right), \quad t_i \in J, \end{cases}$$

whose solution is given by

$$\begin{aligned} w(t) =& \mathcal{X}^{M,A,\mu}_{\beta,1,r}(t,-r)\psi(-r) + \int_{-r}^{0} \mathcal{X}^{M,A,\mu}_{\beta,\beta,r}(t,s)\left[\left({}^{C}_{-r^+}D^{\beta}_{\mu}\psi\right)(s) - A\psi(s)\right]d\mu(s) \\ &+ \int_0^t \mathcal{X}^{M,A,\mu}_{\beta,\beta,r}(t,s)g(s,w(s))d\mu(s) + \sum_{0<t_i<t} \mathcal{X}^{M,A,\mu}_{\beta,1,r}\left(t,t_i\right) f\left(w\left(t_i\right)\right) \\ &+ \int_0^t \mathcal{X}^{M,A,\mu}_{\beta,\beta,r}(t,s)Su(s)d\mu(s) \end{aligned}$$

Unfortunately, we can not control this system without putting extra conditions on the nonlinear function and impulsive function, an extra operator. Now, let us make some assumptions as follows:

A_4 **::** The operator $M : L^2\left(J,\mathbb{R}^n\right) \to \mathbb{R}^n$

$$Mu = \int_0^{\tau} \mathcal{X}^{M,A,\mu}_{\beta,\beta,r}(\tau,s)Su(s)d\mu(s),$$

has an inverse operator M^{-1} which take values in $L^2\left(J,\mathbb{R}^n\right)/kerM$.

Let X_1 and X_2 be Banach spaces. $B(X_1,X_2)$ is the Banach space consisting of all linear bounded operators endowed with the norm $\|.\|_B$

For simplicity, we will set the following notations:

$$R := \left\|M^{-1}\right\|_{B(\mathbb{R}^n, L^2(J,\mathbb{R}^n)/kerM,)},$$

$$R_1 := \left\|\mathcal{X}^{M,A,\mu}_{\beta,1,r}(t,-r)\psi(-r)\right\| + \left\|\int_{-r}^{0} \mathcal{X}^{M,A,\mu}_{\beta,\beta,r}(t,s)\left[\left({}^{C}_{-r^+}D^{\beta}_{\mu}\psi\right)(s) - A\psi(s)\right]d\mu(s)\right\|,$$

$$R_2 := \sum_{0<t_i<t} \left\|\mathcal{X}^{M,A,\mu}_{\beta,1,r}\left(t,t_i\right)\right\| |f(0)| + [\mu(T) - \mu(0)]\mathcal{X}^{||M||,||A||,\mu}_{\beta,\alpha,r}(T,0) \max_{[0,T]} |g(t,0)|,$$

$$R_3 := \left(L_f \sum_{0<t_i<t} \left\|\mathcal{X}^{M,A,\mu}_{\beta,1,r}\left(t,t_i\right)\right\| + L_g[\mu(T) - \mu(0)]\mathcal{X}^{||M||,||A||,\mu}_{\beta,\alpha,r}(T,0)\right)\|w\|_C.$$

From Remark 3.3[13], it is known that

$$R = \sqrt{\|W^{-1}[0,\tau]\|}.$$

Theorem 6.3. *Suppose that $1 \geq \beta > 0.5$. Under the assumptions A_1 :,A_2 :, and A_4 : are fulfilled. Then the system (6.2) is relatively controllable if*

$$\left(1 + R\|S\| \max\{1, R_3\}\right) R_3 < 1.$$

Proof. Based on the assumption A_4 :, one can define the following control function

$$\begin{aligned} u_w =& M^{-1}\Big[w_\tau - \mathcal{X}^{M,A,\mu}_{\beta,1,r}(\tau,-r)\psi(-r) \\ &- \int_{-r}^{0} \mathcal{X}^{M,A,\mu}_{\beta,\beta,r}(\tau,s)\left[\left({}^{C}_{-r^+}D^{\beta}_{\mu}\psi\right)(s) - A\psi(s)\right]d\mu(s) \\ &- \sum_{0<t_i<t} \mathcal{X}^{M,A,\mu}_{\beta,1,r}(\tau,t_i)\, f\left(w\left(t_i\right)\right) - \int_0^t \mathcal{X}^{M,A,\mu}_{\beta,\beta,r}(t,s)g(s,w(s))d\mu(s)\Big]. \end{aligned}$$

By executing this control function, one can also define $\mathcal{K}: C(J,\mathbb{R}^n)\to C(J,\mathbb{R}^n)$ by

$$\begin{aligned} \mathcal{K}w(t) =& \mathcal{X}^{M,A,\mu}_{\beta,1,r}(t,-r)\psi(-r) + \int_{-r}^{0} \mathcal{X}^{M,A,\mu}_{\beta,\beta,r}(t,s)\left[\left({}^{C}_{-r^+}D^{\beta}_{\mu}\psi\right)(s) - A\psi(s)\right]d\mu(s) \\ &+ \int_0^t \mathcal{X}^{M,A,\mu}_{\beta,\beta,r}(t,s)g(s,w(s))d\mu(s) + \sum_{0<t_i<t} \mathcal{X}^{M,A,\mu}_{\beta,1,r}(t,t_i)\, f\left(w\left(t_i\right)\right) \\ &+ \int_0^t \mathcal{X}^{M,A,\mu}_{\beta,\beta,r}(t,s)Su_w(s)d\mu(s). \end{aligned}$$

Now, we need to determine such a radius r for $D_r := \{w\in C(J,\mathbb{R}^n) : \|w\|_C \le r\}$ which is a convex, closed and bounded subset that $\mathcal{K}(D_r)\subseteq D_r$. To do this, start with the norm of the control function:

$$\|u_w\| \le R\left(R_1 + R_2 + R_3\|w\|_C\right).$$

The norm of the operator $\mathcal{K}w(t)$ for $w\in D_r$ is

$$\|\mathcal{K}w(t)\| \le R_1 + R_2 + R_3\|w\|_C + R\|S\|\left(R_1 + R_2 + R_3\|w\|_C\right).$$

If we take

$$r = \frac{\left(1+R\|S\|\right)\left(R_1+R_2\right) + R\|S\|\,\|w_\tau\|}{1-\left(1+R\|S\|\max\{1,R_3\}\right)R_3} > 0,$$

the desired thing is demonstrated. Now we will separate $\mathcal{K}$ in two different operators as follows:

$$\begin{aligned} \mathcal{K}_1 w(t) =& \mathcal{X}^{M,A,\mu}_{\beta,1,r}(t,-r)\psi(-r) + \int_{-r}^{0} \mathcal{X}^{M,A,\mu}_{\beta,\beta,r}(t,s)\left[\left({}^{C}_{-r^+}D^{\beta}_{\mu}\psi\right)(s) - A\psi(s)\right]d\mu(s) \\ &+ \sum_{0<t_i<t} \mathcal{X}^{M,A,\mu}_{\beta,1,r}(t,t_i)\, f\left(w\left(t_i\right)\right) + \int_0^t \mathcal{X}^{M,A,\mu}_{\beta,\beta,r}(t,s)Su_w(s)d\mu(s), \quad t\in J, \end{aligned}$$

and

$$\mathcal{K}_2 w(t) = \int_0^t \mathcal{X}^{M,A,\mu}_{\beta,\beta,r}(t,s)g(s,w(s))d\mu(s) \quad t\in J.$$

For $w, v\in D_r$, one gets

$$\|u_w(t) - u_v(t)\| \le RR_3\|w-v\|_C$$

and

$$\begin{aligned}\|\mathcal{K}_1 w(t)-\mathcal{K}_1 v(t)\| &\leq [\mu(T)-\mu(0)]\mathcal{X}_{\beta,\beta,r}^{||M||,||A||,\mu}(T,0)\,\|S\|\,\|u_w(t)-u_v(t)\| \\ &+ L_f \sum_{0<t_i<t}\left\|\mathcal{X}_{\beta,1,r}^{M,A,\mu}(t,t_i)\right\|\|w-v\|_C \\ &\leq [\mu(T)-\mu(0)]\mathcal{X}_{\beta,\beta,r}^{||M||,||A||,\mu}(T,0)\,\|S\|\,RR_3\,\|w-v\|_C \\ &+ L_f \sum_{0<t_i<t}\left\|\mathcal{X}_{\beta,1,r}^{M,A,\mu}(t,t_i)\right\|\|w-v\|_C \\ &\leq (1+R\,\|S\|\max\{1,R_3\})\,R_3\,\|w-v\|_C\end{aligned}$$

which gives that $\mathcal{K}_1$ is a contraction.

Assume that $w_n \in D_r$ with $w_n \to w$ in D_r. Since g is continuous, $g(t,w_n(t)) \to g(t,w(t))$. By using dominated convergence theorem

$$\|\mathcal{K}_2 w_n(t)-\mathcal{K}_2 w(t)\| \leq \int_0^t \left\|\mathcal{X}_{\beta,\beta,r}^{M,A,\mu}(t,s)\right\|\|g(s,w_n(s))-g(s,w(s))\|\,d\mu(s)$$

goes to zero as n tends to ∞. Thus, $\mathcal{K}_2$ is continuous on D_r. The last task is to show that $\mathcal{K}_2$ is compact. For $w \in D_r$, $0<t<t+h<\tau$

$$\begin{aligned}\mathcal{K}_2 w(t+h)-\mathcal{K}_2 w(t) &= \int_t^{t+h}\mathcal{X}_{\beta,\beta,r}^{M,A,\mu}(t+h,s)g(s,w(s))d\mu(s) \\ &+ \int_0^t\left(\mathcal{X}_{\beta,\beta,r}^{M,A,\mu}(t+h,s)-\mathcal{X}_{\beta,\beta,r}^{M,A,\mu}(t,s)\right)g(s,w(s))d\mu(s).\end{aligned}$$

Introduce the below notations:

$$\lambda_1 := \int_t^{t+h}\mathcal{X}_{\beta,\beta,r}^{M,A,\mu}(t+h,s)g(s,w(s))d\mu(s),$$

$$\lambda_2 := \int_0^t\left(\mathcal{X}_{\beta,\beta,r}^{M,A,\mu}(t+h,s)-\mathcal{X}_{\beta,\beta,r}^{M,A,\mu}(t,s)\right)g(s,w(s))d\mu(s).$$

With an easy calculation, one can acquire

$$\|\lambda_1\| = \left(L_g\,\|w\|_C + \max_{t\in[0,T]}|g(t,0)|\right)\int_t^{t+h}\left\|\mathcal{X}_{\beta,\beta,r}^{M,A,\mu}(t+h,s)\right\|ds \to 0$$

$$\|\lambda_2\| = \left(L_g\,\|w\|_C + \max_{t\in[0,T]}|g(t,0)|\right)\int_0^{t}\left\|\mathcal{X}_{\beta,\beta,r}^{M,A,\mu}(t+h,s)-\mathcal{X}_{\beta,\beta,r}^{M,A,\mu}(t,s)\right\|ds \to 0$$

as $h \to 0$. As a result, one acquires

$$\|\mathcal{K}_2 w(t+h)-\mathcal{K}_2 w(t)\| \leq \|\lambda_1\|+\|\lambda_2\| \to 0 \quad \text{as} \quad h\to 0.$$

$\mathcal{K}_2(D_r)$ is uniformly bounded because one easily reach to the following upper bound for all members of $\mathcal{K}_2(D_r)$ with the familiar computations,

$$\|\mathcal{K}_2\| \leq \left(L_g\rho + + \max_{t\in[0,T]}|g(t,0)|\right)\tau\mathcal{X}_{\beta,\beta,r}^{M,A,\mu}(\tau,0).$$

Because of the equicontinuity and uniform boundedness of $\mathcal{K}_2$, Arzela-Ascoli theorem provides $\mathcal{K}_2$ is compact. Krasnoselskii's fixed point theorem guarantees that $\mathcal{K}$ has a fixed point $w \in D_r$. □

7. Conclusion

The current paper is in brief devoted to investigating the existence and uniqueness of the solution and examining stability and controllability of the system.

For a next problem, neutral version can be taken into consideration and investigated in terms of all aspects considered in the present paper.

References

[1] N. I. Mahmudov, Delayed perturbation of Mittag-Leffler functions and their applications to fractional linear delay differential equations, Mathematical Methods in the Applied Sciences, vol.42, pp.5489–5497, (2019).
[2] M. Aydin, N.I. Mahmudov, H. Aktuğlu, E. Baytunç, M.S. Atamert, On a study of the representation of solutions of a Ψ-Caputo fractional differential equations with a single delay, Electronic Research Archive, vol.30, pp.1016–1034, (2022).
[3] A. Mustafa, N.I. Mahmudov, Iterative learning control for impulsive fractional order time-delay systems with nonpermutable constant coefficient matrices,International Journal of Adaptive Control and Signal Processing, vol.36, N.1, pp.1419–1438, (2022).
[4] D. Y. Khusainov, G. V. Shuklin, Linear autonomous time-delay systemwith permutation matrices solving, Stud Univ Žilina, vol.17, pp.101–108, (2003).
[5] M. Li, J.R. Wang, Exploring delayed Mittag-Leffler type matrix functions to study finite time stability of fractional delay differential equations, Applied Mathematics and Computation, vol.324, pp.254–265, (2018).
[6] N.I. Mahmudov Multi-delayed perturbation of Mittag-Leffler type matrix functions, Journal of Mathematical Analysis and Applications, vol.505, 125589, (2022).
[7] A.M. Elshenhab, X.T. Wang, Representation of solutions for linear fractional systems with pure delay and multiple delays, Mathematical Methods in the Applied Sciences, vol.44, pp.12835–12850, (2021).
[8] A.M. Elshenhab, X.T. Wang, Representation of solutions of linear differential systems with pure delay and multiple delays with linear parts given by non-permutable matrices, Applied Mathematics and Computation, vol.410, 126443, (2021).
[9] N.I. Mahmudov, M. Aydın, Representation of solutions of nonhomogeneous conformable fractional delay differential equations. Chaos Solitons Fractals, vol.150, 111190, (2021).
[10] N.I. Mahmudov, Representation of solutions of discrete linear delay systems with non permutable matrices. Applied Mathematics Letters, vol.85, pp.8–14, (2018).
[11] L. Liu, Q. Dong, G. Li, Exact solutions and Hyers–Ulam stability for fractional oscillation equations with pure delay, Applied Mathematics Letters, vol.112 106666, (2021).
[12] C. Liang, J. Wang, D. O'Regan, Controllability of nonlinear delay oscillating systems, Electronic Journal of Qualitative Theory of Differential Equations, vol.2017, pp.1–18, (2017) .
[13] J. Wang, Z. Luo, M. Fečkan, Relative controllability of semilinear delay differential systems with linear parts defined by permutable matrices, European Journal of Control, vol.38, pp.39–6, (2017).
[14] D.Y. Khusainov, G.V. Shuklin, Relative controllability in systems with pure delay, International Journal of Applied Mathematics. vol.2, pp.210–221, (2005).
[15] Z. You, M. Fečkan, J. Wang, Relative Controllability of Fractional Delay Differential Equations via Delayed Perturbation of Mittag-Leffler Functions, Journal of Computational and Applied Mathematics, vol.378, 112939, (2020). 10.1016/j.cam.2020.112939.
[16] D.D. Bainov, and P.S. Simeonov, Systems with Impulse Effect. Ellis Horwood Series:Mathematics and Its Applications, Ellis Horwood, Chichester, (1989).
[17] D.D. Bainov, and P.S. Simeonov, Impulsive Differential Equations: Periodic Solutions and Applications, Pitman Monographs and Surveys in Pure and Applied Mathematics, vol. 66, Longman Scientific & Technical, Harlow; JohnWiley & Sons, New York, (1993).
[18] V. Lakshmikantham, D.D. Bainov, and P.S. Simeonov, Theory of Impulsive Differential Equations, Series in Modern Applied Mathematics, vol. 6, World Scientific, New Jersy, (1989).
[19] A.M. Samoilenko, N.A. Perestyuk, Impulsive Differential Equations, World Scientific Series on Nonlinear Science. Series A:Monographs and Treatises, vol. 14, World Scientific, New Jersey, (1995). ISBN: 978-981-02-2416-5.

(Mustafa AYDIN) Yuzuncu Yil University, Department of Medical Services and Techniques, 65080, Van, Turkey
Email address: m.aydin@yyu.edu.tr

IFSCOM-E 2023
9th Ifs And Contemporary Mathematics and Engineering Conference
08-11 July 2023 Tarsus, Mersin, Türkiye
ISBN: 978-605-68670-8-8
pp: 50-58

SECOND ORDER MODEL REDUCTION OF HIGHER ORDER SYSTEMS AND PID CONTROLLER DESIGN

A.YÜCE

Abstract. Reduced order systems are used to avoid computational complexity in higher order plant models. Low-order or standardized transfer functions are more suitable for controller design. In addition, Salem presented a non-overshoot and analytical PID controller design technique for standard quadratic systems. In this study, efficient PID controller design for high-order systems is carried out with the help of a second-order reduced model. The curve fitting technique is used to reduce the model to the second-order structure. The open loop unit step response of the higher order system is fitted with the parametric unit step response of the standard quadratic system. Particle Swarm Optimization (PSO) algorithm is used to detect unknown ζ and ω_n parameters. The analytical method proposed by Salem has been applied for the PID controller design of second-order model. Thus, PID controller design for any higher order system is performed in two stages using model reduction and model based PID controller design techniques. It has been seen that the efficient PID controller designed for the second order equivalent models is a suitable design for the higher order system.

1. Introduction

Closed-loop PID control systems have attracted the attention of academic circles and gained an important place in industrial applications due to their ease of implementation and effective control capabilities [1, 2]. It has found widespread use in process control. Due to this intense interest, many studies have been carried out especially for the optimal control problem of the classical PID control structure [2, 3, 4, 5]. Many artificial intelligence techniques and optimization algorithms have been mobilized for self-tuning of the PID controller in order to provide robust control performance in real systems that may contain noise, parameter and model uncertainties [6, 7].
In the literature, the PID controller design problem has been studied in three parts [8]: (i) analytical methods [2, 9], (ii) graphical methods [10, 11] and (iii) empirical and intelligent methods [4, 7]. Analytical methods have generally produced analytical formulas for the determination of PID gains that can provide the targeted

Date: July, 8, 2023.
Key words and phrases. Higher order system, Second order system, Model reduction, Particle Swarm Optimization, PID controller design.

control response for system models of low order generalized structure. If the system to be controlled has a low order generalized system model, the gains that provide the targeted control system performance can be easily calculated with the help of simple analytical formulas. However, practical control systems often have time-delay and high-order system models. Time-delayed or large-scale complex systems can be represented by higher order models. For example, time-delayed systems can be converted to high-order approximate system models with the Pade approach. In this context, the conversion of these models to low-order generalized system models provides important conveniences for the application of analytical methods in high-order systems. Otherwise, the design of the analytical controller turns into a problem whose solution complexity increases exponentially as the system scale increases. At this point, model order reduction techniques have gained importance. Model order reduction methods are expected to produce low-order standard models that provide responses as close as possible to higher-order systems, especially in the low-frequency region where control systems operate effectively.

Some of the main model reduction methods in the literature are as follows: SBL based model reduction method [12] Model reduction with Pade convergence method [13], Routh convergence techniques [14] and continuous fraction method [15]. In this study, we propose a model reduction method based on the standard quadratic system for model reduction. In the proposed method, first, it is aimed to plot unit step response of a high-order system. Second, the error between the unit step response of the higher order system and the parametric unit step response of the second order standard system is calculated. Finally, according to the integral performance criteria, the standard quadratic system parameters ζ and ω_n, which minimize the error, are determined with the PSO algorithm. The appropriate PID controller design for the second-order approximate model obtained by the PSO algorithm was carried out with the model-based PID design formulation proposed by Salem [9]. These formulations have been proposed for the quadratic system to provide non-overshoot and fast enough PID responses. As a sample application, the design of PID controller gains for an eighth-order system has been carried out and the efficiency of the method has been evaluated.

The remainder of this work is organized as follows: Section 2 describes the PSO algorithm and computation method of the approximate quadratic model. Two numerical examples are given in Section 3. In these examples, the proposed method on higher order system models is examined. The results are presented in Section 4.

2. Methodology

2.1. **Particle Swarm Optimization (PSO).**

Particle swarm optimization is a nature-inspired technique developed by Kennedy-Eberhart [16, 17, 18, 19]. PSO is a simple and powerful optimization algorithm. This algorithm has been successfully applied in various fields of science and engineering. Initially, the PSO system randomly chose solution values called populations. Each solution is called a particle. Also, there is a randomly chosen velocity for each particular particle. It is called the best position (P_{best}) for each particle in the algorithm. Particles move and follow Pbest and there is a fitness value for each Pbest. The largest fitness value is called the global best (G_{best}). There are two main equations in the PSO algorithm, velocity and position vectors, and these

are shown in (1) and (2), respectively [20].

$$v_{ij}(t+1) = wv_{ij}(t) + r_1c_1(p_{ij}(t) - x_{ij}(t)) + r_2c_2(g_{ij}(t) - x_{ij}(t)) \tag{2.1}$$

$$x_{ij}(t+1) = x_{ij}(t) + v_{ij}(t+1) \tag{2.2}$$

Where, r_1 and r_2 are two random vectors and their values are between 0 and 1. The c_1 and c_2 parameters represent acceleration constants or learning parameters [20]. The v parameter represents the speed, and the x parameter represents the position. The parameters g and p are G_{best} and P_{best}, respectively.

2.2. **Calculation of the approximate standard quadratic system.**
The schematic representation of the proposed procedure to determine the approximate standard quadratic transfer function using the integral performance index and the error minimizing PSO algorithm is given in Figure 1.

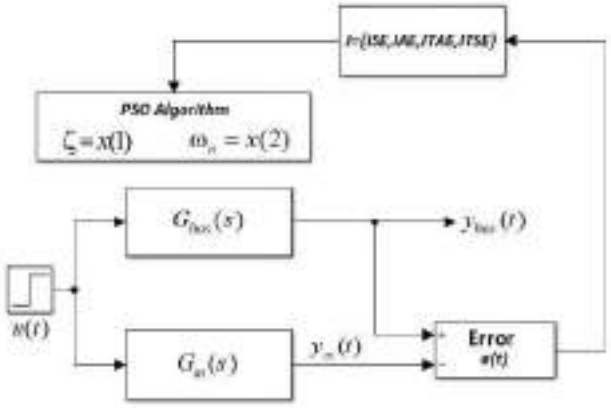

FIGURE 1. The model of the proposed procedure

In Figure 1, $G_{hos}(s)$ and $y_{hos}(t)$ denote the transfer function of the higher-order system and the open-loop unit step response, respectively. $G_{hos}(s)$ is given in (2.3) (3) and it is possible to obtain its open loop unit step response easily.

$$G_{hos} = \frac{a_m s^m + a_{m-1}s^{m-1} + ... + a_1 s + a_0}{b_n s^n + b_{n-1}s^{n-1} + ... + b_1 s + b_0} \{a_m, b_n\} \in R, \{m, n\} \in Z, n > m \tag{2.3}$$

The standard quadratic system model is given in (2.4).

$$G_{hos} = \frac{Y(s)}{U(s)} = \frac{\omega_n^2}{s^2 + 2\zeta\omega_n s + \omega_n^2} \tag{2.4}$$

In (2.4), u denotes the input, y denotes the output, ζ is the damping ratio, and ω_n is the natural frequency. The open loop unit step response of a standard quadratic transfer function is written in time domain as in (2.5).

$$y(t) = 1 - e^{(-\zeta\omega_n t)}(\cos(\omega_n\sqrt{(1-\zeta^2)}t) + (\zeta/\sqrt{(1-\zeta^2)})\sin(\omega_n\sqrt{(1-\zeta^2)}t)) \tag{2.5}$$

It is defined as $\zeta = x(1)$ and $\omega_n = x(2)$ in (2.5). Thus, the quadratic model is reconstructed in the form of (2.6). Where, the $y_m(t)$ is the parametric form of the open-loop unit step response of (2.4).

(2.6)
$$y_m(t) = 1 - e^{(-x(1)x(2)t)}(\cos(x(2)\sqrt{(1-x(1)^2)}t) + (x(1)/\sqrt{(1-x(1)^2)})\sin(x(2)\sqrt{(1-x(1)^2)}t))$$

For the curve fitting in the time domain, we can write the error as (2.7).

$$e(t) = [y_m(t) - y_{norm}(t)] \tag{2.7}$$

Where, $y_{norm}(t)$ specifies the function in which the steady state value of $y_{hos}(t)$ is normalized to 1. Normalization is achieved with a gain multiplier K. Normalization coefficient K and $y_{norm}(t)$ are calculated as in (2.8)-(2.9) respectively.

$$K = \frac{b_0}{a_0} \tag{2.8}$$

$$Ky_{hos}(t) \tag{2.9}$$

The optimum parameters ζ and ω_n can be obtained by minimizing the error signal using integral performance criteria and PSO algorithm. Integral performance criteria are defined as cost functions in optimization algorithms and provide minimization. Firstly, the integral of the square of error (ISE) and the integral of the absolute value of the error (IAE) performance criteria were used by Graham and Lathrop [21] in 1953. Then, the absolute value of the time-weighted error (ITAE) and the integral of the square of the time-weighted error (ITSE) were developed by [22]. These performance criteria and its mathematical expressions in the literature are given in (2.10) [23].

$$J_{ISE} = \int_0^t e^2(t)dt \tag{2.10}$$

The integral performance criteria presented in (2.10) work as a cost function in the PSO algorithm. The proposed process determines the ζ and ω_n parameters that minimize the cost function. In the program, the number of variables is 2, the lower limit is 0.001, the upper limit is 10, the number of particles is 20, the maximum number of iterations is 40, acceleration constants $c_1 = c_2 = 2$, $w_{max} = 0.9$ and $w_{min} = 0.4$ are selected to calculate the inertia weight value.

Equations (2.11) and (2.12)are used to arrive at the quadratic model transfer function as a result of the ζ and ω_n parameters determined by the PSO algorithm.

$$G_{norm}(s) \approx KG_{hos}(s) \tag{2.11}$$

$$G_m(s) = \frac{1}{K}G_{norm}(s) \approx G_{hos}(s) \tag{2.12}$$

2.3. **PID controller design for the standard second order system.** PID controller structure in its general form is written in (2.13).

$$C(s) = k_p + \frac{k_i}{s} + k_d s \tag{2.13}$$

Salem proposed the design formulas given in (2.14) for efficient PID design that provides non-overshoot and fast control response for second order systems in standard form [9].

$$k_p = 1; k_i = \frac{\omega_n}{2\zeta}; k_d = \frac{1}{2\zeta\omega_n} \tag{2.14}$$

3. Examples

Let's consider the higher order transfer function given in (3.1).

(3.1)

$$G_{hos} = \frac{8.51s^6 + 169s^5 + 1279s^4 + 4702s^3 + 8834s^2 + 7990s + 2675}{s^8 + 22.52s^7 + 191.1s^6 + 782.9s^5 + 1684s^4 + 2031s^3 + 1475s^2 + 632.1s + 117.6}$$

In this example, an eighth order transfer function is chosen [24]. The open loop unit step response of the higher order system is fitted with the parametric unit step response of the standard quadratic system. Curve fitting was done using ISE criterion and PSO algorithm. As a result of the PSO algorithm, $\zeta = x(1) = 0.6876$ and $\omega_n = x(2) = 0.5908$.

The normalization gain is calculated as $K = 0.0494$. Thus, $G_{norm}(s)$ and $G_m(s)$ are obtained as (3.2)-(3.3), respectively.

$$G_{norm}(s) = \frac{0.3491}{s^2 + 0.8125s + 0.3491} \tag{3.2}$$

$$G_m(s) = \frac{7.94}{s^2 + 0.8125s + 0.3491} \tag{3.3}$$

In the literature, the second-order approximate model using the SBL method is given in (3.4) [12].

$$G_{SBL}(s) = \frac{10.17}{s^2 + 1.067s + 0.4420} \tag{3.4}$$

In Figure 2, the Bode diagrams of the higher order transfer function, the reduced second order approximation model $G_m(s)$ and model reduction method using SBL are compared. It was observed that the amplitude and phase responses were quite close to each other in the low frequency region. The proposed method gives better frequency response than the SBL method. The mean square error in the Bode diagram is 0.5168 for the proposed method and 0.5925 for the SBL method. This indicates that a good reduced approximate model can be obtained for proposed prosedure.

In Figure 3, the open loop unit step responses of $G_{hos}(s)$, $G_m(s)$ and G_{SBL} are compared. It was observed that the rise and settling times in the open loop unit

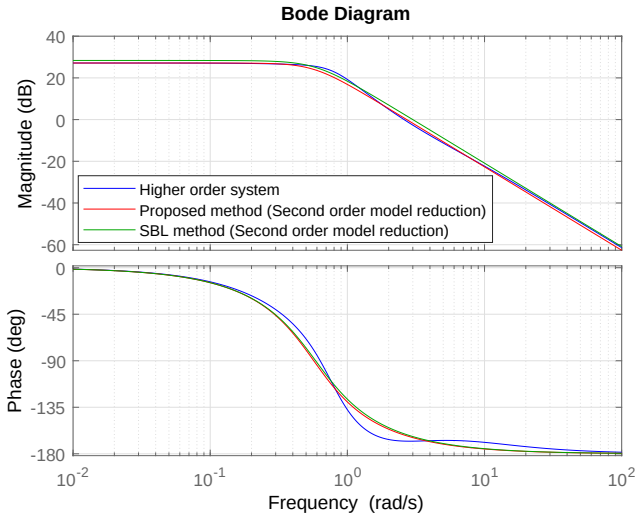

FIGURE 2. Comparison of Bode diagrams of higher order system, $G_m(s)$ and G_{SBL}.

step responses were quite close, and there was a slight difference in the maximum overshoot. The mean square errors of $G_m(s)$ and G_{SBL} are 0.2625 and 0.2878, respectively.

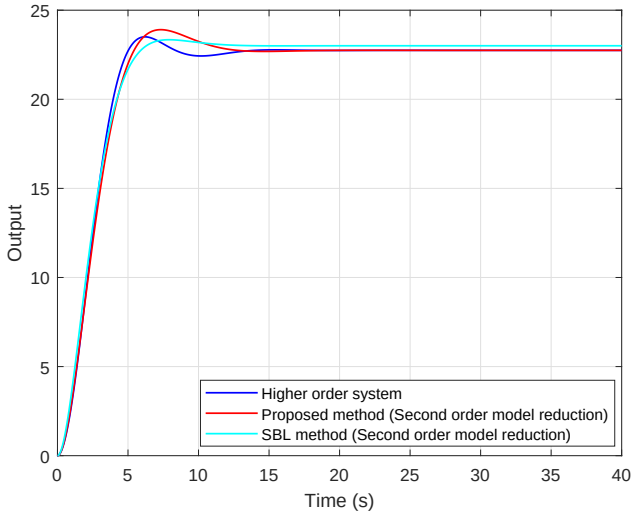

FIGURE 3. Comparison of open loop unit step responses of higher order system, $G_m(s)$ and G_{SBL}.

For the second-order reduced system model, the Salem PID design that provides a non-overshoot control response is arranged according to (2.14). Thus, the PID parameters for normalized transfer function are computed as (3.5).

$$k_{p\_norm} = 1; k_{i\_norm} = 0.4297; k_{d\_norm} = 1.2308 \tag{3.5}$$

The PID parameters for the model transfer function $G_m(s)$ are calculated as (3.6) depending on the normalization gain.

$$k_{p\_m} = 1.\frac{1}{K} = 22.7466; k_{i\_m} = 0.4297.\frac{1}{K} = 9.774; k_{d\_m} = 1.2308.\frac{1}{K} = 28 \tag{3.6}$$

In addition, the PID parameters calculated according to the second-order transfer function determined using the SBL method are given in (3.7).

(3.7)

$$k_{p\_SBL} = 1.\frac{1}{K} = 22.7466; k_{i\_SBL} = 0.4142.\frac{1}{K} = 9.422; k_{d\_SBL} = 0.9372.\frac{1}{K} = 21.32$$

In Figure 4, the unit step response of closed loop control system with designed PID controller for both proposed method and SBL method are shown.

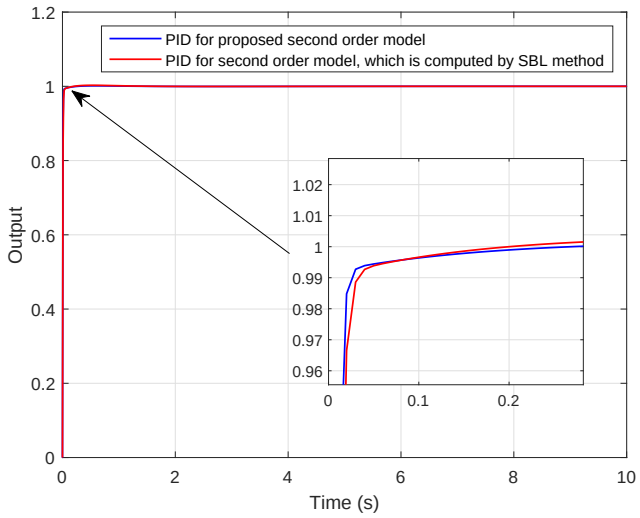

FIGURE 4. Closed-loop unit step response of PID controllers designed by model order reduction method for higher order system

The control performances of the PID controllers determined by the proposed method and the SBL method for the high-order system are given in Table 1. From the performance data in Table 1, it is seen that the proposed method makes more successful model reduction and PID controller design.

Table 1: Performance characteristics of closed loop control system for different methods.

Methods	Rise Time (s)	Settling Time (s)	Peak Time (s)	Overshoot (%)
Proposed Model Reduction	0.0089	0.0194	0.5800	0.1374
SBL Model Reduction	0.0138	0.0261	0.5300	0.2836

4. Conclusion

In this study, second-order approximate equivalent models of a higher-order transfer function were obtained by the PSO algorithm and integral performance criteria. In the sample application, it has been seen that the amplitude, phase, and unit step responses of the second-order reduced model can get quite close to the responses of the higher-order system. It has been seen that the PID controller, which is analytically designed for the second-order reduced model, can respond appropriately within the higher-order model. Thus, analytical controller design within higher order systems has been simplified and optimal PID design formulations proposed for second order systems have been made available for higher order systems. Future work can be done on obtaining approximate equivalent models for time-delayed systems.

References

[1] K. J. Åström and T. Hägglund, The future of PID control, Control engineering practice, Vol. 9, N. 11, pp. 1163-1175, (2001).
[2] K. J. Åström and T. Hägglund, PID controllers: theory, design, and tuning. Isa Research Triangle Park, NC, (1995).
[3] J.-G. Juang, R.-W. Lin, and W.-K. Liu, Comparison of classical control and intelligent control for a MIMO system, Applied Mathematics and computation, Vol. 205, N. 2, pp. 778-791, (2008).
[4] M. S. Saad, H. Jamaluddin, and I. Z. M. Darus, Implementation of PID controller tuning using differential evolution and genetic algorithms, International Journal of Innovative Computing, Information and Control, Vol. 8, N. 11, pp. 7761-7779, (2012).
[5] R. Sanchis, J. A. Romero, and P. Balaguer, Tuning of PID controllers based on simplified single parameter optimisation, International Journal of Control, Vol. 83, N. 9, pp. 1785-1798, (2010).
[6] Z.-Y. Zhao, M. Tomizuka, and S. Isaka, Fuzzy gain scheduling of PID controllers, IEEE transactions on systems, man, and cybernetics, Vol. 23, N. 5, pp. 1392-1398, (1993).
[7] D. Karaboga and B. Akay, Proportional—integral—derivative controller design by using artificial bee colony, harmony search, and the bees algorithms, Proceedings of the Institution of Mechanical Engineers, Part I: Journal of Systems and Control Engineering, Vol. 224, N. 7, pp. 869-883, (2010).
[8] V. Nicolau, On PID controller design by combining pole placement technique with symmetrical optimum criterion, Mathematical Problems in Engineering, Vol. 2013, (2013).
[9] F. A. Salem, New efficient model-based PID design method, European scientific journal, Vol. 9, N. 15, pp. 181-199, (2013).
[10] K. J. Åström and T. Hägglund, Automatic tuning of simple regulators with specifications on phase and amplitude margins, Automatica, Vol. 20, N. 5, pp. 645-651, (1984).
[11] Y. Tang and R. Ortega, Adaptive tuning to frequency response specifications, Automatica, Vol. 29, N. 6, pp. 1557-1563, (1993).
[12] B. B. Alagöz, F. N. Deniz, and N. Tan, Yüksek dereceli sistemlerin kararlılık sınır eğrileri ile ikinci derece yaklaşık modele indirgenmesi ve uygun PID kontrolör tasarımı, Otomatik Kontrol Ulusal Kongresi, Kocaeli, Türkiye, (2014).

[13] T.N. Lucas, Constrained optimal Padé model reduction, J. Dyn. Sys., Meas., Control, Vol. 119, N.4, pp. 685-690, (1997).
[14] D. K. Sambariya, O. Sharma, Routh approximation: an approach of model order reduction in SISO and MIMO systems, Indonesian Journal of Electrical Engineering and Computer Science, Vol. 2, N.3, pp. 486-500, (2016).
[15] B. B.Duddeti, Order reduction of large-scale linear dynamic systems using balanced truncation with modified Cauer continued fraction, IETE Journal of Education, pp. 1-12, (2023). 10.1080/09747338.2023.2178530
[16] Y. Shi and R. C. Eberhart, Empirical study of particle swarm optimization, in Proceedings of the 1999 congress on evolutionary computation-CEC99, Vol. 3, pp. 1945-1950, (1999).
[17] J. Kennedy and R. Eberhart, Particle swarm optimization, in Proceedings of ICNN'95-international conference on neural networks, Vol. 4, pp. 1942-1948, (1995).
[18] Y. Shi, Particle swarm optimization: developments, applications and resources, in Proceedings of the 2001 congress on evolutionary computation, 2001, Vol. 1, pp. 81-86, (2001).
[19] Y. Shi and R. C. Eberhart, Parameter selection in particle swarm optimization, in Evolutionary Programming VII: 7th International Conference, EP98 San Diego, California, USA, March 25–27, 1998 Proceedings 7, 1998: Springer, pp. 591-600, (1998).
[20] X.-S. Yang, Nature-inspired optimization algorithms. Academic Press, (2020).
[21] D. Graham and R. C. Lathrop, The synthesis of optimum transient response: criteria and standard forms, Transactions of the American Institute of Electrical Engineers, Part II: Applications and Industry, Vol. 72, N. 5, pp. 273-288, (1953).
[22] D. Atherton and A. Boz, Using standard forms for controller design, in UKACC International Conference on Control'98 (Conf. Publ. No. 455), 1998: IET, pp. 1066-1071, (1998).
[23] S. B. Joseph, E. G. Dada, A. Abidemi, D. O. Oyewola, and B. M. Khammas, Metaheuristic algorithms for PID controller parameters tuning: Review, approaches and open problems, Heliyon, Vol. 8, pp. 1-29 (2022).
[24] R. Mansouri, M. Bettaye, S. Djennoune, Approximation of high order integer systems by fractional order reduced-parameters models, Mathematical and Computer Modelling, Vol. 51, pp. 53-62 (2010).

Malatya Turgut Özal University, Department of Electrical and Electronics Engineering, 44300, Malatya, Turkey

Email address: ali.yuce@ozal.edu.tr

IFSCOM-E 2023
9th Ifs And Contemporary Mathematics and Engineering Conference
08-11 July 2023 Tarsus, Mersin, Türkiye
ISBN: 978-605-68670-8-8
pp: 59-64

VISLIT-TEST: DESIGNING EFFECTIVE VISUALIZATION LITERACY ASSESSMENT TEST

ELIF E. FIRAT

0000-0001-9497-7928

Abstract. Data volume and complexity continue to increase, and the ability to comprehend and interpret visual representations becomes crucial for making informed decisions and identifying meaningful insights. Understanding the ability of users to analyze and extract relevant insights from visuals requires evaluating their visualization literacy skills. However, creating an efficient visualization literacy assessment test is a non-trivial task. This paper recommends key practices for creating assessment tests to gauge users' visualization literacy skills. These practices are presented based on designing an effective visualization literacy assessment and the structure of the literacy test.

1. Introduction

Visualizations are graphical representations of data that can be used to make complex information more understandable. The significance of understanding and comprehending data visualizations is growing as data expands rapidly. As the exploration and analysis of vast and complex datasets increasingly rely on visual representations, the need for individuals without expertise in the field to possess visualization literacy skills becomes crucial. Visualization literacy is defined as "*the ability to make meaning from and interpret patterns, trends, and correlations in visual representations of data*" [1] and "a concept generally understood as the ability to create and interpret visual representations of data confidently" [2]. Visualization literacy can help people make informed decisions and identify insights within the data. Evaluating users' visualization literacy abilities is essential for potential improvements. However, there is currently a lack of efficient, practical, and time-saving tools to assess individuals' comprehension and interpretation of visual designs [3].

In recent years, several tests and assessments have been introduced to measure visualization literacy skills [2, 3, 4, 5, 6]. These tests typically assess people's ability to understand the different elements of visualizations, such as the type of data being represented, the visual encodings used, and the underlying statistical

Date: July, 8, 2023.
Key words and phrases. Information visualization, Visualization literacy.

relationships. They also gauge people's ability to interpret visual representations, identify patterns, and evaluate their visualization literacy abilities.

This paper provides a guideline and recommends that researchers and practitioners focus on key criteria and test elements when developing assessments of visualization literacy to ensure their reliability and effectiveness. The paper starts with motivation. This is followed by rules for creating test questions, structuring an assessment test, and then a conclusion.

2. Motivation and Previous Work

Visualization literacy is becoming increasingly important in today's data-rich world. Developing comprehensive and reliable tests of visualization literacy is challenging because visualization literacy encompasses a range of cognitive, perceptual, and analytical skills. However, testing visualization literacy skills can help researchers and practitioners to gain insights into users' proficiency and identify areas for improvement.

Boy *et al.* [2] introduce an assessment test that includes tasks that require only basic intelligence, such as identifying minimum, maximum, variation, intersection, average, and comparison. They test the user's ability to find these characteristics on line charts, bar charts and scatterplots. Delmas *et al.* [7]present an assessment test consisting of multiple-choice items designed to evaluate students' understanding and reasoning abilities in the area of variability. It specifically focuses on their skills in interpreting distributions and making comparisons. Similarly, Lee *et al.* [4] develop the Visualization Literacy Assessment Test (VLAT) to gauge novice users' visualization literacy skills with the most common visualization techniques from different sources: K-12 curriculum, data visualization authoring tools, and news articles to determine the content of the test. Firat *et al.* [5, 6] focused on an individual visual design to create two assessment tests for treemap and parallel coordinates plots, respectively. Designing comprehensive and reliable tests for visualization literacy involves considering a range of factors. Lastly, Pandey and Ottley [3] use a 12-item short form of the 53-item VLAT in their study.

By understanding and addressing the challenges of developing comprehensive and reliable tests of visualization literacy, researchers and practitioners can advance the field of visualization literacy and contribute to the effective use of visualizations in various domains. Several practices must be considered when designing a visualization literacy test to assess users' skills. These practices can help ensure the assessment's reliability, validity, and fairness. Here are some key practices to create assessment tests to gauge users' visualization literacy skills. These practices are presented based on designing effective visualization literacy assessment questions and the formatting of the assessment test.

3. Designing an Effective Visualization Literacy Test

This section explores key considerations for creating effective visualization literacy tests. We begin by emphasizing the importance of defining clear test objectives, which provide a clear direction and purpose for evaluating participants' visualization literacy skills. Next, we discuss the significance of selecting appropriate tasks and stimuli, including various visualizations and complexity levels. We also highlight the importance of incorporating diverse datasets and contexts and ensuring high-quality and clear images. Lastly, we address the need for considering diverse

user backgrounds to create inclusive assessments that promote equal opportunities for participants. By attending to these considerations, researchers and practitioners can design assessment tools that accurately measure and advance individuals' visualization literacy skills.

3.1. **Defining Clear Test Objectives:** To ensure clarity and focus in the design of a visualization literacy test, it is essential to clearly articulate the objectives of the assessment. This involves explicitly stating the intended goals and outcomes of the test. The goals can be to determine if the test assesses literacy skills for a single or multiple visual designs or testing specific target users such as young children etc. By doing so, researchers can provide a clear direction and purpose for evaluating participants' visualization literacy skills.

In addition to defining test objectives, it is important to determine the specific aspects of visualization literacy that will be measured. Visualization literacy encompasses various dimensions, including understanding the key features of visual designs to understand visual encodings and the ability to recognize patterns and interpret the meaning of the information. By identifying and prioritizing these aspects, researchers can align the test with the desired outcomes and ensure that the assessment comprehensively captures the core components of visualization literacy.

3.2. **Selecting Appropriate Tasks:** When designing a visualization literacy test, including a diverse range of tasks and visualizations is crucial. By doing so, the assessment can effectively gauge participants' ability to apply their visualization literacy skills in practical contexts. It is important to include various visualizations in the test to capture the breadth of visualization literacy. Unless the focus is a single visual technique, the test can include bar charts, scatter plots, network diagrams, treemaps, parallel coordinates and other commonly used visualization forms. The diversity in visualizations allows for a comprehensive assessment of participants' visualization literacy skills across different visualization forms and contexts.

Furthermore, it is important to consider the complexity levels of the tasks and stimuli. Include simple and complex visualizations to assess participants' abilities to interpret and analyze visual representations of varying intricacy. This range of complexity ensures that the test can effectively measure users' skills across different levels of visual complexity encountered in real-world data analysis and decision-making scenarios.

3.3. **Diverse Data and Contexts:** In addition to diverse visualizations, incorporating diverse datasets and contexts in the test is crucial. Real-world datasets from different domains can expose participants to various data characteristics, including varying scales, distributions, and relationships. This helps assess their ability to interpret visualizations in different contexts and apply their visualization literacy skills to various scenarios.

3.4. **Image Quality:** Ensure that the visualizations presented in the test are of high quality and clarity. Poor image quality can introduce unnecessary ambiguity and hinder participants' ability to accurately interpret and analyze the visualizations. Use appropriate resolution, colors, and labels to enhance readability and avoid visual distortions. It is necessary to consider optimizing the visualizations for different display sizes and devices to accommodate a diverse range of participants.

3.5. **Considering Diverse User Backgrounds:** To create an inclusive visualization literacy test, it is vital to consider the target audience's diverse backgrounds, experiences, and expertise levels. By doing so, the assessment can accommodate a wide range of participants and provide a fair and unbiased evaluation of their visualization literacy skills.

One key aspect of inclusivity is avoiding bias and stereotypical assumptions that could disadvantage certain participants. Ensure that the test content, language, and examples used are free from cultural or gender biases. By promoting a neutral and inclusive environment, the assessment can provide an equal opportunity for all participants to demonstrate their visualization literacy skills.

4. Formatting an Effective Assessment Test

Creating visualization literacy assessment requires careful consideration of various factors to collect and analyze results effectively. This section explores key aspects of forming a visualization literacy assessment test.

4.1. **Using a Variety of Response Formats:** To comprehensively assess different aspects of visualization literacy, it is important to incorporate a mix of response formats in the test. One effective response format to include is multiple-choice questions. These questions can evaluate participants' knowledge of visualization concepts, such as understanding different visual encodings or identifying appropriate visualization types for specific data scenarios.

To capture the diverse aspects of visualization literacy, it is crucial to incorporate a mix of response formats in the test. This includes open-ended responses and ranking or sorting tasks. These are valuable for assessing participants' ability to articulate interpretations and insights from visualizations, compare and prioritize visual elements, and identify patterns within visual representations. Open-ended responses allow participants to demonstrate their critical thinking skills by explaining the rationale behind their visual analysis. Participants can effectively communicate their understanding of the visual representations by expressing their interpretations and insights. Integrating ranking or sorting tasks allows for assessing participants' skills in comparing and prioritizing visual elements. These tasks require participants to make informed judgments about the relative importance or relationships between different components within a visualization. By discerning patterns and hierarchies, participants demonstrate their ability to extract meaningful information and identify key insights from the visual representations.

Furthermore, interactive tasks that involve filtering, zooming, or interacting with linked views provide participants with opportunities to demonstrate their proficiency in using interaction techniques to gain deeper insights from visual representations. These tasks assess participants' ability to dynamically manipulate visualizations to explore specific aspects or uncover hidden patterns and relationships.

4.2. **Establishing Scoring Criteria:** To ensure consistency in scoring and enhance the reliability of the visualization literacy assessment, it is crucial to develop clear and objective scoring criteria for each test item. These criteria should align with the specific skills and knowledge being assessed and ideally include multiple performance levels. To develop effective scoring criteria, align them with the specific skills and knowledge the assessment targets. For example, if the test item assesses

the ability to interpret visual encoding, the scoring criteria should outline the expected understanding of different visual properties, such as color, size, or position, and how they relate to the data representation. Moreover, the number of correct answers in each task (for example, comparing and prioritising visual elements and identifying patterns) enables a more comprehensive assessment of participants' abilities, highlighting strengths and improvement areas. The scoring criteria are a robust framework for evaluating participants' performance and enabling meaningful individual comparisons.

4.3. **Considering Time Constraints:** Determining appropriate time limits for completing the visualization literacy test is crucial to ensure a balanced assessment experience. When setting the time constraints, the tasks' complexity and the target audience's skill level should be considered. Tasks with higher complexity or requiring more in-depth analysis may require longer time limits to allow participants to engage thoroughly with the visualizations and provide thoughtful responses. On the other hand, tasks with lower complexity or shorter response formats may require shorter time limits to maintain an efficient testing process.

4.4. **Pilot study and Validating the Test:** Conducting a pilot study is essential to ensure the quality and effectiveness of the visualization literacy test. This pilot study evaluates the clarity of the test items, assesses the validity and reliability of the assessment, refines the scoring criteria, and validates the test through comparison with established measures or expert judgments. The pilot study involves recruiting a small group of participants who represent the target audience of the test. These participants should possess various visualization literacy skills and backgrounds relevant to the assessment. Additionally, involving experts in visualization literacy can provide valuable insights and expertise during the pilot study. During the pilot study, participants are asked to complete the test while providing feedback on the clarity of the test items. This feedback helps identify any potential issues or ambiguities in the wording, instructions, or visual representations used in the test. Participants' input is invaluable for refining and improving the overall design and clarity of the assessment.

4.5. **Maintaining Ethical Considerations:** To ensure ethical conduct during the visualization literacy test, it is imperative to follow ethical guidelines prioritising participants' rights and well-being. Obtaining informed consent is a fundamental requirement, wherein participants must be fully informed about the test's purpose, procedures, and any potential risks or benefits involved. It is essential to provide participants with a clear understanding of their participation and the right to withdraw from the study at any time. Ensuring the confidentiality and anonymity of participants' responses and personal information is crucial. Moreover, taking measures to minimize potential harm or stress and providing clear and easily comprehensible instructions to reduce confusion or anxiety are vital aspects of the study. Safeguarding collected data through secure storage and limited access only to authorized individuals and seeking ethical approval from appropriate ethics committees before conducting the test is necessary to uphold the research study's integrity and ethicality.

4.6. **Improving the Test:** Maintaining a continuous improvement process for the test is essential by actively incorporating participant feedback and conducting pilot

studies. This iterative approach identifies areas that require enhancement, whether in terms of test content, methodology, or usability. By actively checking participants' feedback and observing their experiences, the test can be refined to assess visualization literacy better and address potential shortcomings.

Additionally, it is necessary to address any limitations or gaps identified in previous test versions, ensuring that it aligns with the evolving understanding of visualization literacy and incorporates best practices in the field. This ongoing refinement and alignment with current knowledge contribute to the test's validity, reliability, and relevance in assessing visualization literacy effectively.

5. Conclusion

The power of visualizations for data analysis and decision-making requires users to have visualization literacy abilities. Developing comprehensive and reliable assessment tests to evaluate users' visualization literacy skills is crucial in light of visualizations' increasing importance and utilization. This paper provides recommendations and emphasizes the importance of incorporating practices for creating an assessment test. By following these recommendations, researchers and practitioners can actively contribute to evaluating and improving individuals' visualization literacy skills.

References

[1] Katy Börner, Adam Maltese, Russell Nelson Balliet, and Joe Heimlich. Investigating aspects of data visualization literacy using 20 information visualizations and 273 science museum visitors. *Information Visualization*, 15(3):198–213, 2016.

[2] Jeremy Boy, Ronald A Rensink, Enrico Bertini, and Jean-Daniel Fekete. A principled way of assessing visualization literacy. *IEEE Transactions on Visualization and Computer Graphics*, 20(12):1963–1972, 2014.

[3] Saugat Pandey and Alvitta Ottley. Mini-vlat: A short and effective measure of visualization literacy. *Computer Graphics Forum*, 42(3):1–11, 2023.

[4] Sukwon Lee, Sung-Hee Kim, and Bum Chul Kwon. Vlat: Development of a visualization literacy assessment test. *IEEE Transactions on Visualization and Computer Graphics*, 23(1):551–560, 2017.

[5] Elif E. Firat, Alena Denisova, and Robert S. Laramee. Treemap Literacy: A Classroom-Based Investigation. In *Eurographics 2020 - Education Papers*, pages 29–38, 2020.

[6] Elif E Firat, Alena Denisova, Max L Wilson, and Robert S Laramee. P-lite: A study of parallel coordinate plot literacy. *Visual Informatics*, 6(3):81–99, 2022.

[7] Robert Delmas, Joan Garfield, and Ann Ooms. Using assessment items to study students' difficulty reading and interpreting graphical representations of distributions. In *Fourth Forum on Statistical Reasoning, Thinking, and Literacy (SRTL-4)*, pages –, 2005.

Cukurova University, Computer Engineering Department, 01380, Adana, Turkiye
Email address: elifemelfirat@gmail.com

IFSCOM-E 2023
9th Ifs And Contemporary Mathematics and Engineering Conference
08-11 July 2023 Tarsus, Mersin, Türkiye
ISBN: 978-605-68670-8-8
pp: 65-69

A GUIDELINE TO DESIGNING CROWDSOURCED ONLINE EXPERIMENTS FOR EVALUATING VISUALIZATION LITERACY

ELIF E. FIRAT

0000-0001-9497-7928

Abstract. As data becomes increasingly complex, comprehending and interpreting visual representations becomes essential for informed decision-making and valuable insights. With visualizations gaining significance across various domains, it is vital to effectively assess users' visualization literacy skills and provide opportunities to enhance them. This paper offers a comprehensive guide on organizing online experiments for evaluating visualization literacy, leveraging advantages such as scalability and accessibility, and reaching a diverse participant pool. However, successfully organising these experiments requires planning and considering various factors. The paper outlines practices and considerations for online experiments to evaluate visualization literacy.

1. introduction

In the data-driven world, the volume and complexity of data are continuously increasing. The ability to comprehend and make sense of visual representations has become increasingly important. Visualizations are powerful tools for understanding complex information, enabling us to make informed decisions and uncover valuable insights. To determine users' ability to understand and comprehend the data to suggest improvements, assessing users' visualization literacy skills has gained significant importance across various domains [1, 2].

This paper aims to provide a comprehensive guide on organizing crowdsourced online experiments specifically designed to evaluate visualization literacy. Online experiments offer numerous advantages over traditional methods, e.g. classroom-based, such as scalability, accessibility, and the ability to reach diverse participants. Leveraging the benefits of online platforms, researchers and practitioners can conduct experiments that effectively assess users' skills in understanding and interpreting visual representations. However, organizing online experiments for evaluating visualization literacy requires thoughtful planning and consideration of several factors [3]. This paper will discuss the best practices and considerations for organizing

Date: July, 8, 2023.
Key words and phrases. Information visualization, Visualization literacy.

crowdsourced experiments to evaluate visualization literacy. By providing practical guidance, we aim to assist researchers and practitioners in conducting successful crowdsourced experiments that advance our knowledge of visualization literacy and its assessment. The paper starts with motivation. This is followed by recommendations for creating a crowdsourced online experiment and a conclusion.

2. Motivation

Online experiments enable researchers to access a larger and more diverse participant pool [3, 4]. Online experiments offer increased sample size, enhance the generalizability of findings and provide a better understanding of visualization literacy than traditional classroom experiments. When designing an online experiment, there are several key factors to consider. These practices are shaped based on the experimental settings from previous studies on visualization literacy. Boy *et al.* [5] designed online experiments using Amazon Mechanical Turk (MTurk) [6] with an average of 36 participants for each stage. They test the user's ability to find these characteristics on line graphs, bar charts and scatterplots. Ruchikachorn and Mueller [7] present a learning-by-analogy technique that explains an unfamiliar visualization method by showing a step-by-step conversion between two visual designs. A total of 44 participants were recruited via MTurk and were asked to understand the uncommon visual designs more quickly after interacting with the transitions. Kwon and Lee [8] focus on Parallel Coordinates, an efficient method to display multidimensional data, to study the impacts of multimedia learning environments for teaching data visualization to non-expert users. An experiment was conducted using MTurk with 120 participants. Firat *et al.* [9] presents the process of conducting a crowdsourcing experiment to gauge users' parallel coordinates plot literacy skills with 60 participants recruited via MTurk. We recommend steps for designing a crowdsourcing online experiment based on related literature. By giving attention to the design of an online experiment and conducting thorough checks, researchers can ensure the study's reliability, validity, and overall success, leading to meaningful insights into visualization literacy.

3. Recommendations to Design a Crowdsourced Online Experiment

Here are the steps for designing a crowdsourcing online experiment.

3.1. **Experimental Design:**

Designing an online experiment for visualization literacy evaluation requires careful consideration of various factors to ensure reliable and valid results. When selecting tasks and stimuli for the online experiment, choosing those that effectively assess participants' visualization literacy skills is essential. Tasks should align with the aspects of visualization literacy being evaluated, such as interpreting visual encodings, identifying patterns, or deriving insights from complex visualizations. The tasks should represent real-world scenarios and challenges, encompassing a range of data and visualization types and complexity levels to capture users' abilities across different visual representations.

Determining the appropriate sample size is critical for the generalizability of the study. Researchers should consider expected variability in participants' visualization literacy skills. Additionally, the test could have two parts: a pre-test and post-test or a control group, allowing for comparing participants' performance against a baseline or reference group, providing a clearer understanding of their

visualization literacy levels. Moreover, the randomization of participants should be applied to minimize potential biases and confounding variables. Randomization ensures that participants are assigned to different experimental conditions or tasks randomly, reducing systematic biases and increasing the generalizability of the findings.

3.2. **Platform Selection:** Choosing the appropriate online platform is crucial for conducting visualization literacy experiments effectively. One popular platform for online experiments is Qualtrics [10], a web-based survey platform that offers a range of features for designing and administering experiments. Qualtrics provides a user-friendly interface with customizable survey templates, allowing researchers to create interactive and engaging tasks for assessing visualization literacy. It also offers options for participant recruitment, data collection, and basic analysis, making it suitable for researchers seeking a comprehensive platform for their experiments.

Another commonly used platform is Amazon Mechanical Turk (MTurk) [6], an online crowdsourcing marketplace allowing researchers to recruit study participants. MTurk offers a large and diverse pool of participants, providing access to a broader demographic range. However, it is important to consider potential limitations, such as the need for careful participant screening and quality control measures to ensure reliable data. Additionally, MTurk may be more suitable for simpler tasks or initial pilot studies rather than complex visualization literacy assessments.

Sometimes, researchers may opt for custom-built web applications tailored specifically to their visualization literacy experiments. Developing a custom platform offers flexibility regarding experimental design, data collection methods, and user interface customization. This approach gives researchers full control over the experiment's features and functionality. However, it requires technical expertise and resources for development. Regardless of the platform, privacy and security measures should be a priority. Researchers must securely collect and store participant data, complying with relevant privacy regulations and ethical guidelines. Anonymization of data and restricted access to sensitive information are essential considerations when selecting an online platform.

3.3. **Participant Recruitment and Sampling:** Recruiting participants for online experiments is a critical step in ensuring the validity and generalizability of the findings. There are several potential sources for participant recruitment in online experiments. Prolific [11] is a platform that offers to reach more attentive participants and can be an alternative platform to MTurk for online studies. Also, such online platforms, consisting of pre-screened individuals who have agreed to participate in research studies, offer a convenient and accessible option. These platforms can provide a diverse pool of participants with various demographic backgrounds. Furthermore, social media platforms can also effectively reach a wider audience and engage novice individuals to participate in visualization literacy studies. Additionally, academic networks and research participant pools offer access to individuals within educational institutions, providing an opportunity to target specific populations.

Defining clear inclusion and exclusion criteria minimises biases. Researchers should establish criteria for the target population, such as age, educational background, or prior experience with visualizations. This helps to ensure that the sample reflects the intended user group and allows for meaningful comparisons and

generalizations. Inclusion criteria should be carefully defined to capture the characteristics and diversity of the population of interest, while exclusion criteria help to mitigate potential confounding factors or outliers that could affect the results.

3.4. **Experimental Procedure:** The experimental procedure is important to ensure the smooth execution and reliable results of visualization literacy experiments. The first step in the experiment is to obtain informed consent from participants, which involves providing a detailed explanation of the purpose, procedures, potential risks or benefits, and any necessary ethical considerations. Clear instructions and task descriptions are essential for guiding participants through the experiment. These instructions should include a brief overview of the study, the specific tasks participants are expected to perform, and the evaluation criteria for assessing their visualization literacy skills. Researchers should be available to address participants' questions or concerns throughout the experimental procedure.

3.5. **Data Collection and Analysis:** The data collection and analysis phase of an online experiment for visualization literacy plays a critical role in deriving meaningful insights. When collecting quantitative data, researchers can design survey questions that assess various aspects of users' understanding of visual designs, such as participants' ability to interpret visual encodings, recognize patterns, or derive insights from complex visualizations. Adding Likert charts can capture participants' level of agreement or questions with multiple options can aid the analysis. It is important to carefully design the response options to adequately capture the desired information without biasing participant responses. The analysis of participants' data to gauge their visualization literacy skills, the data can be analysed using both quantitative and qualitative methods. For quantitative data, statistical tests, such as t-tests, ANOVA, or correlation analysis, can examine relationships, differences, or associations between variables. Qualitative data can be analyzed through thematic analysis or coding to identify patterns within participants' responses.

3.6. **Ethical Considerations:** It is essential to consider ethical considerations when recruiting participants. Researchers should obtain informed consent from participants, clearly explaining the purpose, procedures, and any potential risks or benefits associated with the study. Confidentiality and privacy measures should be implemented to protect participant data, and participants should be allowed to withdraw from the study at any time.

3.7. **Validation and Reliability:** Ensuring the reliability and validity of an online experiment is necessary to establish the credibility of the findings. Pilot testing is an essential step in validating the reliability of the experiment. Conducting a pilot study with a small group of participants helps identify potential experimental design or task issues. Feedback from pilot participants can provide valuable insights for refining the experiment and making necessary adjustments before conducting the full-scale study.

4. Conclusion:

Increasing data volume and complexity, comprehending and interpreting visual representations are necessary for making informed decisions and discovering meaningful insights. To advance users' ability to understand and comprehend the data,

assessing users' visualization literacy skills is an important step. This paper has provided researchers and practitioners with a comprehensive guide to organizing crowdsourced online experiments for evaluating visualization literacy due to reaching a broader pool of participants with different levels and backgrounds. By following the recommended practices and considerations, researchers can conduct reliable and valid experiments, leading to meaningful insights into participants' visualization literacy skills. The findings from such experiments contribute to advancing our understanding of visualization literacy and its assessment in the data-driven world.

References

[1] Elif E. Firat, Alena Denisova, and Robert S. Laramee. Treemap Literacy: A Classroom-Based Investigation. In *Eurographics 2020 - Education Papers*, pages 29–38, 2020.

[2] Elif E Firat, Alark Joshi, and Robert S Laramee. Interactive visualization literacy: The state-of-the-art. *Information Visualization*, 21(3):285–310, 2022.

[3] Rita Borgo, Bongshin Lee, Benjamin Bach, Sara Fabrikant, Radu Jianu, Andreas Kerren, Stephen Kobourov, Fintan McGee, Luana Micallef, Tatiana von Landesberger, et al. Crowdsourcing for information visualization: Promises and pitfalls. In *Evaluation in the Crowd. Crowdsourcing and Human-Centered Experiments: Dagstuhl Seminar 15481, Dagstuhl Castle, Germany, November 22–27, 2015, Revised Contributions*, pages 96–138. Springer, 2017.

[4] Rita Borgo, Luana Micallef, Benjamin Bach, Fintan McGee, and Bongshin Lee. Information visualization evaluation using crowdsourcing. In *Computer Graphics Forum*, volume 37, pages 573–595. Wiley Online Library, 2018.

[5] Jeremy Boy, Ronald A Rensink, Enrico Bertini, and Jean-Daniel Fekete. A principled way of assessing visualization literacy. *IEEE Transactions on Visualization and Computer Graphics*, 20(12):1963–1972, 2014.

[6] Amazon Mechanical Turk. https://www.mturk.com/, 2023. Last Accessed: June, 2023.

[7] Puripant Ruchikachorn and Klaus Mueller. Learning visualizations by analogy: Promoting visual literacy through visualization morphing. *IEEE Transactions on Visualization and Computer Graphics*, 21(9):1028–1044, 2015.

[8] Bum Chul Kwon and Bongshin Lee. A comparative evaluation on online learning approaches using parallel coordinate visualization. In *Proceedings of the 2016 CHI Conference on Human Factors in Computing Systems*, pages 993–997. ACM, 2016.

[9] Elif E Firat, Ben Swallow, and Robert S Laramee. Pcp-ed: Parallel coordinate plots for ensemble data. *Visual Informatics*, 7(1):56–65, 2023.

[10] Qualtrics. https://www.qualtrics.com/, 2023. Last Accessed: June, 2023.

[11] Stefan Palan and Christian Schitter. Prolific. ac—a subject pool for online experiments. *Journal of Behavioral and Experimental Finance*, 17:22–27, 2018.

Cukurova University, Computer Engineering Department, 01380, Adana, Turkiye
Email address: elifemelfirat@gmail.com

IFSCOM-E 2023
9th Ifs And Contemporary Mathematics and Engineering Conference
08-11 July 2023 Tarsus, Mersin, Türkiye
ISBN: 978-605-68670-8-8
pp: 70-79

SOLVING NONLINEAR SHE EQUATIONS USING HHO ALGORITHM

YASİN BEKTAŞ

0000-0002-3681-0123

Abstract. Selective Harmonic Elimination-Pulse Width Modulation (SHE-PWM) is a widely used modulation technique in power electronics. However, solving SHE equations requires complex and computationally intensive calculations. To tackle this complexity, algorithms inspired by nature have been developed. This study focuses on the solution of 11-level nonlinear SHE equations using the Harris Hawks Optimization (HHO) algorithm. The results demonstrate the effectiveness of the HHO algorithm in solving nonlinear SHE equations for 11-level modulation schemes within the modulation index range of 0.1 to 1.0.

1. Introduction

Nonlinear equations are mathematical equations that do not exhibit a linear relationship between variables. These equations involve terms with variables of different degrees and can include products or powers of variables, making their solutions more complex than linear equations [1-2]. Nonlinear equations arise in various fields such as physics, engineering, economics, and mathematics. They play a significant role in accurately understanding and modelling real-world phenomena [3]. For example, nonlinear equations describe the behaviour of resistors in conjunction with diodes in electrical systems. Ohm's Law, which assumes a linear relationship between these two variables, typically explains the relationship between voltage and current in standard resistors in electrical systems. However, when diodes are included in electrical circuits, resistors become nonlinear and depend on the current and voltage. Solving nonlinear equations can be challenging due to their complex nature and absence of direct analytical solutions. Various numerical methods have been developed to solve nonlinear equations, such as the Newton-Raphson method and gradient-based algorithms [4-5]. These methods iteratively improve estimates to find approximate solutions for unknown variables.
The Newton-Raphson method is one of the most commonly used and effective procedures for solving nonlinear equations. This method aims to iteratively approach

Date: July, 8, 2023.

a solution by utilizing the first derivative of a function. However, the Newton-Raphson method may have limitations in convergence when dealing with highly nonlinear and ill-conditioned systems. Researchers have recently investigated alternative optimization algorithms to enhance the efficiency and effectiveness of solving nonlinear equations [6-9]. One unique optimization algorithm in this context is the Harris Hawks Optimization (HHO) algorithm [10]. The Harris Hawk Optimization algorithm is a population-based metaheuristic optimization method that draws inspiration from Harris Hawk's hunting techniques. This algorithm mimics the collaboration of Harris Hawks in optimizing their hunting abilities and increasing their chances of successful hunting. The Harris-Hawk Optimization algorithm has shown promising results in solving nonlinear equations. It has successfully improved the convergence process and found optimal global solutions. Utilizing the Harris Hawk Optimization algorithm for solving nonlinear equations is particularly beneficial when dealing with complex systems where nonlinear and analytical solutions are unavailable. The Harris-Hawk Optimization algorithm effectively tackles the challenges of solving nonlinear equations by employing a nature-inspired population-based approach. The algorithm iteratively improves the positions of potential solutions, effectively searching for optimal solutions to nonlinear equations.

Although the Newton-Raphson method is widely used and practical, it can encounter limitations in terms of convergence when dealing with highly nonlinear and ill-conditioned systems. In such cases, the Harris Hawks Optimization (HHO) algorithm provides an alternative approach to overcome these limitations.

2. Mathematical Model of SHE-PWM Technique

The development and application of efficient modulation techniques is very important in the field of power electronics. These techniques play a vital role in controlling the switching of power electronic devices, thereby providing the desired output voltage or current waveform. One such modulation technique is Selective Harmonic Elimination Pulse Width Modulation (SHE-PWM) [11]. SHE-PWM is a basic switching frequency technique commonly used to control multilevel inverters' output waveform and eliminate low-order harmonics. Compared to traditional PWM techniques, this technique offers several advantages, such as linear control of converter output voltage by eliminating preselected low-order harmonics, the possibility to optimize specific performance parameters, improved transient response, and improved input power factor. The mathematical model of the SHE-PWM technique is concerned with calculating a set of switching angles that reduce the harmonic components for a given modulation index (m) value.

There are many SHE-PWM waveforms in the literature. The stepped waveform is the most broadcast waveform used in multilevel inverters. The purpose of using this waveform is to generate the signal for low harmonic similar to the sine waveform. The output voltage waveform for a single phase of a 3-phase 11-level multilevel inverter is shown in Figure 1.

Using the Fourier series, the amplitudes and phase angles of the harmonic components of a waveform at certain frequencies can be calculated, and the actual waveform can be obtained as the sum of these components. The Fourier series of

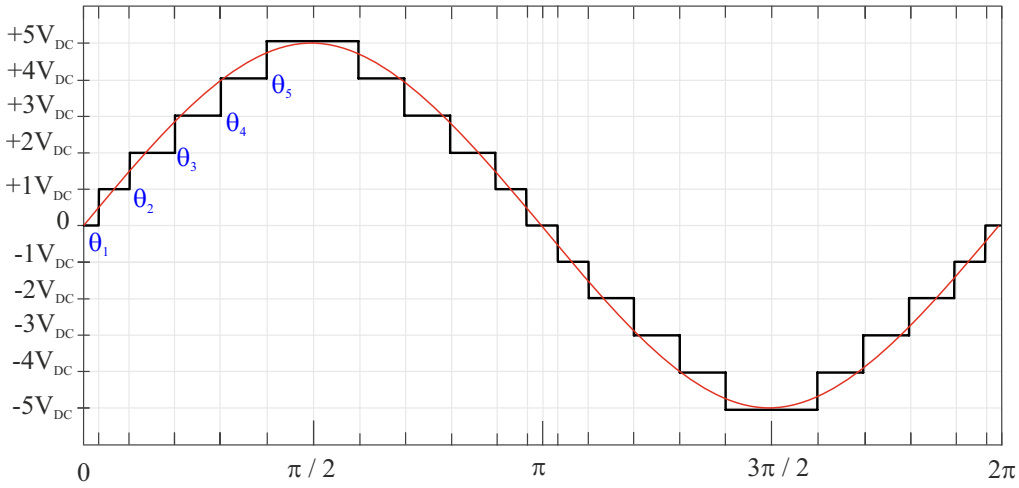

FIGURE 1. 11-Level Multi-level inverter SHE-PWM waveform.

the output voltage waveform can be expressed as

$$v_o(t) = \frac{a_o}{2} + \sum_{i=0}^{n} a_n \cos\left(\frac{2\pi nt}{T}\right) + b_n \sin\left(\frac{2\pi nt}{T}\right) \tag{2.1}$$

where ao is the constant DC term, an is the Fourier cosine coefficient and bn is the Fourier sine coefficient. Since the output voltage has quarter-wave symmetry, the odd harmonics with a_0, a_n, and sine terms take the value zero. Therefore, the output voltage waveform equation can be expressed more simply as in Eq. (2.1).

$$v_o(t) = \sum_{i=1,3,5,\ldots}^{n} b_n \sin\left(n\theta_i\right). \tag{2.2}$$

For the step output voltage bn can be expressed as:

$$b_n = \frac{4V_{dc}}{n\pi} \sum_{\mathrm{i}=1,3,5,\ldots}^{\mathrm{n}} \cos\left(n\theta_i\right) \tag{2.3}$$

For the 11-level output voltage waveform shown in Figure 1, five switching angles θ_1, θ_2, θ_3, θ_4 and θ_5 must be calculated. One of the switching angles is used to control the fundamental harmonics, and the remaining four are used to eliminate or reduce the selected harmonics. In three-phase systems, 3 and multiple harmonics are eliminated due to the nature of the system. In this study, 5^{th},7^{th}, 11^{th}, and 13^{th} harmonics will be considered. If the harmonic equations are to be rewritten in Eq.(2.4);

$$
\begin{aligned}
\mathrm{V}_1 &= \cos(\theta_1) + \cos(\theta_2) + \cos(\theta_3) + \cos(\theta_4) + \cos(\theta_5) = Ms\pi/4 \\
\mathrm{V}_5 &= \cos(5\theta_1) + \cos(5\theta_2) + \cos(5\theta_3) + \cos(5\theta_4) + \cos(5\theta_5) = 0 \\
\mathrm{V}_7 &= \cos(7\theta_1) + \cos(7\theta_2) + \cos(7\theta_3) + \cos(5\theta_4) + \cos(7\theta_5) = 0 \\
\mathrm{V}_{11} &= \cos(11\theta_1) + \cos(11\theta_2) + \cos(11\theta_3) + \cos(11\theta_4) + \cos(11\theta_5) = 0 \\
\mathrm{V}_{13} &= \cos(13\theta_1) + \cos(13\theta_2) + \cos(13\theta_3) + \cos(13\theta_4) + \cos(13\theta_5) = 0
\end{aligned} \tag{2.4}
$$

Due to the quarter-wave symmetry, the switching angles must satisfy the constraint given in Eq. (2.5).

$$0 \leq \theta_1 < \theta_2 < \theta_3 < \theta_4 < \theta_5 \leq \frac{\pi}{2} \tag{2.5}$$

The expression M given in Eq. (2.4) represents the modulation index. It is defined as the peak value (V1p) ratio of the desired base voltage to the total DC input voltage. Modulation index (M) can be represented mathematically as:

$$M = \frac{V_{1p}}{sV_{DC}} \tag{2.6}$$

Total harmonic distortion (THD) is mathematically shown in Eq. (2.7). THD_{13}, which is the THD of the harmonics up to the 13th harmonic, is given in Eq. (2.8).

$$THD = \frac{\sqrt{V_5^2 + V_7^2 + V_{11}^2 + \cdots V_{49}^2}}{|V_1|} \tag{2.7}$$

$$THD_{13} = \frac{\sqrt{V_5^2 + V_7^2 + V_{11}^2 + V_{13}^2}}{|V_1|} \tag{2.8}$$

3. Harris Hawks Optimization Algorithm

Harris Hawks Optimization (HHO) is a metaheuristic optimization algorithm developed by Heidari et al. in 2017. Inspired by the hunting behaviour of Harris Hawks, the algorithm mimics their collaborative hunting strategy. Harris Hawks work together in groups to optimize their hunting abilities, tracking the prey's location and moving swiftly. This collaboration and fast movement strategy increase their chances of capturing the prey. The algorithm utilizes these natural strategies to solve optimization problems. It adopts a population-based approach and iteratively improves potential solutions. Harris Hawks Optimization effectively explores the potential solution space by considering the exploration and exploitation phases. The algorithm has been used in various studies, demonstrating successful results in solving optimization problems, particularly in complex, multidimensional, and real-world problems. Harris hawks randomly perch in some locations and wait based

on two strategies to detect the prey. The first strategy is called "Exploration." According to this strategy, hawks perch randomly and scan the surrounding area to search for the prey. They observe and try to identify potential locations of the prey. In this stage, there is no communication or collaboration among the hawks; each one independently conducts its own exploration. The second strategy is called "Exploitation". This strategy involves hawks quickly taking action and moving towards the prey after detecting it. The hawks move rapidly and coordinate their movements while tracking the prey. This strategy aims to facilitate collaboration among the hawks for capturing the prey and minimizing the prey's chances of escape. The HHO algorithm combines and iteratively uses these two strategies. Initially, the hawks settle in random locations and try to detect the prey. Then, upon finding the prey, they swiftly move towards it, applying the exploitation strategy. This process is repeated, effectively scanning the potential solution space. The fundamental philosophy of HHO is to mimic the hunting strategies observed in Harris hawks in nature. These strategies maintain a proper balance between prey detection and capture. The HHO algorithm aims to solve optimization problems by utilizing these strategies. In conclusion, the HHO algorithm is an optimization algorithm developed by drawing inspiration from nature. By mimicking Harris Hawks' exploration and exploitation strategies, it explores the potential solution space and aims to find optimal solutions effectively [10].

The stages of the HHO algorithm are as follows:

3.1. Exploration Phase

$$X(t+1) = \begin{cases} X_{\text{rand}}\ (t) - r_1 \left| X_{\text{rand}}\ (t) - 2r_2 X(t) \right| & q \geq 0.5 \\ (X_{\text{prey}}(t) - X_m(t)) - r_3 \left(LB + r_4 (UB - LB) \right) & q < 0.5 \end{cases} \tag{3.1}$$

$X(t+1)$ is the position vector of the hawks in the next iteration. X(t) is currently the position vector of the hawks. r1, r2, r3, r4, and q are random numbers in the range (0,1) that are updated at each iteration. LB and UB indicate the upper and lower bounds of the variables. Xrand(t) is a hawk randomly selected from the current population, and Xm is the average position of the current population of hawks. The following equation obtains the average position of the hawks:

$$X_m(t) = \frac{1}{N} \sum_{i=1}^{N} X_i(t) \tag{3.2}$$

3.2. Transition from exploration to exploitation

To model this step, a victim's (prey) energy is modeled as:

$$E = 2E_0 \left(1 - \frac{t}{T} \right) \tag{3.3}$$

where E is the energy of the escaped prey, T is the maximum number of iterations, and Eo is the initial state of the prey's energy.

3.3. Exploitation phase

3.3.1. Soft besiege

This behaviour is modeled by the following rules:

$$X(t+1) = \Delta X(t) - E\,|JX_{\text{prey}}(t) - X(t)| \tag{3.4}$$

$$\Delta X(t) = X_{\text{prey}}(t) - X(t) \tag{3.5}$$

where $\Delta X(t)$ is the difference between the rabbit's position vector and the current position in iteration t, r5 is a random number between 0 and 1, and J represents the rabbit's random jump power during the escape procedure. Calculated as J = 2(1 — r5), the J value changes randomly with each iteration to simulate the nature of the Rabbit's movements.

3.3.2. Hard besiege

In this case, the current positions are updated using Eq. (3.6).

$$X(t+1) = X_{\text{prey}}(t) - E|\Delta X(t)| \tag{3.6}$$

3.3.3. Soft besiege with progressive rapid dives

The next movements of the hawks to perform a soft encirclement are represented by Eq. (3.7).

$$Y = X_{\text{prey}}(t) - E\,|JX_{\text{prey}}(t) - X(t)| \tag{3.7}$$

It is assumed that falcons will dive with respect to LF-based models using the following rule:

$$Z = Y + S \times LF(D) \tag{3.8}$$

Here D is the problem's dimension, S is a random vector with respect to dimension 1 x D, and LF is the flight function calculated using Eq. (3.9).

$$LF(x) = 0.01 \times \frac{u \times \sigma}{|v|^{\frac{1}{\beta}}}, \sigma = \left(\frac{\Gamma(1+\beta) \times \sin\left(\frac{\pi\beta}{2}\right)}{\Gamma\left(\frac{1+\beta}{2}\right) \times \beta \times 2^{\left(\frac{\beta-1}{2}\right)}} \right)^{\frac{1}{\beta}} \tag{3.9}$$

Where u, and v are coefficients that take random values between 0 and 1, β is a default constant set to 1.5. Therefore, the final strategy to update the positions of the hawks during the soft encirclement phase can be accomplished by Eq. (3.10).

$$X(t+1) = \begin{cases} Y \text{ if } F(Y) < F(X(t)) \\ Z \text{ if } F(Z) < F(X(t)) \end{cases} \tag{3.10}$$

Here Y and Z are obtained using Eqs. (3.7), and (3.8).

3.3.4. Hard besiege with progressive rapid dives

In case of hard siege, the following rule applies:

$$X(t+1) = \begin{cases} Y \text{ if } F(Y^*) < F(X(t)) \\ Z^* \text{ if } F(Z^*) < F(X(t)) \end{cases} \tag{3.11}$$

Here Y* and Z* are obtained using equations (3.12) and (3.13).

$$Y^* = X_{\text{prey}}(t) - E\,|JX_{\text{prey}}(t) - X_m(t)| \tag{3.12}$$

$$Z^* = Y^* + S \times LF(D) \tag{3.13}$$

3.4. The stages of the HHO algorithm

The stages of the HHO algorithm are in Table 1.

4. Application of Harris Hawks Optimization Algorithm to SHE equations

The HHO algorithm we proposed was used with MATLAB software to solve the SHE Eq. (4), which describe the chosen harmonics in the 11-level inverter. We chose a population size of 100 and 100 repetitions for the algorithm. The solutions were calculated by gradually increasing the modulation index M from 0 to 1, with

TABLE 1. The stages of the HHO algorithm

1.	Initialize the populatıon of hawks.
2.	Evaluate the fıtness of each hawk based on the objective functıon.
3.	Update the global best positıon.
4.	Update the positıon and velocıty of each hawk based on exploration and exploitation strategıesn.
5.	Check for convergence crıterıa or maxımum ıteratıons.
6.	Repeat steps 2 to 5 untıl convergence or maximum ıteratıons ar e reached.
7.	Return the best solutıon obtamed.

a step size of 0.1. We performed the computations on a personal computer with an Intel(R) Core (TM) i7-10870H CPU @ 2.20GHz, 16.0 GB RAM, and a GeForce RTX 2060 NVIDIA graphics card. At each step, we evaluated the solution using a fitness function. Our objective was to determine the switching angles in a way that eliminates or reduces the selected low-order harmonics to an acceptable level while maintaining the fundamental voltage at the desired value. We used the fitness function defined in Eq. (4.1) to assess the quality of each solution set.

$$f = \min_{\theta_i} \left\{ |V_{ref} - V_{1p}| + (V_5)^2 + (V_7)^2 + (V_{11})^2 + (V_{13})^2 \right\} = 0 \tag{4.1}$$

In Eq. (4.1), the variable Vref represents the maximum desired base voltage, while V1p represents the maximum base voltage obtained at the output of the inverter when the calculated switching angles are applied. The fundamental frequency of the base voltage is set at 50Hz. The total source voltage is determined to have a maximum value of 311 volts. For the eleven-level inverter, each source is selected to have a voltage of 311/5 volts.
To verify the accuracy and effectiveness of the algorithm, it was executed five times for ten different modulation values ranging from 0.1 to 1.0. The obtained results, including the best, worst, and standard deviation values, are presented in Table 2. The statistical values in Table 2 illustrate the relationship between the modulation index and the fitness function. As the modulation index increases, the fitness function value tends to decrease. This indicates that higher modulation indices lead to improved results.

Table 3 displays the switching angles obtained from the best-fit function calculated for the given modulation indices. Meanwhile, Table 4 presents the results of the simulation applied to the multi-level inverter on Matlab Simulink, using the switching angles found in Table 3.

Table 4 shows the effect of different modulation indices on the performance of the HHO (Harris Hawks Optimizer) algorithm. According to this table, the HHO algorithm was able to find suitable solutions for modulation indices between 0.1 and 1.0. However, while higher harmonic distortion values were observed in systems with low modulation index, lower harmonic distortion values were obtained in systems with high modulation index. The modulation index range where the algorithm performs best is between 0.5 and 1.0. In these ranges, it appears that

TABLE 2. Statistical Values for the Relationship Between Modulation Index and Fitness Function

M	**Best**	**Worst**	**Standard deviation**
0.1	292.5	951	296.5
0.2	112.6	132.6	1.6
0.3	53.3	195.5	62.2
0.4	6.8	33.9	10.3
0.5	1.3	25.4	9.9
0.6	0	2.8	1.1
0.7	0	0.6	0.3
0.8	0	0.4	0.2
0.9	0	0.2	0.1
1	0	0.3	0.1

TABLE 3. Calculated switching angles with HHO versus modulation index

Modulation Index (M)		Switching Angles (radians)				
		θ_1	θ_2	θ_3	θ_4	θ_5
Low	0.1	1.1775	1.5614	1.5708	1.5708	1.5708
	0.2	0.6675	1.5708	1.5708	1.5708	1.5708
	0.3	0.1063	1.386	1.5708	1.5708	1.5708
Middle	14	0.7883	0.9972	1.2418	1.5708	1.5708
	0.5	0.6407	0.8642	1.1415	1.468	1.5708
	0.6	0.6168	0.8195	1.0224	1.2673	1.5331
High	0.7	0.3364	0.6722	0.982	1.1081	1.5399
	0.8	0.1606	0.4358	0.7335	1.0667	1.5386
	0.9	0.1308	0.477	0.7096	0.9136	1.274
	1.0	0.1335	0.3363	0.5102	0.8245	1.1007

the selected harmonics are effectively suppressed.

5. Conclusion

This research proves that the Harris Hawks Optimization Algorithm is a reliable method to optimize the modulation of multilevel inverters in power electronics. The HHO algorithm was successful in controlling the fundamental voltage with an error margin of less than 0.38% for the specified modulation indices. These findings indicate that the HHO algorithm can minimize harmonic distortion and accurately control the fundamental voltage, making power electronics systems more efficient and achieving the desired output characteristics.

References

[1] M. Ohkita,Y. Kobayashi,M. Inoue,Application of the Haar functions to solution of differential equations, Mathematics and Computers in Simulation,25(1), 31-38 (1983)

[2] S. K. Chhabra, R. Kumar, V. Mittal, Prediction equations for spirometry for children from northern India, Indian pediatrics, 53, 781-785, (2016).

TABLE 4. Simulation results by modulation index

M		Vref(rms)	V1p(rms)	error (%)	THD (%)	THDe (%)	5th (%)	7th (%)	11th (%)	13th (%)
Low	0.1	22	21.98	**0.09%**	62.42	57.71	49.64	16.26	19.04	15.44
	0.2	44	43.86	**0.32%**	**29.03**	26.67	25.03	0.78	5.72	7.18
	0.3	66	65.82	**0.27%**	**30.82**	29.42	28.41	2.85	4.03	5.78
Middle	14	88	87.75	**0.28%**	14.34	10.61	7.34	6.75	1.77	3.18
	0.5	110	110	**0.00%**	**9.08**	**1.14**	**0.45**	**0.37**	**0.87**	**0.45**
	0.6	132	131.5	**0.38%**	**6.84**	**0.04**	**0.01**	**0.01**	**0.02**	**0.02**
High	0.7	154	153.9	**0.06%**	7.78	**0.07**	**0.01**	**0.01**	**0.02**	**0.03**
	0.8	176	175.8	**0.11%**	**6.52**	**0.04**	**0.01**	**0**	**0.01**	**0.02**
	0.9	198	197.5	**0.25%**	**6.22**	**0.04**	**0.01**	**0.01**	**0.02**	**0.01**
	1.0	220	219.8	**0.09%**	**4.89**	**0.03**	**0.02**	**0.01**	**0.01**	**0.01**

[3] A. Akbulut, and F. Taşcan, Application of conservation theorem and modified extended tanh-function method to (1+ 1)-dimensional nonlinear coupled Klein–Gordon–Zakharov equation, Chaos, Solitons and Fractals, 104, 33-40, (2017).

[4] M. Y. Lada, M. S. A. Khiar, S. A. Ghani, M. R. M. Nawawi, A. S. M. Nor, and , J. G. M. Yuen, Performance analysis of SHE-PWM using Fourier Series and Newton-Raphson analysis, In AIP Conference Proceedings (Vol. 1660, No. 1, p. 070046). AIP Publishing LLC, (2015).

[5] P. F., Rasmussen and N. Gautam ,Alternative PWM-estimators of the Gumbel distribution, Journal of Hydrology, 280(1-4), 265-271. (2003).

[6] H. Karaca, and E. Bektas, Selective Harmonic Elimination Using Genetic Algorithm for Multilevel Inverter with Reduced Number of Power Switches. Engineering Letters, 24(2), (2016).

[7] B. Ahmadi, O. Ceylan, and A. Özdemir, Grey wolf optimizer for allocation and sizing of distributed renewable generation, In 2019 54th international universities power engineering conference (UPEC) (pp. 1-6). IEEE, (2019).

[8] B. Ahmadi, O. Ceylan, and A. Ozdemir. A multi-objective optimization evaluation framework for integration of distributed energy resources, Journal of Energy Storage, 41, 103005, (2021).

[9] E. Amini, D. Golbaz, R. Asadi, M. Nasiri, O. Ceylan, M. Majidi Nezhad, and M. Neshat, A comparative study of metaheuristic algorithms for wave energy converter power take-off optimisation: A case study for eastern Australia, Journal of Marine Science and Engineering, 9(5), 490, (2021).

[10] A. A. Heidari, S. Mirjalili, Faris, H., Aljarah, I., Mafarja, M., and Chen, H. , Harris hawks optimization: Algorithm and applications, Future generation computer systems, 97, 849-872, (2019).

[11] Y. Sahali, and M. K. Fellah, Selective harmonic eliminated pulse-width modulation technique (SHE PWM) applied to three-level inverter/converter, In 2003 IEEE International Symposium on Industrial Electronics (Cat. No. 03TH8692) (Vol. 2, pp. 1112-1117), IEEE, (2003).

AKSARAY UNIVERSITY, VOCATIONAL SCHOOL OF TECHNICAL SCIENCES, CENTER/AKSARAY, TURKEY

Email address: yasinbektas@aksaray.edu.tr

IFSCOM-E 2023
9th Ifs And Contemporary Mathematics and Engineering Conference
08-11 July 2023 Tarsus, Mersin, Türkiye
ISBN: 978-605-68670-8-8
pp: 80-84

SIGN LANGUAGE RECOGNITION MOBILE APPLICATION FOR TURKISH LANGUAGE

ERDEM DEMIROGLU, FURKAN AYAKDAS, ASUDE TANRIBUYURDU, AND GULSUM AKKUZU KAYA

Abstract. Sign language is a common and reliable way of communicating with deaf and dumb people. This language can be done anywhere around the world however most people do not know and understand sign language. When people do not understand that special group of people, they either try to isolate themselves from the community or they get angry. In order to overcome that type of problem, sign language applications have been developed which help deaf and dumb people to convey their ideas to others. Sign language tools simply convert sign language into text in real-time. This research aims to develop a mobile application that converts sign language into text for the Turkish Language. This research focuses on the accuracy of the recognition. Our Application resulted in 96,3% accuracy for three words.

1. Introduction

According to the Turkish Statistical Institute (TÜİK), hearing-impaired individuals, who constitute approximately a percent 3 of society, are among the special groups within the community [1]. Among those people, hearing-impaired individuals can communicate through sign language. This language also known as body language, is a language that helps people to use visual signs instead of spoken words [2]. With this language, especially deaf and dumb people can communicate with other people in their daily activities. However, that special group of people still have difficulties that have negative effects on their lives. Because they get angry when they can not convey their needs to others.

In order to overcome this issue, a tool is needed which should receive photo or video as input from deaf and dumb people and translate it into text for other people. The aim of this study is to provide a real-time sign-language translator. We intend to develop a mobile application for people to use on their phones and integrate it with a chatbot. Artificial intelligence and image processing techniques will be used for developing a real-time sign language translator. This application holds great importance in terms of enabling people to use it easily and improving their quality of life.

Date: July, 8, 2023.
Key words and phrases. Sign language recognition, Turkish Sign Language, Hand Gesture recognition, LSTM.

The structure of the rest of the paper is as follows. Section 2 discusses works in the literature related to our approach and analysis. Section 3 gives a road map of the methodological steps taken for completing this research. In Section 4, we present and discuss the results of our analysis. In this section, we also conclude the paper and list the limitations of this work.

2. Related Works

Recognition technology has helped researchers to recognize hand movements, patterns, faces, body movements for various purposes. The first real-time gesture recognition tool was introduced in 2013 [3], it used a face detector. It was a quite successful tool as it had a success rate of around 70%. A hand gesture recognition study was then introduced by *Tarek Frikha and Abir Presentche* [4]. After this study, a dataset called EgoGesture was created in 2018, on this dataset various techniques such as Hidden Markov Model and classification models were applied [5]. However, it was claimed that sign-language is more effective for communication [6, 7, 8]. This language has different forms and gestures in each country around the world. Therefore researchers have started to develop sign-language tools for their own language. For example, the American Sign Language tool was introduced by Shruti Chavan, Xinrui Yu, and Jafar Saniie [10]. Similarly, Indonisian Sign Lamguage tool was developed by Zulkarnain Iyw [9]. Chinese Sign Language tool has been started to develop in this year [11].

As it is highlighted above, each country needs its own sign language tool. With respect to this idea, we aim to develop Turkish Sign Language. In existing systems, a limited number of words have been translated into sign language by generating videos for each word. Our innovative approach aims to be open-source with libraries, and additionally, with the collaboration of expert sign language interpreters, it continuously incorporates new sign language equivalents of words into our library. Once added to the library, the chatbot is enabled to interpret new words.

3. Method and Application Development Stage

For this study, we first searched similar research papers and tools to discover what is missing and our requirements. Figure 1 represents the main taken steps to develop this study. The methods employed in our project are as follows:

- We aim to create a sign language recognition library using image processing techniques. Through this library, a dataset will be generated by capturing images using a camera and associating them with their corresponding words.
- We plan to develop a mobile application and integrate it with artificial intelligence. By combining the mobile application with AI capabilities, our goal is to create a real-time sign language translation application.
- The dataset used in the model will be created using everyday Turkish words that are commonly used.
- The model will be trained using the Mediapipe framework, which will record the instantaneous images of the movements and create a dataset.
- The dataset will be generated by recording the instantaneous images of the movements using the Mediapipe framework.

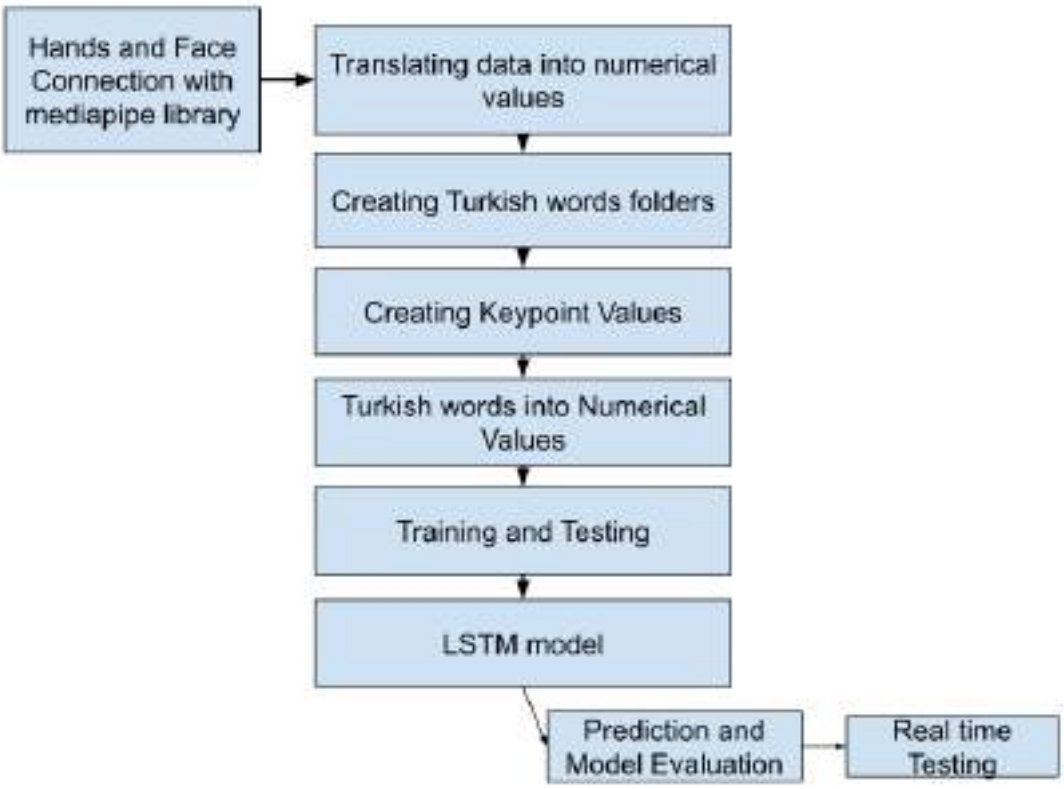

FIGURE 1. Methodological Steps

4. Results with Users' Interactions on the Application

The model has worked with four Turkish words. The dataset will be extended with more Turkish words, especially the most frequent words used in a person's daily life. The accuracy resulting from the confusion matrix is 96,3%. Once the model has been implemented, our application recognizes and converts sign languages to texts in real-time. The application has been affected by various factors such as lighting and background. Therefore, we needed good lighting and a plain background that does not have objects on the box that reads hand gestures for receiving successful results.

We perform the training and testing stages of a model by utilizing the Mediapipe library to create the Hands and Face model, which involves addressing the process of mapping words to their corresponding signs in sign language, creating folders for Turkish words, and generating significant numerical values that represent body or facial keypoints. Subsequently, we employ the Long-Short Term Memory (LSTM) model to convert the representation of Turkish words in sign language into numerical values, enabling us to construct a language processing or time series model. We evaluate the performance of the trained model by testing its predictions against real-time data. Figure 2, Figure 3, and Figure 4 illustrate the different results of this project. The tool is able to recognize three words in its current version. How-

FIGURE 2. "Tesekkürler" Translate

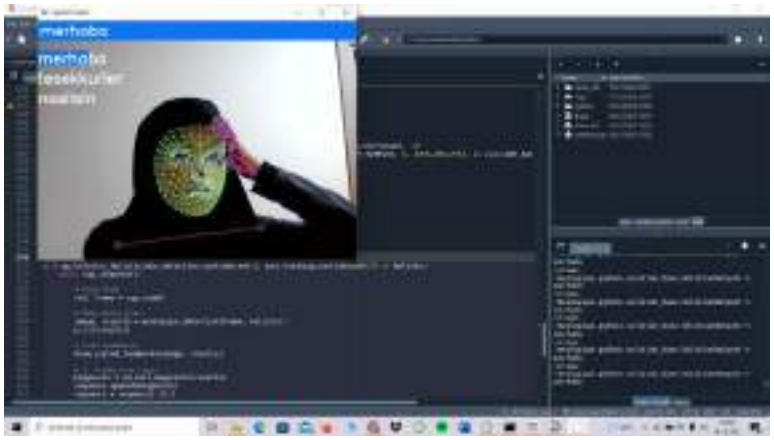

FIGURE 3. "Merhaba" Translate

FIGURE 4. "Nasilsin" Translate

ever, we still work on it to enrich our dictionary. The aimed dictionary will cover as much as possible daily life activities. We also intent to use different techniques to increase the success rate of our application.

References

[1] ERTEN, H., and ARICI, N. İşaret dilinin tarihi serüveni ve Türk İşaret Dili. Afyon Kocatepe Üniversitesi Sosyal Bilimler Dergisi,
24(1), 1-14, (2022).
[2] Pfau, R. Sign language. M. Steinbach, and B. Woll (Eds.). De Gruyter Mouton, (2012).
[3] Bayazit M, Couture-Beil A, Mori G. Real-time Motion-based Gesture Recognition Using the GPU. In: MVA. Citeseer; p. 9-12, (2009).
[4] Zeineb A, Chaala C, Frikha T, Hadriche A. Hand gesture recognition system. International Journal of Computer Science and Information Security (IJCSIS).14(6), (2016).
[5] Zengeler N, Kopinski T, Handmann U. Hand gesture recognition in automotive human machine interaction using depth cameras. Sensors. 19(1):59, (2018).
[6] Nivedita S, Ramyapriya Y, Tanmaya H, et al. Sign Language Recognition System using Machine Learning. (2022).
[7] Kadhim RA, Khamees M. A real-time American sign language recognition system using convolutional neural network for real datasets. TemJournal. 9(3):937, (2020).
[8] Pigou L, Dieleman S, Kindermans PJ, Schrauwen B. Sign language recognition using convolutional neural networks. In: European conferenceon computer vision. Springer; p. 572-8, (2014).
[9] Zulkarnain Iyw. Indonesian Sign Language Converter Into Text And Voice As Social Interaction Tool For Inclusion Student In Vocational High Schools Conference on Electro Information Technology (EIT). IEEE; p. 188-92, (2021).
[10] Chavan S, Yu X, Saniie J. Convolutional Neural Network Hand Gesture Recognition for American Sign Language. In: 2021 IEEE Int ernational Conference on Electro Information Technology (EIT). IEEE; p. 188-92, (2021).
[11] Obi, Y., Claudio, K. S., Budiman, V. M., Achmad, S., and Kurniawan, A. Sign language recognition system for communicating to people with disabilities. Procedia Computer Science, 216, 13-20, (2023).

(Erdem Demiroglu) Computer Engineering, Faculty of Engineering and Architecture, Recep Tayyip Erdogan University, Rize, TURKIYE
Email address: edemiroglu138@gmail.com

(Furkan Ayakdas) Computer Engineering, Faculty of Engineering and Architecture, Isparta Uygulamali Bilimler University, Isparta, TURKIYE
Email address: furkanayakdas@gmail.com

(Asude Tanribuyurdu) Computer Engineering, Faculty of Engineering and Architecture, Kirsehir Ahi Evran University, Kirsehir, TURKIYE
Email address: asudetb@gmail.com

(Gulsum Akkuzu Kaya) Computer Engineering, Faculty of Engineering and Architecture, Kirsehir Ahi Evran University, Kirsehir, TURKIYE
Email address: gulsum.akkuzukaya@ahievran.edu.tr

IFSCOM-E 2023
9th Ifs And Contemporary Mathematics and Engineering Conference
08-11 July 2023 Tarsus, Mersin, Türkiye
ISBN: 978-605-68670-8-8
pp: 85-94

SPACELIKE f-RECTIFYING CURVES IN MINKOWSKI SPACE E_1^4

HÜLYA GÜN BOZOK AND ÖNDER KORKMAZ

Abstract. In this paper, spacelike f-rectifying curves are introduced in Minkowski Space E_1^4 and using this definition some characterizations and classifications are researched in Minkowski Space E_1^4.

1. Introduction

Rectifying curve is a curve whose position vector always lie in its rectifying plane[1]. In Minkowski space the rectifying curves have similar geometric properties as in the Euclidean space. After the definition of rectifying curves many studies are done in Minkowski space [2, 3, 4]. Similar to this definition, an f-rectifying curve definition was given by Iqbal and Sengupta in both Euclidean space and Minkowski space. Firstly they studied f-Rectifying Curves in Minkowski space such that Non-null (spacelike or timelike) f-rectifying curves in the Minkowski 3-space [5], null (lightlike) f-rectifying curves in the Minkowski 3-space [6] and differential geometric aspects of lightlike f-rectifying curves in Minkowski space-time [7]. Then they researched f-rectifying curves in Euclidean n-Space [8] and Euclidean 4-space [9]. Moreover some new characterizations of f-rectifying curves respect to type-2 quaternionic frame in $\mathbb{R}^4$ is investigated in [10].

In this study in analogy to rectifying curve we define spacelike f-rectifying curve in Minkowski space E_1^4 as a spacelike curve γ parametrized by its arclength s such that its f-position vector field γ_f introduced by $\gamma_f(s) = \int f(s)\, d\gamma$ always lies its rectifying plane, here f is a nowhere vanishing integrable function with parameter s. Then using this definition of spacelike f-rectifying curve we characterize and classify these curves in E_1^4.

2. Preliminaries

Minkowski space-time E_1^4 is an 4-dimensional pseudo-Euclidean space on which metric has index $\nu = 1$ and defined by the Lorentzian inner product

$$\langle v, w\rangle = -v_1w_1 + v_2w_2 + v_3w_3 + v_4w_4 \tag{2.1}$$

Date: July, 8, 2023.
2000 *Mathematics Subject Classification.* 53B30,53C40,53C50.
Key words and phrases. Rectifying curve, Minkowski space-time , Spacelike curve.

where $v=(v_1,v_2,v_3,v_4)$ and $w=(w_1,w_2,w_3,w_4)$ are vectors in E_1^4. Any arbitrary vector v is called timelike, lightlike or spacelike if the Lorentzian inner product $\langle v,v\rangle$ is negative definite, zero or positive definite, respectively. The norm of a vector v in E_1^4 is given by $\|v\|=\sqrt{\langle v,v\rangle}$ and if $\|v\|=1$ the vector v is called unit vector in E_1^4. Also the pseudo-sphere of unit radius with centre at the origin in E_1^4 can be given by

$$S_1^3(1)=\left\{v\in E_1^4:\langle v,v\rangle=1\right\}$$

Let $\gamma: I\longrightarrow E_1^4$ be an arbitrary curve in E_1^4 and $\gamma'(t)$ denote its velocity vector.Then γ is spacelike if and only if $\gamma'(t)$ is spacelike i.e. $\langle\gamma',\gamma'\rangle>0$, γ is timelike if and only if $\gamma'(t)$ is timelike i.e. $\langle\gamma',\gamma'\rangle<0$ and γ is null(lightlike) if and only if $\gamma'(t)$ is null i.e. $\langle\gamma',\gamma'\rangle=0$.
Let $\{T,N,B_1,B_2\}$ the moving Frenet frame along the curve $\gamma(s)$ in the space E_1^4 , consisting of the tangent, the principal normal, the binormal and the trinormal vector fields respectively. For an arbitrary spacelike curve $\gamma(s)$ in E_1^4 the following Frenet formulae can be given

i. If $\gamma(s)$ be a spacelike curve with timelike principal normal then Frenet equations are

$$\begin{bmatrix}T'(s)\\N'(s)\\B_1'(s)\\B_2'(s)\end{bmatrix}=\begin{bmatrix}0&k_1&0&0\\k_1&0&k_2&0\\0&k_2&0&k_3\\0&0&-k_3&0\end{bmatrix}\begin{bmatrix}T(s)\\N(s)\\B_1(s)\\B_2(s)\end{bmatrix}\tag{2.2}$$

ii. If $\gamma(s)$ be a spacelike curve with timelike binormal then Frenet equations are

$$\begin{bmatrix}T'(s)\\N'(s)\\B_1'(s)\\B_2'(s)\end{bmatrix}=\begin{bmatrix}0&k_1&0&0\\-k_1&0&k_2&0\\0&k_2&0&k_3\\0&0&k_3&0\end{bmatrix}\begin{bmatrix}T(s)\\N(s)\\B_1(s)\\B_2(s)\end{bmatrix}\tag{2.3}$$

iii. If $\gamma(s)$ be a spacelike curve with timelike trinormal then Frenet equations are

$$\begin{bmatrix}T'(s)\\N'(s)\\B_1'(s)\\B_2'(s)\end{bmatrix}=\begin{bmatrix}0&k_1&0&0\\-k_1&0&k_2&0\\0&-k_2&0&k_3\\0&0&k_3&0\end{bmatrix}\begin{bmatrix}T(s)\\N(s)\\B_1(s)\\B_2(s)\end{bmatrix}\tag{2.4}$$

where k_1,k_2,k_3 are first, second and third curvatures of the spacelike curve respectively [11].

3. Spacelike f-rectifying curve in E_1^4

Let $\gamma: I\longrightarrow E_1^4$ be a unit speed spacelike curve with Frenet aparatus $\{T_\gamma,N_\gamma,B_{\gamma_1},B_{\gamma_2},k_{\gamma_1},k_{\gamma_2},k_{\gamma_3}\}$. Then $\gamma: I\longrightarrow E_1^4$ is a rectifying curve in E_1^4 if and only if its position vector always lies in its rectifying space, i.e., if and only if its position vector is denoted by

$$\gamma(s)=\lambda(s)T_\gamma(s)+\mu_1(s)B_{\gamma_1}(s)+\mu_2(s)B_{\gamma_2}(s)$$

for all $s\in I$, where $\lambda,\mu_1,\mu_2: I\longrightarrow\mathbb{R}$ are differentiable functions in parameter s.[12]. Let $f: I\longrightarrow\mathbb{R}$ be a non-zero integrable function in parameter s. Then

f-position vector field of the curve γ in E_1^4 is expressed by γ_f and defined by

$$\gamma_f(s) = \int f(s)\, d\gamma \tag{3.1}$$

for all $s \in I$. Here the integral sign is used in this sense that after differentiating previous equation, the following equation can be found

$$\gamma_f'(s) = f(s)\, T_\gamma(s)$$

for all $s \in I$.

Definition 3.1. Let $\gamma : I \longrightarrow E_1^4$ be a unit speed spacelike curve with Frenet aparatus $\{T_\gamma, N_\gamma, B_{\gamma_1}, B_{\gamma_2}, k_{\gamma_1}, k_{\gamma_2}, k_{\gamma_3}\}$ and $f : I \longrightarrow \mathbb{R}$ be a nowhere vanishing integrable function in parameter s with at least twice differentiable primitive function F. Then the curve γ is called spacelike f-rectifying curve in E_1^4 if its f-position vector field $\gamma_f = \int f d\gamma$ always lies in its rectifying plane of γ in E_1^4, i.e., if its f-position vector field $\gamma_f = \int f d\gamma$ can be denoted as,

$$\gamma_f(s) = \lambda(s)\, T_\gamma(s) + \mu_1(s)\, B_{\gamma_1}(s) + \mu_2(s)\, B_{\gamma_2}(s) \tag{3.2}$$

for all $s \in I$, where $\lambda, \mu_1, \mu_2 : I \longrightarrow \mathbb{R}$ are smooth functions in parameter s.

4. Characterizations of Spacelike f-rectifying curve in E_1^4

Theorem 4.1. *Let $\gamma : I \longrightarrow E_1^4$ be a unit speed spacelike f-rectifying curve in E_1^4 parametrized by the arclength function s and having non-zero curvatures $k_{\gamma_1}, k_{\gamma_2}, k_{\gamma_3}$. Moreover assume that $f : I \longrightarrow \mathbb{R}$ be a nowhere vanishing integrable function in parameter s with primitive function F (i.e. $F'(s) = f(s)$ for all $s \in I$). Then up to isometries of E_1^4, γ is congruent to an f-rectifying curve in E_1^4 if and only if the following equations hold;*

i. *For spacelike f-rectifying curve with timelike binormal*

$$\frac{d}{ds}\left[\frac{\frac{d}{ds}\left(\frac{k_{\gamma_1}(s)}{k_{\gamma_2(s)}}F(s)\right)}{k_{\gamma_3}(s)}\right] - \frac{k_{\gamma_1}(s)\, k_{\gamma_3}(s)}{k_{\gamma_2}(s)}F(s) = 0 \tag{4.1}$$

ii. *For spacelike f-rectifying curve with timelike trinormal*

$$-\frac{d}{ds}\left[\frac{\frac{d}{ds}\left(\frac{k_{\gamma_1}(s)}{k_{\gamma_2(s)}}F(s)\right)}{k_{\gamma_3}(s)}\right] + \frac{k_{\gamma_1}(s)\, k_{\gamma_3}(s)}{k_{\gamma_2}(s)}F(s) = 0 \tag{4.2}$$

iii. *For spacelike f-rectifying curve with timelike principal normal*

$$-\frac{d}{ds}\left[\frac{\frac{d}{ds}\left(\frac{k_{\gamma_1}(s)}{k_{\gamma_2(s)}}F(s)\right)}{k_{\gamma_3}(s)}\right] - \frac{k_{\gamma_1}(s)\, k_{\gamma_3}(s)}{k_{\gamma_2}(s)}F(s) = 0 \tag{4.3}$$

for all $s \in I$.

Proof. Suppose that $\gamma : I \longrightarrow E_1^4$ be a unit speed spacelike f-rectifying curve with timelike binormal in E_1^4 parametrized by the arclength function s and having non-zero curvatures $k_{\gamma_1}, k_{\gamma_2}, k_{\gamma_3}$. Then for some smooth functions $\lambda, \mu_1, \mu_2 : I \longrightarrow \mathbb{R}$ we have f-position vector which satisfied the equation (3.2). So if we differentiate the equation (3.2) and considering the equation (2.3) we find,

$$\begin{aligned} f(s)\, T_\gamma(s) &= \lambda'(s)\, T_\gamma(s) + (\lambda(s)\, k_{\gamma_1}(s) + \mu_1(s)\, k_{\gamma_2}(s))\, N_\gamma(s) \\ &+ (\mu_1'(s) + \mu_2(s)\, k_{\gamma_3}(s))\, B_{\gamma_1}(s) + (\mu_2'(s) + \mu_1(s)\, k_{\gamma_3}(s))\, B_{\gamma_2}(s) \end{aligned} \tag{4.4}$$

for all $s \in I$. Equating the coefficients of equation (4.4) we obtain,

$$\begin{aligned} \lambda'(s) &= f(s) \ , \\ \lambda(s) k_{\gamma_1}(s) + \mu_1(s) k_{\gamma_2}(s) &= 0 \ , \\ -\mu_1'(s) - \mu_2(s) k_{\gamma_3}(s) &= 0 \ , \\ \mu_2'(s) + \mu_1(s) k_{\gamma_3}(s) &= 0 \ . \end{aligned} \tag{4.5}$$

Therefore from the firs equations of (4.5) and after some calculations we get

$$\begin{aligned} \lambda(s) &= F(s) \ , \\ \mu_1(s) &= -\frac{k_{\gamma_1}(s)}{k_{\gamma_2}(s)} F(s) \ , \\ \mu_2(s) &= \frac{1}{k_{\gamma_3}} \frac{d}{ds} \left(\frac{k_{\gamma_1}(s)}{k_{\gamma_2}(s)} F(s) \right) \ . \end{aligned} \tag{4.6}$$

Conversely we suppose that $\gamma : I \longrightarrow E_1^4$ be a unit speed spacelike curve with timelike binormal in E_1^4 parametrized by the arclength function s and having non-zero curvatures $k_{\gamma_1}, k_{\gamma_2}, k_{\gamma_3}$ and $f : I \longrightarrow \mathbb{R}$ be a non-zero integrable function in parameter s and the equation (4.1) is satisfied. Let define a vector field V along γ by

$$\begin{aligned} V(s) &= \gamma_f(s) - F(s) T_\gamma(s) + \frac{k_{\gamma_1}(s)}{k_{\gamma_2}(s)} F(s) B_{\gamma_1}(s) \\ &- \frac{1}{k_{\gamma_3}} \frac{d}{ds} \left(\frac{k_{\gamma_1}(s)}{k_{\gamma_2}(s)} F(s) \right) B_{\gamma_2}(s) \end{aligned} \tag{4.7}$$

for all $s \in I$. Differentiating (4.7) and using (2.3) and (4.1) we obtain $V'(s) = 0$ which implies that V is constant along γ. Hence up to isometries of E_1^4, γ is congruent to an spacelike f-rectifying curve in E_1^4. The equation (4.2) and (4.3) can be found by using the equations (2.2), (2.4) and the similar method above. So, the proof is completed. □

Remark 4.2. For a spacelike f-rectifying curve in E_1^4 if all of its curvature functions $k_{\gamma_1}, k_{\gamma_2}, k_{\gamma_3}$ are non-zero constants, let's say $k_{\gamma_1} = a_1 \neq 0, k_{\gamma_2} = a_2 \neq 0, k_{\gamma_3} = a_3 \neq 0$ for all $s \in I$, then we have

i. For a spacelike f-rectifying curve with timelike binormal

$$F''(s) - a_3^2 F(s) = 0 \ , \tag{4.8}$$

ii. For a spacelike f-rectifying curve with timelike trinormal

$$-F''(s) + a_3^2 F(s) = 0 \ , \tag{4.9}$$

iii. For a spacelike f-rectifying curve with timelike principal normal

$$-F''(s) - a_3^2 F(s) = 0 \ . \tag{4.10}$$

If f is non-zero constant or linear, then from (4.8),(4.9) and (4.10) we find $a_3 = 0$ which is a contradiction. Again, if f is non-linear then from (4.8),(4.9) and (4.10) we find a_3 is non-constant which is also a contradiction.

So the following theorem can be given;

Theorem 4.3. *Let $\gamma : I \longrightarrow E_1^4$ be a unit speed spacelike f-rectifying curve in E_1^4 parametrized by the arclength function s and having non-zero curvatures $k_{\gamma_1}, k_{\gamma_2}, k_{\gamma_3}$. Then γ is not congruent to an f-rectifying curve for any choice of f if and only if all of its curvatures $k_{\gamma_1}, k_{\gamma_2}, k_{\gamma_3}$ are constants.*

Theorem 4.4. *Let $\gamma : I \longrightarrow E_1^4$ be a unit speed spacelike f-rectifying curve in E_1^4 parametrized by the arclength function s and having non-zero curvatures $k_{\gamma_1}, k_{\gamma_2}, k_{\gamma_3}$. Also let $f : I \longrightarrow \mathbb{R}$ be a nowhere vanishing integrable function in parameter s with primitive function F. If γ is a spacelike f-rectifying curve in E_1^4 then the following equations are satisfied,*

i. *For spacelike f-rectifying curve with timelike binormal (timelike trinormal or timelike principal normal) the norm function $\rho = \|\gamma_f\|$ is given*
$$\rho(s) = \sqrt{F^2(s) + c^2}$$
for all $s \in I$, where c is a non-zero constant.

ii. *For spacelike f-rectifying curve with timelike binormal (timelike trinormal or timelike principal normal) the tangential component $\langle \gamma_f, T_\gamma \rangle$ of the f-position vector γ_f of γ can be given by,*
$$\langle \gamma_f, T_\gamma \rangle = F(s)$$

iii. *For spacelike f-rectifying curve with timelike principal normal (timelike trinormal or timelike principal normal) the normal component $\gamma_f^{N_\gamma}$ of the f-position vector γ_f of γ has constant length and the norm function is non-constant*

iv. *For spacelike f-rectifying curve with timelike binormal (timelike trinormal or timelike principal normal) the first component $\langle \gamma_f, B_{\gamma_1} \rangle$ and the second component $\langle \gamma_f, B_{\gamma_2} \rangle$ of the f-position vector γ_f of γ can be given by,*
$$\begin{aligned} \langle \gamma_f, B_{\gamma_1} \rangle &= \frac{k_{\gamma_1}(s)}{k_{\gamma_2}(s)} F(s) \\ \langle \gamma_f, B_{\gamma_2} \rangle &= \frac{1}{k_{\gamma_3}(s)} \frac{d}{ds} \left(\frac{k_{\gamma_1}(s)}{k_{\gamma_2}(s)} F(s) \right) \end{aligned}$$

for all $s \in I$.
Conversely $\gamma : I \longrightarrow E_1^4$ be a unit speed spacelike curve in E_1^4 parametrized by the arclength function s and having non-zero curvatures $k_{\gamma_1}, k_{\gamma_2}, k_{\gamma_3}$. Also let $f : I \longrightarrow \mathbb{R}$ be a nowhere vanishing integrable function in parameter s with primitive function F (i.e. $F'(s) = f(s)$ for all $s \in I$). If any one of the statements (i),(ii),(iii),(iv) is true then γ is a unit speed spacelike f-rectifying curve in E_1^4.

Proof. Suppose that $\gamma : I \longrightarrow E_1^4$ be a unit speed spacelike f-rectifying curve with timelike binormal in E_1^4 parametrized by the arclength function s and having non-zero curvatures $k_{\gamma_1}, k_{\gamma_2}, k_{\gamma_3}$. Then for some differential functions $\lambda, \mu_1, \mu_2 : I \longrightarrow \mathbb{R}$ with arclength parameter s the f-position vector γ_f of γ in E_1^4 satisfies equation (3.2) and from (4.5) and (4.6) we find

$$-\mu_1 \mu_1' + \mu_2 \mu_2' = 0 \tag{4.11}$$

for all $s \in I$. If we integrate the equation (4.12) we get

$$-\mu_1^2 + \mu_2^2 = c^2 \tag{4.12}$$

where c is a non-zero constant.So we have

i. Considering (3.2),(4.6) and (4.12) we get

$$\rho^2 = \|\gamma_f(s)\|^2 = \langle \gamma_f, \gamma_f \rangle = F^2(s) + c^2$$

then,

$$\rho(s) = \sqrt{F^2(s) + c^2}$$

where c is a non-zero constant.

ii. Using (3.2) and (4.6) we find

$$\langle \gamma_f(s), T_\gamma(s) \rangle = \lambda(s) = F(s) \ .$$

iii. Let $\alpha : J \longrightarrow E_1^4$ be an arbitrary curve then its f-position vector α_f can be written as follows,

$$\alpha_f(t) = \nu(t) T_\gamma(t) + \alpha_f^{N_\gamma}(t), t \in J,$$

for some smooth function $\nu : I \longrightarrow E_1^4$, here $\alpha_f^{N_\gamma}(t)$ is the normal component of α_f. If γ is a spacelike f-rectifying curve in E_1^4 then satisfies equation (3.2) so we can write

$$\gamma_f^{N_\gamma}(s) = \mu_1(s) B_{\gamma_1}(s) + \mu_2(s) B_{\gamma_2}(s) \ .$$

Then we get

$$\left\| \gamma_f^{N_\gamma}(s) \right\| = \sqrt{-\mu_1^2(s) + \mu_2^2(s)}$$

for all $s \in I$. From the above equation we obtain $\left\| \gamma_f^{N_\gamma}(s) \right\| = c$. So it satisfies that $\gamma_f^{N_\gamma}$ has constant length. Moreover using the statement (i) we have $\rho = \|\gamma_f\|$ is non constant.

iv. Considering (3.2)and (4.6), the first component $\langle \gamma_f, B_{\gamma_1} \rangle$ of γ_f is given by

$$\langle \gamma_f, B_{\gamma_1} \rangle = -\mu_1(s) = \frac{k_{\gamma_1}(s)}{k_{\gamma_2}(s)} F(s)$$

and the first component $\langle \gamma_f, B_{\gamma_1} \rangle$ of γ_f is given by

$$\langle \gamma_f, B_{\gamma_2} \rangle = \mu_2(s) = \frac{1}{k_{\gamma_3}(s)} \frac{d}{ds} \left(\frac{k_{\gamma_1}(s)}{k_{\gamma_2}(s)} F(s) \right)$$

for all $s \in I$.

Conversely let $\gamma : I \longrightarrow E_1^4$ be a unit speed spacelike curve in E_1^4 parametrized by the arclength function s and having non-zero curvatures $k_{\gamma_1}, k_{\gamma_2}, k_{\gamma_3}$. Also let $f : I \longrightarrow \mathbb{R}$ be a nowhere vanishing integrable function in parameter s with primitive function F (i.e. $F'(s) = f(s)$ for all $s \in I$). Assume that the statement (i) or (ii) is true such that if (i) is true we have

$$\langle \gamma_f(s), \gamma_f(s) \rangle = F^2(s) + c^2$$

where c is a non-zero constant. If we differentiate the above equation we find

$$\langle \gamma_f(s), T_\gamma(s) \rangle = F(s). \tag{4.13}$$

differentiate again and considering (2.3) we have

$$\langle \gamma_f(s), N_\gamma(s) \rangle = 0 \ .$$

Therefore we can say that γ is a spacelike f-rectifying curve in E_1^4.
If (iii) is true we get $\left\|\gamma_f^{N_\gamma}(s)\right\| = c$, then we can write

$$\gamma_f(s) = F(s)\,T_\gamma(s) + \gamma_f^{N_\gamma}(s)$$

for all $s \in I$. Then we find

$$\langle \gamma_f(s), \gamma_f(s)\rangle = \langle \gamma_f(s), T_\gamma(s)\rangle^2 + c^2$$

and if we differentiate this and using (2.3) we have

$$\langle \gamma_f(s), N_\gamma(s)\rangle = 0$$

for all $s \in I$. Therefore we can say that γ is a spacelike f-rectifying curve in E_1^4.
If (iv) is true we have

$$\langle \gamma_f, B_{\gamma_1}\rangle = \frac{k_{\gamma_1}(s)}{k_{\gamma_2}(s)} F(s) \tag{4.14}$$

$$\langle \gamma_f, B_{\gamma_2}\rangle = \frac{1}{k_{\gamma_3}(s)} \frac{d}{ds}\left(\frac{k_{\gamma_1}(s)}{k_{\gamma_2}(s)} F(s)\right) \tag{4.15}$$

for all $s \in I$.If we differentiate the equation (4.14) and using (2.3) we get

$$k_{\gamma_2}\langle \gamma_f(s), N_\gamma(s)\rangle + k_{\gamma_3}\langle \gamma_f(s), B_{\gamma_2}(s)\rangle = \frac{d}{ds}\left(\frac{k_{\gamma_1}(s)}{k_{\gamma_2}(s)} F(s)\right)$$

and from the equation (4.15) and the above equation we calculate

$$\langle \gamma_f(s), N_\gamma(s)\rangle = 0\ .$$

Consequently γ is a spacelike f-rectifying curve in E_1^4. □

5. Classification of Spacelike f-rectifying curve in E_1^4

Theorem 5.1. *Let $\gamma : I \longrightarrow E_1^4$ be a unit speed spacelike f-rectifying curve in E_1^4 parametrized by the arclength function s and having non-zero curvatures $k_{\gamma_1}, k_{\gamma_2}, k_{\gamma_3}$. Also let $f : I \longrightarrow \mathbb{R}$ be a nowhere vanishing integrable function in parameter s with primitive function F (i.e. $F'(s) = f(s)$ for all $s \in I$). If γ is a spacelike f-rectifying curve in E_1^4 iff its f-position γ_f is satisfied the following equation,*

$$\gamma_f(t) = c\sec\left(t + \arctan\left(\frac{F(s_0)}{c}\right)\right)\alpha(t) \tag{5.1}$$

for all $t \in I$, where c is a positive constant, $s_0 \in I$ and $\alpha : J \longrightarrow S_1^3(1)$ is a unit speed curve having $t : I \longrightarrow J$ as arclength function based at s_0.

Proof. Suppose that $\gamma : I \longrightarrow E_1^4$ be a unit speed spacelike f-rectifying curve in E_1^4 and having non-zero curvatures $k_{\gamma_1}, k_{\gamma_2}, k_{\gamma_3}$. Then using theorem 4.3. we have,

$$\rho(s) = \sqrt{F^2(s) + c^2} \tag{5.2}$$

for all $s \in I$ and where c is a positive constant. If we define a new curve α in E_1^4 by

$$\alpha(s) = \frac{1}{\rho(s)}\gamma_f(s)\ . \tag{5.3}$$

Therefore we obtain

$$\langle \alpha(s), \alpha(s)\rangle = 1 \tag{5.4}$$

for all $s \in I$. So α is a curve in S_1^3. If we differentiate above equation we have

$$\langle \alpha(s), \alpha'(s) \rangle = 0 . \tag{5.5}$$

Moreover using the equations (5.2) and (5.3) we find

$$\gamma_f(s) = \alpha(s) \sqrt{F^2(s) + c^2} . \tag{5.6}$$

Differentiating (5.6) and considering (5.4) and (5.5) we obtain

$$\langle \alpha'(s), \alpha'(s) \rangle = \frac{c^2 f^2(s)}{(F^2(s) + c^2)^2} .$$

Also we have

$$\|\alpha'(s)\| = \frac{c f(s)}{F^2(s) + c^2}$$

for all $s \in I$. Assume that $t : I \longrightarrow J$ be the arc length function of α based at $s_0 \in I$ given by

$$t = \int_{s_0}^{s} \|\alpha'(u)\| \, du.$$

Then we get

$$t = \arctan\left(\frac{F(s)}{c}\right) - \arctan\left(\frac{F(s_0)}{c}\right).$$

Therefore we obtain

$$F(s) = c \tan\left(t + \arctan\left(\frac{F(s_0)}{c}\right)\right). \tag{5.7}$$

Moreover using the equations (5.6) and (5.7) we have

$$\gamma_f(t) = \frac{c}{\cos\left(t + \arctan\left(\frac{F(s_0)}{c}\right)\right)} \alpha(t) . \tag{5.8}$$

for all $t \in J$. Conversely let $\gamma : I \longrightarrow E_1^4$ be a unit speed spacelike curve in E_1^4 given by (5.1), $s_0 \in I$ and $\alpha : J \longrightarrow S_1^3$ is a unit speed curve with $t : I \longrightarrow J$ as arclength function based at s_0. If we differentiate (5.1) we get

$$\gamma_f'(t) = \frac{c \sin\left(t + \arctan\left(\frac{F(s_0)}{c}\right)\right)}{\cos^2\left(t + \arctan\left(\frac{F(s_0)}{c}\right)\right)} \alpha(t) + \frac{c}{\cos\left(t + \arctan\left(\frac{F(s_0)}{c}\right)\right)} \alpha'(t) . \tag{5.9}$$

for all $t \in J$. We know that α is a unit speed curve in the unit sphere $S_1^3(1)$ so we obtain $\langle \alpha'(t), \alpha'(t) \rangle = 1$, $\langle \alpha(t), \alpha(t) \rangle = 1$ and $\langle \alpha(t), \alpha'(t) \rangle = 0$ for all $t \in J$. Then consider the equations (5.1) and (5.9) we have

$$\begin{aligned}
\langle \gamma_f(t), \gamma_f(t) \rangle &= \frac{c^2}{\cos^2\left(t + \arctan\left(\frac{F(s_0)}{c}\right)\right)} , \\
\langle \gamma_f(t), \gamma_f'(t) \rangle &= \frac{c^2 \sin\left(t + \arctan\left(\frac{F(s_0)}{c}\right)\right)}{\cos^3\left(t + \arctan\left(\frac{F(s_0)}{c}\right)\right)} , \\
\langle \gamma_f'(t), \gamma_f'(t) \rangle &= \frac{c^2}{\cos^4\left(t + \arctan\left(\frac{F(s_0)}{c}\right)\right)} .
\end{aligned} \tag{5.10}$$

If we put

$$t = \arctan\left(\frac{F(s)}{c}\right) - \arctan\left(\frac{F(s_0)}{c}\right).$$

then s becomes arclength parameter of γ and we get

$$\begin{aligned} \langle \gamma_f(s), \gamma_f(s) \rangle &= \frac{c^2}{\cos^2\left(\arctan\left(\frac{F(s)}{c}\right)\right)} \\ \langle \gamma_f(s), \gamma_f'(s) \rangle &= \frac{c^2 \sin\left(\arctan\left(\frac{F(s)}{c}\right)\right)}{\cos^3\left(\arctan\left(\frac{F(s)}{c}\right)\right)} \qquad (5.11) \\ \langle \gamma_f'(s), \gamma_f'(s) \rangle &= \frac{c^2}{\cos^4\left(\arctan\left(\frac{F(s)}{c}\right)\right)} \end{aligned}$$

for all $s \in I$. The normal component $\gamma_f^{N_\gamma}$ of γ_f can be given by

$$\left\langle \gamma_f^{N_\gamma}(s), \gamma_f^{N_\gamma}(s) \right\rangle = \langle \gamma_f(s), \gamma_f(s) \rangle - \frac{\left\langle \gamma_f(s), \gamma_f'(s) \right\rangle^2}{\left\langle \gamma_f'(s), \gamma_f'(s) \right\rangle}$$

for all $s \in I$. Then considering the equation (5.11) in above equation we obtain

$$\left\langle \gamma_f^{N_\gamma}(s), \gamma_f^{N_\gamma}(s) \right\rangle = \left\| \gamma_f^{N_\gamma}(s) \right\|^2 = c^2$$

for all $s \in I$. Consequently the normal component $\gamma_f^{N_\gamma}$ of γ_f has a constant length. Also we have

$$\rho(s) = \sqrt{\langle \gamma_f(s), \gamma_f(s) \rangle} = \frac{c}{\cos\left(\arctan\left(\frac{F(s)}{c}\right)\right)}$$

for all $s \in I$ and it is non constant. Then applying theorem 4.3 we can say that γ is a spacelike f-rectifying curve in E_1^4. □

References

[1] B.Y. Chen, When does the position vector of a space curve always lie in its rectifying plane?, Amer. Math. Monthly, 110, 147-152, (2003).

[2] K. Ilarslan , E. Nesovic, Some characterizations of null, pseudo null and partially null rectifying curves in Minkowski space-time, Taiwanese J Math, 12(5), 1035-1044, (2008).

[3] K. Ilarslan , E. Nesovic, On rectifying curves as centodes and extremal curves in the Minkowski 3-space. Novi Sad J Math, 37, 53-64, (2007).

[4] T. Tunahan,, On Rectifying Curves and Their Characterization in Lorentz n-Space, International Electronic Journal of Geometry, 11(1), 26-36, (2018).

[5] Z. Iqbal, J.Sengupta, Non-null (spacelike or timelike) f-rectifying curves in the Minkowski 3-space ., Eurasian Bul. Math., 3(1), 38-55, (2020).

[6] Z. Iqbal, J. Sengupta, Null (lightlike) f-rectifying curves in the Minkowski 3-space . Fundam. J.Math. Appl., 3(1), 8-16, (2020).

[7] Z. Iqbal, J. Sengupta, Differential geometric aspects of lightlike f-rectifying curves in Minkowski space-time, Differential Geometry - Dynamical Systems, 22, 113-129, (2020).

[8] Z. Iqbal , J. Sengupta, A Study on f-Rectifying Curves in Euclidean n-Space. Univ. J. Math. Appl., 4(3), 107-113, (2021).

[9] Z. Iqbal, J. Sengupta, On f-rectifying curves in the Euclidean 4-space. Acta Universitatis Sapientiae, Mathematica., 13(1), 192-208, (2021).

[10] E. Erdem, Some New Characterizations of f-Rectifying Curves Respect to Type-2 Quaternionic Frame in $\mathbb{R}^4$, Prespacetime Journal,14(2), 344-353, (2023).

[11] J. Walrave, Curves and Surfaces in Minkowski Space, (1995).
[12] A.T. Ali , Onder M. Some Characterizations of Space-Like Rectifying Curves in the Minkowski Space-Time, Global Journal of Science Frontier Research Mathematics and Decision Sciences, 2(1), 57-63, (2012).

Osmaniye Korkut Ata University, Department of Mathematics, 80000, Osmaniye, Turkey
Email address: hulyagun@osmaniye.edu.tr

Osmaniye Korkut Ata University, Department of Mathematics, 80000, Osmaniye, Turkey
Email address: krkmz.1990@hotmail.com